

# Performance modeling of a centrifugal pump

P6 PROJECT  
GROUP TE6-601  
DEPARTMENT OF ENERGY TECHNOLOGY  
AALBORG UNIVERSITY  
25<sup>th</sup> OF MAY 2012



## Abstract

The purpose of this project is to produce a model for prediction of the performance of the Grundfos NK 32-125 pump, verify the model by setting up and carrying out an ISO 9906 approved pump test and achieve an understanding of the theories applied for centrifugal pump modeling.

For describing the fundamental theory of pump modeling, the different types of pumps and impellers are examined. The Grundfos NK32-125 endsuction pump is determined by calculations of specific speed to be a radial pump.

The model is based on the theory of velocity triangles and the influence of the angles of the fluid velocity throughout the impeller. The calculation with velocity triangles includes blockage, incidence, deviation and slip. The accuracy of the model is adjusted by taking hydraulic and mechanical losses in the impeller into account. The model is designed with a fixed rotational speed.

Compliance of the model with the general impeller theory is tested. The model is tested for optimization of number of blades as a function of flow rate through the system. According to the theory, the highest efficiencies should be found in the range of 5-10 blades independent of the flow. The model predicted highest efficiency for 6-9 blades, followed closely by 5 and 10 blades. A closer examination shows the highest efficiency curves occur for impellers with 7 or 8 blades. The significance of blade number increases with the flow rate. Additionally it is shown that especially for low flow rates, a higher number of blades results in a higher head gain.

The model is tested by changing the outlet angle. The model follows the theory that a larger outlet angle should change the slope of the theoretical head as a function of flow, having a negative slope below 90° and a positive slope above 90°.

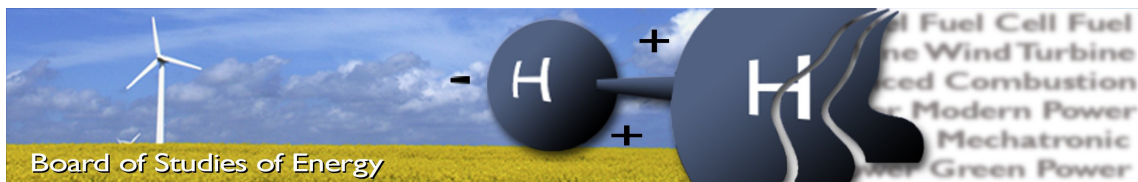
Verification of the model is based on data sheet comparison and the deviation between the two is found to be too high. To further improve the accuracy of the model the diffuser loss is taken into account based on [Gülich, 2008] theory about *the influence of losses and recirculation on pump characteristics*.

An impeller with blades perpendicular to the side discs is designed in order to perform tests with parameters more alike those the model is limited to. Due to lack of time for construction, this impeller was not tested.

A final verification of the model is possible by setting up a pump test in accordance to International Standard, ISO 9906. Due to problems with the setup construction, the final pump test setup is not valid in accordance with the ISO. Scaling of rotational speed makes it possible to verify the validity of the test data to the data sheet with varying rotational speed. The model is compared to the unscaled data.

The model deviates significantly in the low flow area but the accuracy of the model increase with the flow. The model is therefore considered valid in the high flow area and at the rated flow at the NK 32-125.





**Title:** Performance modeling of a centrifugal pump  
**Semester:** 6  
**Semester theme:** Thermo Mechanical Energy Systems  
**Project period:** 01.02.12 to 25.05.2012  
**ECTS:** 19  
**Supervisor:** Henrik Sørensen  
**Project group:** TE6-601

---

Katrine Arnoldsen Juhl

---

Gregers Nis Søborg Larsen

---

Morten Lind Andreasen

---

Copies: 5  
 Pages, total: 120  
 Appendices: 7  
 Supplements: CD

#### SYNOPSIS:

The purpose of this project is to produce a model for prediction of the performance of the Grundfos NK 32-125 pump, verify the model by setting up and carrying out an ISO 9906 approved pump test and achieve an understanding of the theories applied for centrifugal pump modeling. A model is established based on impeller theory and pump losses after a description of centrifugal pumps. The model is verified by comparing the model results to theory, data sheet and experiment. The model has several limitations based on simplifications of the system, e.g. fixed rotational speed. A new impeller is designed with blades perpendicular to the side discs but have not been tested. The pump test is conducted on a setup which is designed after the International Standard, ISO 9906. Due to differences between the designed and the constructed test setup, the test setup is not valid under the ISO. Comparing the model to the test data shows that a significant deviation occurs in the low flow area, while the model fits in the high flow area. The model does not predict the pump performance exactly, but gives a good estimate of it in and around the highest efficiency point.

By signing this document, each member of the group confirms that all participated in the project work, that the content of the project is our own work and thereby all members are collectively liable for the content of the report.



# Preface

---

This report is the work of group TE6-601 on 6<sup>th</sup> semester at Department of Energy Technology at Aalborg University. The theme for the semester is *Thermo Mechanical Energy Systems*. The purpose of this project is to produce a model for prediction of the performance of the Grundfos NK 32-125 pump, verify the model by setting up and carrying out an ISO approved pump test and achieve an understanding of the theories applied for centrifugal pump modeling.

Following programs has been used: MATLAB, LabVIEW, SolidWorks, Excel and AutoCAD. Some knowledge to these programs are assumed in order to get the full benefit of this report.

## Topical organization

The report is divided into four parts.

Part I: Chapter 1 gives a short introduction to the usage of pumps and is followed by the problem statement in Chapter 2. The problem statement contains the goals, limitations and the strategy of the project.

Part II: *Identification and modeling of a centrifugal pump* gives a general description of pumps and makes the reader aware of some of the fundamental aspects of pump theory including velocity triangles and losses. Chapter 4 in Part I ends with an overview of the model, that describes the pump impeller theory for a radial impeller.

Part III: *Model verification* gives a description of the Grundfos NK32-125 pump performance, the design of the impellers and the experiment results, which can be seen in Chapter 5, 6 and 7. In Chapter 7 the experimental data will be compared to the model results.

Chapter 8 holds the conclusion of the report and Chapter 9 ideas for further work.

Part IV: Appendices.

The two main parts of the report, part II and part III, can be read independent of each other, but to get a satisfactory insight into how the impeller and the model are designed, the authors recommend that the report is read from one end to the other.

## Reading guide

Throughout the report there will be references to sources, these can be found in the Bibliography. The used method for referring to sources is the Harvard method, with references listed as [Author, Year]. If the reference is included in a sentence before the dot, the reference covers the sentence. If the reference is after a dot, it covers the prior

paragraph or section. If there are more than one source with the same name and year the source gets a letter after the year. A reference leads to the Bibliography where the source is given by the author, title, edition, publisher, hyperlink and year. In the report transcript will be clearly marked as a quotation in italic with its own reference.

Figures, tables, equations and calculations have numbers that indicates which chapter they belong to and their order of appearance. E.g. the first figure in Chapter 3 is Figure 3.1 and the next, Figure 3.2. There is a caption to each figure and table. Appendixes are indicated with a letter.

Some figures have been modified in order to better show certain details. These figures will have a reference to the source and a comment saying “Modified” in the caption.

A CD is attached to the report, which includes all data given, data sheets, program files, the report in PDF and PDF-copies of all websites. All the files on the CD have a number. A reference to a file on the CD appears by referring to the CD appendix (Appendix A) and the number on the CD, e.g. Appendix A.3.

Publication of the entire or parts of this report is allowed only with reference and by approval from the authors.

# Nomenclature list

---

Symbol	Definition	Unit
$A$	Area	$m^2$
$a$	Distance between vanes	$m$
$b$	Blade height	$m$
$c$	Absolute velocity	$\frac{m}{s}$
$c_d$	Dissipation coefficient	—
$c_f$	Friction coefficient	—
$d$	Diameter	$m$
$D_h$	Hydraulic diameter	$m$
$d_{inlet}$	Diameter of the pump inlet	$m$
$d_{outlet}$	Diameter of the pump outlet	$m$
$E$	Axial distance to wall	$m$
$e$	Blade width	$m$
$f$	Darcy friction factor	—
$g$	Local gravitational acceleration (9,82)	$\frac{m}{s^2}$
$H, h$	Head	$m$
$I$	Current	$A$
$i$	Incidence angle	°
$K$	Type number	—
$k$	Factor	—
$L$	Length	$m$
$n$	Rotational speed	$rpm$
$n_q$	Specific speed	—
$O$	The wetted circumference	$m$
$P$	Power	$W$
$p$	Pressure	$Pa$
$Q$	Flow rate	$\frac{m^3}{s}$
$R$	Resistance	$\Omega$
$r$	Radius	$m$
$Re$	Reynolds number	—
$s$	Seal width	$m$
$T$	Torque	$Nm$
$u$	Circumferential velocity	$\frac{m}{s}$
$V$	Voltage	$V$
$v$	Velocity	$\frac{m}{s}$

*Continued on next page*

---

<i>Continued from previous page</i>		
Symbol	Definition	
$w$	Relative velocity	$\frac{m}{s}$
$y$	Factor	—
$Z$	Head loss	$m$
$z$	Height	$m$
$z_{La}$	Number of impeller blades	—
$\alpha$	Absolute flow angle	$^{\circ}$
$\beta$	Relative flow angle	$^{\circ}$
$\gamma$	Slip factor	—
$\delta$	Deviation angle	$^{\circ}$
$\epsilon$	Relative roughness	—
$\zeta$	Loss Coefficient	—
$\eta$	Efficiency	%
$\lambda$	Disc angle	$^{\circ}$
$\nu$	Kinematic viscosity	$\frac{m^2}{s}$
$\rho$	Density	$\frac{kg}{m^3}$
$\tau$	Blockage	—
$\varphi$	Flow coefficient	-
$\omega$	Rotational speed	$\frac{rad}{s}$

Subscripts and abbreviations	
1	Impeller inlet
2	Impeller outlet
3	Diffuser outlet
4	Volute outlet
<i>av</i>	Average relative
<i>ax</i>	Axial
<i>B</i>	Blade
<i>C</i>	Shock
<i>D</i>	Design point
<i>d</i>	Discharge side
<i>dyn</i>	Dynamic
<i>EA</i>	In- and outlet
<i>geo</i>	Geodetic
<i>hyd</i>	Hydraulic
<i>i</i>	Second impeller seal
<i>K</i>	Chamber
<i>La</i>	Impeller
<i>Le</i>	Diffuser
<i>ls</i>	Shock
<i>lr</i>	Friction
<i>m</i>	Meridional
<i>Opt</i>	Optimal
<i>p</i>	Static
<i>q</i>	Impeller throat
<i>R</i>	Friction and mixing

*Continued on next page*

---

*Continued from previous page*

Symbol	Definition
<i>ref</i>	Reference
<i>s</i>	Suction side
<i>si</i>	Second impeller seal
<i>sch</i>	Blade
<i>shaft</i>	Shaft
<i>sp</i>	Leakage
<i>stat</i>	Static
<i>th</i>	Theoretical
<i>tot</i>	Total
<i>u</i>	Circumferential component
$\infty$	Blade-congruent

---

Superscript

'	Blockage
*	Dimensionless quantity referred to $d_2$

---

Prescript

$\Delta$	Change
----------	--------

---



# Table of Contents

---

<b>I Introduction</b>	<b>1</b>
<b>1 The usage of pumps</b>	<b>3</b>
<b>2 Problem statement</b>	<b>5</b>
<b>II Identification and modeling of a centrifugal pump</b>	<b>7</b>
<b>3 Description of centrifugal pumps</b>	<b>9</b>
3.1 Description of the different parts of a centrifugal pump . . . . .	10
3.1.1 Radial impeller pumps . . . . .	12
<b>4 Pump impeller theory</b>	<b>17</b>
4.1 Velocity triangles for a radial impeller . . . . .	18
4.1.1 Inlet triangle . . . . .	18
4.1.2 Outlet triangle . . . . .	21
4.1.3 Outlet angle impact on the head . . . . .	22
4.1.4 Slip . . . . .	23
4.2 Overview of losses . . . . .	24
4.2.1 Mechanical losses . . . . .	25
4.2.2 Hydraulic losses . . . . .	26
4.3 Overview of impeller model . . . . .	30
<b>III Model verification</b>	<b>33</b>
<b>5 Verification of the model by product data sheet</b>	<b>35</b>
5.1 Reference pump data . . . . .	35
5.2 Comparison between model and reference impeller. . . . .	37
5.3 Evaluation of model . . . . .	39
5.3.1 Number of blades influence on the head . . . . .	39
5.3.2 The outlet angle influence on the head . . . . .	41
5.4 Additional model loss . . . . .	42
5.5 Influence of diffuser loss . . . . .	45
<b>6 Design of model test impeller</b>	<b>49</b>
6.1 Design of the non-twisted blade impeller . . . . .	49
<b>7 Test data verification of model</b>	<b>53</b>
7.1 Pump characteristics from test data . . . . .	56
<b>8 Conclusion</b>	<b>61</b>

<b>9 Model improvement proposals</b>	<b>63</b>
<b>Bibliography</b>	<b>65</b>
<b>IV Appendices</b>	<b>I</b>
<b>A Contents on the CD</b>	<b>III</b>
<b>B Documentation of model</b>	<b>V</b>
<b>C Loss equations</b>	<b>XI</b>
<b>D Standard measurement criteria</b>	<b>XV</b>
<b>E Testing of pump system</b>	<b>XXI</b>
<b>F Measurement devices</b>	<b>XXIX</b>
<b>G LabVIEW program</b>	<b>XXXV</b>

# **Part I**

# **Introduction**



# The usage of pumps

1

---

Pumps are used for producing and maintaining flows and pressures in fluid systems. The applications of pumps are many and diverse. Pumps are widely used throughout industrial, commercial, public and domestic purposes.

Some examples of pump usages are listed below.

- Circulation pumps
- Pumps for pressure boosting
- Water supply pumps
- Industrial pumps
- Wastewater pumps

Circulation is one of the main usages for pumps. Circulation pumps are used in closed flow systems. Examples of closed flow systems could be heating and cooling. There are installed circulation pumps in most households for domestic heating or cooling, providing air conditioning and transportation of heated consumption water. Domestic circulation pumps are constantly on for minimizing the waiting time for the consumer. New models uses as low as a tenth of energy compared to older models of the same use [The Danish Energy Saving Trust, 2012]. [Department of Structural and Fluid Mechanics, 2008,p. 24]

For hydraulic systems in industrial use, the pump is the main energy consumer of the fluid system. In 2001 pumps consumed 20% of the total electricity usage in the world and a considerably larger percentage in some industries [Hydraulic Institute et al., 2001]. Due to better modeling, the energy consumption for industrial pumps, like pump for circulation in households, have decreased.

During the life cycle of an industrial flow system, the energy cost for the pump is the main expense, as seen in Figure 1.1. Lowering the energy usage will mean savings for the individual user and the energy system. Figure 1.1 is dated 2001 and it is therefore presumed that the efficiency have increased since, causing the energy cost to have a smaller part of the life cycle cost.

As the amount of energy used for pumps is excessive, optimization of efficiency is crucial. One method of optimizing a pump is to design the impeller to satisfy the specific characteristics of the systems. The optimal impeller geometrics are dependent on the required flow and pressure in the system. If the pump impeller is optimized for a certain flow, less power is needed as the efficiency will be maximized.

In order to optimize a pump, a precise modeling tool is needed. A modeling tool could be used for predicting the performance of the pump under different circumstances in the

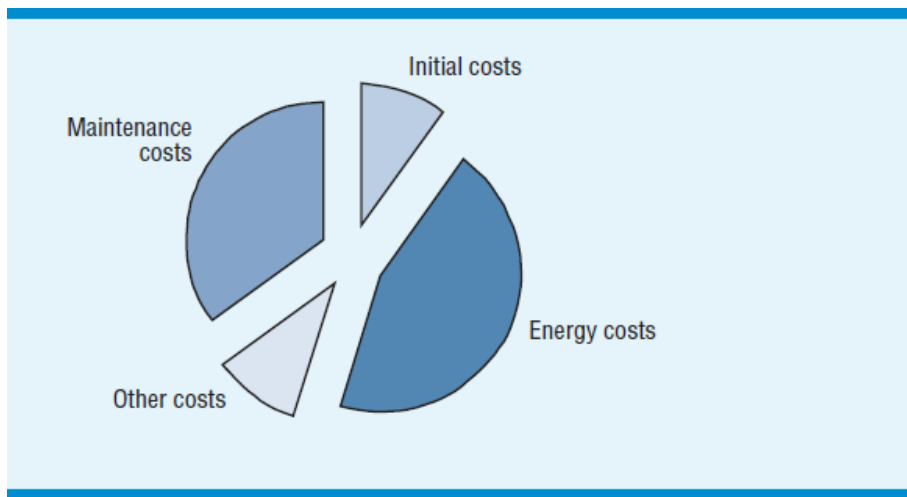


Figure 1.1: Typical life cycle costs for a medium-sized industrial pump [Hydraulic Institute et al., 2001].

system. The tool could as well be used for testing the parameters of the pump such as the number of blades and the blade angles of the impeller.

# Problem statement 2

---

The main objective of this project is to produce a model for prediction of the performance of the Grundfos NK 32-125 pump, verify the model by setting up and carrying out an ISO 9906 approved pump test and achieve an understanding of the theories applied for centrifugal pump modeling. The model will be based on pump theory and will be verified by experiment and by comparison to the NK 32-125/142 pump data sheet. The overall goals of the report are as follows:

## Goals

- Description of the main parts of a centrifugal pump and their purpose.
- Modeling of impeller based on the pump theory.
- Verification of the model by using the NK 32-125/142 data sheet.
- Design of a new impeller for testing the model.
- Set up a pump test corresponding to the ISO 9906 standard.
- Build of ISO 9906 standard verified test stand.
- Final verification of the model by comparison to test data.

## General limitations

This project is based on an already existing Grundfos pump. The focus will be on making a valid model for prediction of the pump performance, and on designing and testing an impeller to verify the model. The project will be limited to the impeller, both in term of modeling and practical work. To verify the model by test data, a test stand valid according to ISO 9906 will be build. The model and the test analysis will focus on the impeller and its losses.

## Project strategy

The project is divided into four parts containing the following:

1. Introduction
2. Identification and modeling of centrifugal pump
  - The main parts of the centrifugal pump will be described.
  - The theory used in the modeling of the impeller will be described.
  - An overview of the model will be presented.
3. Model verification
  - The model will be verified by comparison to the NK 32-125/142 data sheet.
  - A new impeller will be designed for use in an experiment.
  - Experiments with new and original impeller.

- Comparison between the model results and the experimental data.
  - A final evaluation and possible verification of the model will be made.
4. Appendices

## **Part II**

# **Identification and modeling of a centrifugal pump**



# Description of centrifugal pumps 3

---

*This chapter will give a short description of the fluid machine, the centrifugal pump. It will explain the basic principles of the centrifugal pump and pump technology in general. This chapter is build mainly on theory from [Department of Structural and Fluid Mechanics, 2008]*

Fluid machines can be divided into two main categories: positive displacement machines and turbomachines.

The positive displacement machines are denoted as the static type of fluid machines. Positive displacement machines force a fluid into and out of a chamber which is done by changing the volume of the chamber e.g. like a human heart, a bicycle pump or the piston in a compression engine.

Turbomachines are denoted as the dynamic type, which means that they consist of a number of blades, buckets, flow channels or passages around an axis of rotation, which forms a rotor. The turbomachine rotation of the rotor produces dynamic effect which either adds energy to the fluid or extracts energy from the fluid. The energy is either supplied to the rotating shaft e.g. by a motor and transferred to the fluid by the blades, or the energy is transferred from the fluid to the shaft by the blades. Turbines extract energy from the fluid and pumps add energy to the fluid; fans, propellers on ships and airplanes and water pumps are examples of types of turbomachine pumps. An example of a turbine could be a steam turbine used to drive generators for an electrical power plant. [Munson, Young and Okiishi, 2006]

## Principle of the centrifugal pump

The centrifugal pump belongs to the turbomachine category which adds energy to the fluid. The fluid through a system is driven by the pressure difference created by the pump. When the pump is operating, an increase in the fluid pressure from the inlet to the outlet of the pump is created. Bernoulli's general energy equation seen in Equation 3.1 describes the energy flow in the system.

$$\frac{p_1}{\rho_1 \cdot g} + \frac{v_1^2}{2g} + z_1 + h_{Added} - h_{Extracted} - h_{Loss} = \frac{p_2}{\rho_2 \cdot g} + \frac{v_2^2}{2g} + z_2 \quad [m] \quad (3.1)$$

Equation 3.1 is a revised version of Bernoulli's energy equation, where the first part describes the work of the flow, the second part describes the kinetic energy and the third part is the potential energy. Where  $h_{Added}$  is the energy added to the system (e.g. a

pump),  $h_{Extracted}$  is the extracted energy from the system (e.g. a turbine) and  $h_{Loss}$  is the energy loss in the system (e.g. friction).

In the centrifugal pump the motor transfers mechanical energy to the fluid through the rotating impeller, which creates the increase in pressure. The fluid flows from the inlet in the impeller center and out along its blades. The centrifugal force increases the fluid velocity and consequently the kinetic energy is transformed to pressure.

### 3.1 Description of the different parts of a centrifugal pump

In this section a short description of the different parts of the pump, which will be based on Figure 3.1, will be given.

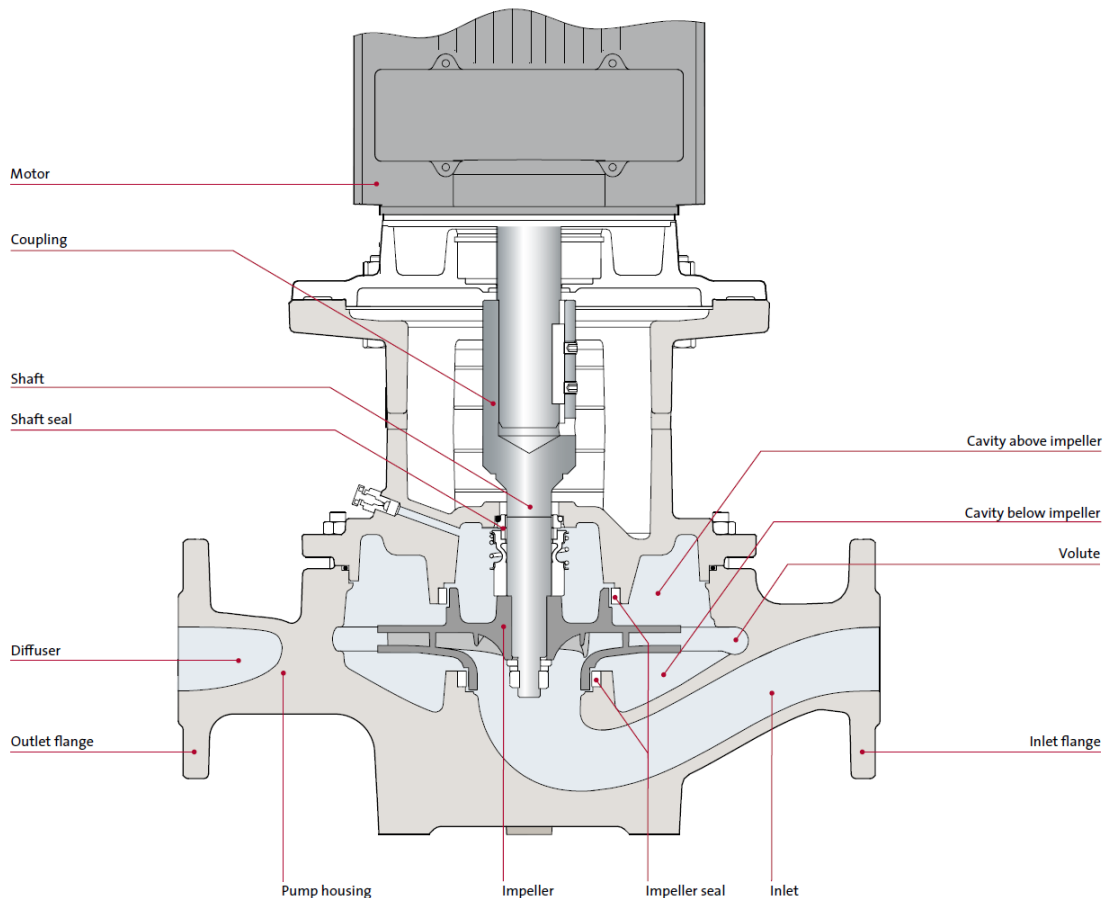


Figure 3.1: The hydraulic components from a single-stage inline pump. [Department of Structural and Fluid Mechanics, 2008,p. 13]

#### Impeller

Turbomachines are classified as radial flow, mixed flow (also called semiaxial flow) or axial flow machines. The fluid can run radially (Figure 3.2 left), axially (Figure 3.2 right) or a

cross between these (Figure 3.2 middle) through the impeller which effects the impellers ability to increase the pressure and create flow.

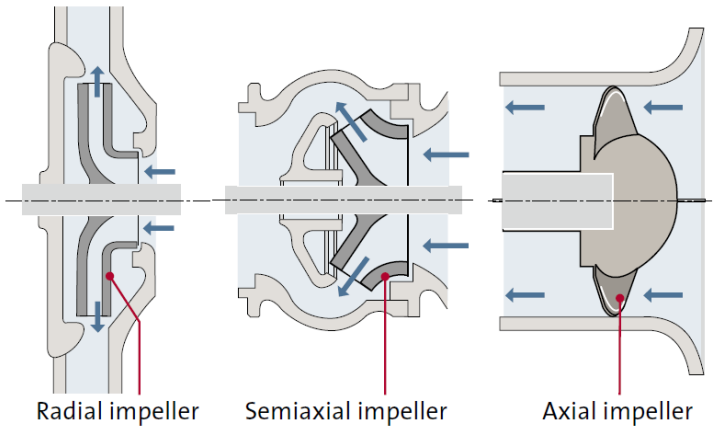


Figure 3.2: The different types of impellers [Department of Structural and Fluid Mechanics, 2008,p. 16].

- In a radial impeller (Figure 3.2 left), the fluid runs radially through the impeller. There is a considerable difference between the inlet diameter and the outlet diameter along with a difference between the outlet diameter and the outlet width. The centrifugal forces in a radial impeller gives a high pressure increase and a low flow.
- The axial impeller (Figure 3.2 right) has a large outlet width. There is no change in radial direction in the axial impeller. In the case of an axial impeller, the fluid flows through the blades in a straight line, relative to the pump axis. An axial impeller gives a low pressure difference and a high flow.
- A semiaxial impeller (Figure 3.2 mid) is used when a medium flow and pressure is required. For semiaxial and axial impellers, the fluid flows through the inlet into the impeller eye and out along the blades of the impellers, as it can be seen for the appropriate impeller types on Figure 3.2.

The impeller eye is the hole in the center of the impeller, where the fluid is sucked through, when the impeller rotates. From the impeller eye the fluid flows out along the vanes created by the blades in the impeller. The blades of the rotating impeller transfers the mechanical energy from the motor to the fluid thereby increasing the fluid pressure. The number of blades depends mainly on three parameters, the desired performance, the noise constraints and the amount and size of solid particles in the fluid.

The connection between the required flow, head and type of impeller is seen in Figure 3.3

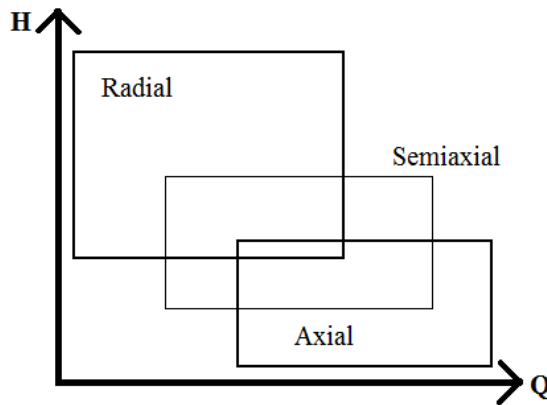


Figure 3.3: The different type of impellers are used under different circumstances e.g. a certain head is needed for a certain flow.

The specific speed,  $n_q$ , is used when selecting the design of the pump. Knowing the pump application, which is characterized by the flow,  $Q_D$ , head,  $H_D$ , and rotational speed,  $n_D$ , in the design point. The specific speed can be found by Equation 3.2 [Department of Structural and Fluid Mechanics, 2008].

$$n_q = n_D \cdot \frac{Q_D^{1/2}}{H_D^{3/4}} \quad [-] \quad (3.2)$$

To a large extent the specific speed determines the design of the impeller shape. Table 3.1 lists the different impeller types based on the specific speed.[Gülich, 2008,p. 50]

Type	Radial pumps	Semiaxial pump	Axial pump
$n_q$	<100	35-160	160-400

Table 3.1: Impeller shape based on the specific speed.

### 3.1.1 Radial impeller pumps

The pump used for modeling and testing is a Grundfos NK32-125, see Appendix A.3. The NK32-125 uses a radial impeller, why this type will be the focus of the further description.

#### Inlet

The pump is connected to the piping system through the inlet and the outlet flange of the pump. The design of the flange can change depending on the applications of the pump. The inlet leads the fluid into the impeller eye. The three most common types of inlets are the endsuction, the doublesuction and the inline. These can be seen at Figure 3.4.

The inline pump (Figure 3.1 left), is constructed to be mounted on a straight pipe and has a curved inlet section. The endsuction pump has a very short and straight inlet section which leads the fluid straight into the impeller eye. The inlet flanges are placed right under the impeller eye. The doublesuction pump splits the inlet in two and leads the fluid into two impeller eyes.

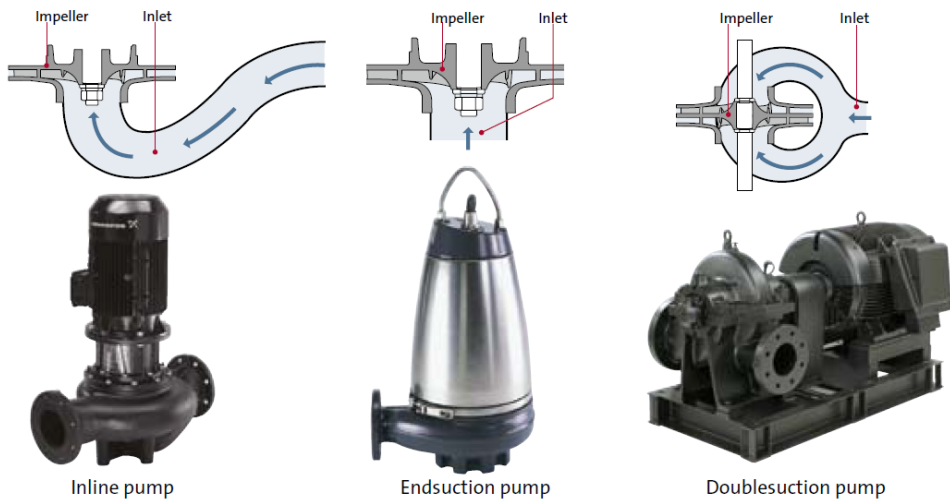


Figure 3.4: The three most common types of inlets; inline, endsuction and doublesuction. [Department of Structural and Fluid Mechanics, 2008,p. 14]

The design of the inlet depends mainly on the application of the pump. The design of the inlet is important, since a good designed inlet creates a symmetrical velocity profile into the impeller, which leads to the best performance. An example of a non-symmetrical velocity profile can be seen at Figure 3.5. For an endsuction pump, the velocity distribution will be more symmetrical, as there are no bends at the inlet.

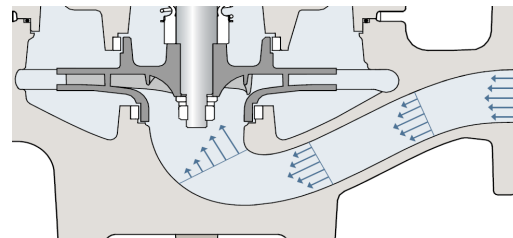


Figure 3.5: Velocity distribution at different cross-sections in an inline inlet. [Department of Structural and Fluid Mechanics, 2008,p. 15]

## Coupling

The pump consists of a rotating shaft driven by e.g. a motor and hydraulic components. The hydraulic components are in contact with the fluid. The coupling between the rotating shaft and the hydraulic parts of the pump causes some problems with the separation of the fluid from the mechanical and electrical components which drive the shaft. For a pump driven by an electrical motor there are two ways of coupling the motor and the hydraulic parts, the dry-runner pump and the canned rotor type pump.

The dry-runner pump has the advantage that it uses a standard motor. The disadvantage is the sealing between the motor and the impeller, which can cause friction losses and can be worn down over time. A dry-runner pump separates the fluid and the motor by either a shaft seal, a separation with a long shaft or a magnetic coupling.

The canned rotor type pump uses a different kind of motor, which has the rotor and the impeller physically separated from the motor stator. The fluid from the pump surrounds the rotor, thereby cooling the motor and lubricating the bearings. [Department of Structural and Fluid Mechanics, 2008,p. 18]

### Impeller seal

Between the rotating impeller and the stationary pump housing there is a gap. Due to the higher pressure on the outlet side of the gap, this gap will cause a leakage flow when the pump is operating. The leakage flow will run back through the gap and return to the impeller eye, which can be observed in Figure 3.6. This means that the impeller flow is higher than the pump flow, and thereby the pump requires more power to operate for the same output. Impeller seals can be mounted on the pump housing in order to minimize the leakage flow. The seals can be seen at Figure 3.1. The impeller seals lower the leakage flow but increase the friction. Losses related to leakage flow will be described in Section 4.2.2.

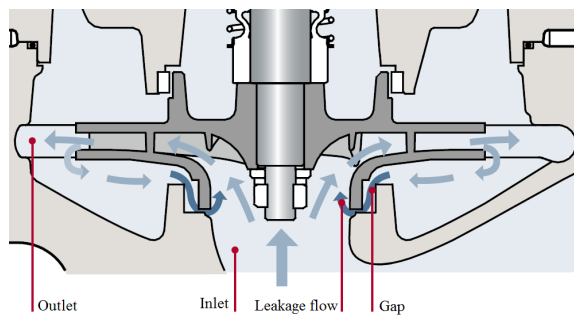


Figure 3.6: Leakage flow in a radial impeller. [Department of Structural and Fluid Mechanics, 2008,p. 18]

### Cavities

The design of the pump housing and the impeller gives the dimensions for the cavities. The cavities are both above and below the impeller, which can be seen at Figure 3.1. The cavities affect the flow around the impeller. Primary and secondary flows are created in the cavities when the impeller rotates. Primary flows are vortices rotating in the cavities along with the impeller. Secondary flows flow around the primary flows. The primary flows are considerably stronger than the secondary flows. The primary and secondary flows can be seen at Figure 3.7.

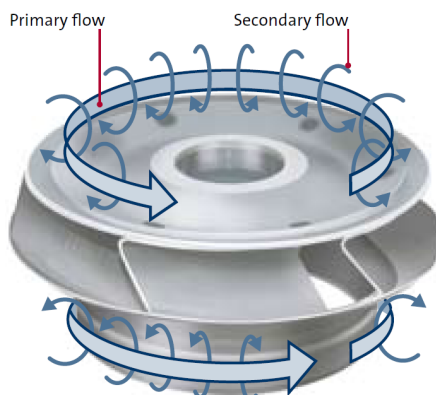


Figure 3.7: Primary and secondary flows in the cavities above the impeller. [Department of Structural and Fluid Mechanics, 2008,p. 19]

### Volute, diffuser and outlet flange

Figure 3.8 shows the components of the volute casing. The dynamic pressure rise in the impeller is converted to static pressure in the volute casing. From Figure 3.8 it can be seen that the fluid flows from the impeller into the ring diffuser, from there to the volute and out through the outlet diffuser to the outlet.

The ring diffuser guides the fluid into the volute from the impeller. The volute collects the fluid from the ring diffuser and leads it to the outlet diffuser. The cross-section area in the volute increases along the periphery from the tongue to the throat to have the same pressure along the volute. The position of the throat, the tongue and the outlet flange can be seen at Figure 3.8. The outlet diffuser increases the cross-sectional area from the throat to the outlet flange, thereby lowering the fluid velocity and dynamic pressure and increasing the static pressure. The throat is the beginning of the outlet diffuser and where the smallest cross-section area in the outlet diffuser is found.

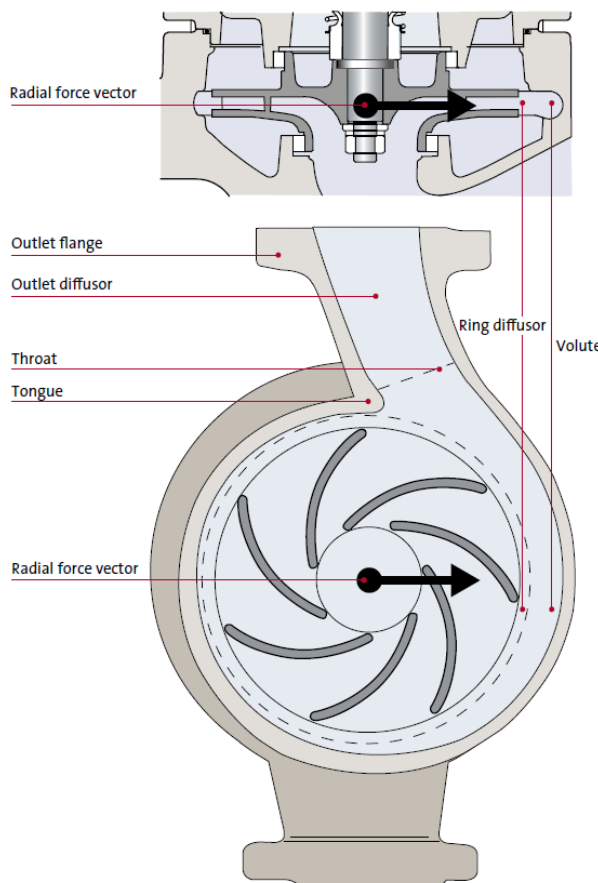


Figure 3.8: The components of the volute casing. [Department of Structural and Fluid Mechanics, 2008,p. 22]

The Grundfos NK32-125 is an endsuction dry-runner pump. As is an endsuction pump, it is assumed the velocity distribution at the inlet is symmetrical.



# Pump impeller theory 4

---

This chapter will cover the physical relations and formulas related to the pump impeller, including mechanical and hydraulic losses. In this chapter they will be presented as general formulas and theory only. Practical implementation will be covered in the model, presented in Section 4.3. Reflecting the general direction of the report, all theory will focus on the changes occurring in and around the pump impeller. The chapter will first deal with calculation of the theoretical performance, and then calculation of losses in the impeller. All the equations, if noting else is mentioned, are from [Gülich, 2008].

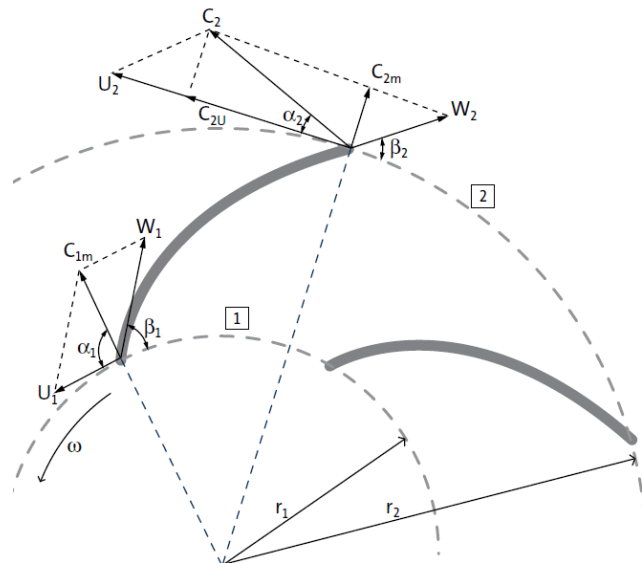
The purpose of the pump is to generate an increase in pressure at a given flow. The pressure increase is usually calculated as an increase in head. Neglecting losses, the head is found using Euler's pump equation, which calculates the increase in head over the impeller as a function of fluid velocities before and after the impeller. Throughout the report the subscripts 1 and 2 denotes inlet and outlet of the impeller.

$$H = \frac{u_2^2 - u_1^2}{2 \cdot g} + \frac{w_1^2 - w_2^2}{2 \cdot g} + \frac{c_2^2 - c_1^2}{2 \cdot g} \quad [m] \quad (4.1)$$

$u$  is the circumferential velocity of the impeller,  $w$  is the relative velocity of the flow, and  $c$  is the absolute velocity of the flow. Equation 4.1 consists of three parts, where the third is the dynamic head, and the first two make up the static head. The velocities can be seen in Figure 4.1 and will be further explained in the chapter. In the model, the theoretical head has been used, seen in Equation 4.2, which describes the head for ideal cases.

$$H_{th} = \frac{u_2 \cdot c_{2u} - u_1 \cdot c_{1u}}{g} \quad [m] \quad (4.2)$$

The flow through the pump is described by velocity triangles. These are vector representations of the speeds of the flow and the impeller blades, used to calculate properties of the pump, see Figure 4.1. The velocity triangles of the impeller are calculated from the geometry of the impeller, the speed of the impeller and the flow through the impeller. In addition to being used for calculating the impeller head, as in Equation 4.1, the sizes and shapes of the velocity triangles are used for calculating losses. This is described in Section 4.2.2.

**Legend**

- W**: Relative velocity
- C**: Absolute velocity
- U**: Circumferential Velocity
- C<sub>m</sub>**: Meridional component of absolute velocity
- C<sub>u</sub>**: Circumferential component of absolute velocity
- α**: Absolute flow angle
- β**: Relative flow angle

Figure 4.1: The velocity triangles of the impeller. The terms will be described in the following text. [Department of Structural and Fluid Mechanics, 2008,p. 61] Modified

When calculating velocities through the impeller, it is important to distinguish between absolute and relative velocities. The relative velocity is the velocity relative to the impeller, while the absolute velocity is the velocity relative to the pump casing. The absolute velocity is always equal to the sum of the relative velocity and the circumferential velocity of the impeller. The impeller moves in a circular motion around the pump shaft axis. The circumferential velocity of any point on the impeller can be calculated from Equation 4.3, where  $u$  is the circumferential velocity,  $r$  is the radius from the pump shaft center and  $n$  is the rotational speed of the pump in rpm.[Stepanoff, 1957]

$$u = \frac{2 \cdot r \cdot \pi \cdot n}{60} \left[ \frac{m}{s} \right] \quad (4.3)$$

The flow running through the impeller is described by two planes in order to take all three dimensions into account. The vane height is included in the meridional place, turning a three dimensional flow into a two dimensional vector (See Equation 4.6). Section 4.1 will describe first the inlet- and then the outlet-triangle, as well as the relevant equations and flow parameters. [Gülich, 2008]

## 4.1 Velocity triangles for a radial impeller

### 4.1.1 Inlet triangle

The inlet velocity triangle can be drawn as seen in Figure 4.2 and 4.3.

The meridional velocity before the impeller blade,  $c_{1m}$ , is calculated by the cross-section area,  $A_1$ , and the flow running into the impeller,  $Q_{La}$ .  $Q_{La}$  is the sum of the useful flow running through the pipe,  $Q$ , the leakage flow from the impeller seals,  $Q_{leakage}$ , and the balance flow,  $Q_{balance}$ , which is deliberately being led back through the balance holes to

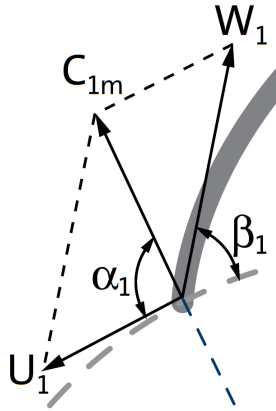


Figure 4.2: The velocity triangle at the impeller inlet. [Department of Structural and Fluid Mechanics, 2008,p. 61] Modified

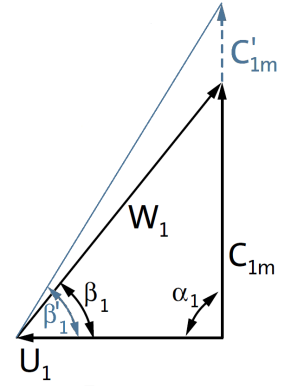


Figure 4.3: Inlet triangle, with blockage, as used in calculations. [Department of Structural and Fluid Mechanics, 2008,p. 61] Modified

ensure the stability of the impeller (See Equation 4.4). Balance flow deals with the axial thrust and occurs at design wish. The cross-section area of the impeller inlet is calculated from the inner radius of the impeller,  $r_1$ , and the inlet blade height,  $b_1$ . [Gülich, 2008]

$$Q_{La} = Q + Q_{leakage} + Q_{balance} \left[ \frac{m^3}{s} \right] \quad (4.4)$$

$$A_1 = 2 \cdot r_1 \cdot \pi \cdot b_1 \left[ m^2 \right] \quad (4.5)$$

$$c_{1m} = \frac{Q_{La}}{A_1} \left[ \frac{m}{s} \right] \quad (4.6)$$

The impeller vanes are separated by the impeller blades. Since these take up some physical space, the vane inlet area is that much smaller. Since the flow does not change, and the area becomes smaller, the velocity of the fluid increases. Therefore, immediately after the leading edge of the impeller, the meridional velocity will have increased to  $c'_{1m}$  due to the blade blockage,  $\tau_1$ . Blockage is dependent on the geometry of the impeller, see Equation 4.7 and 4.8. The effect of blockage on the inlet velocity triangle is illustrated in Figure 4.3. A "''" is used to denote that the blockage has been taken into account.

$$c'_{1m} = c_{1m} \cdot \tau_1 \left[ \frac{m}{s} \right] \quad (4.7)$$

$$\tau_1 = \left( 1 - \frac{z_{La} \cdot e_1}{\pi \cdot d_1 \cdot \sin \beta_{1B} \cdot \sin \lambda_{La}} \right)^{-1} [-] \quad (4.8)$$

$z_{La}$  is the number of impeller blades,  $e_1$  is the blade thickness at the inlet,  $\beta_{1B}$  is the blade angle and  $\lambda_{La}$  is the angle between vanes and side discs. Description of  $\lambda$  can be seen in Figure 4.4.

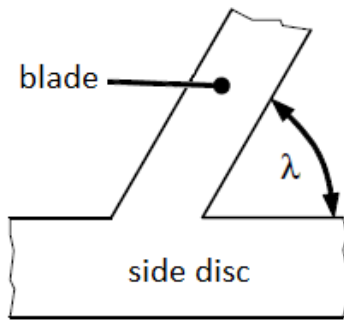


Figure 4.4: The angle between the blades and side disc,  $\lambda$ . [Gülich, 2008,p. XXXI] Modified

The circumferential velocities remain unaffected by blockage. Additionally, the flow to the impeller is largely axial, meaning that the absolute flow angle  $\alpha_1 = 90^\circ$ . Hence the circumferential component of the absolute inlet flow,  $c_{1u}$ , is zero. This can be seen in Equation 4.9. If, due to pre-inlet swirl, the angle is not 90 degrees,  $c_{1u}$  is calculated from the flow angle and the meridional velocity.

$$c_{1u} = \frac{c_{1m}}{\tan(\alpha_1)} \left[ \frac{m}{s} \right] \quad (4.9)$$

The flow angle,  $\beta_1$  is affected by the blade blockage. The blade angle is a function of the meridional velocity and the circumferential velocities of the pump and the streamline. The angle between the blade angle and the flow angle including blockage is called the incidence angle, and is denoted  $i'$ . In praxis the incidence angle is often the factor chosen and the blade angle is calculated based on this.

$$\beta'_1 = \arctan \left( \frac{c_{1m} \cdot \tau_1}{u_1 - c_{1u}} \right) [^\circ] \quad (4.10)$$

$$i' = \beta_{1B} - \beta'_1 [^\circ] \quad (4.11)$$

The incidence angle can be seen in Figure 4.5.

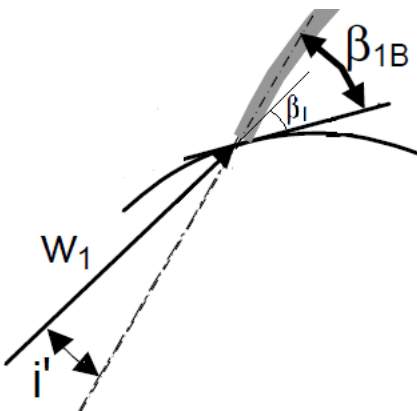


Figure 4.5: The incidence, blade and relative flow angles and the relative velocity at the impeller inlet. [Department of Structural and Fluid Mechanics, 2008,p. ] Modified

The remaining parameters, total relative and absolute velocity,  $c_1$  and  $w_1$ , are simply calculated from basic Pythagoras once  $c_{1m}$ ,  $c_{1u}$  and the tangential velocity  $u_1$  have been determined.

#### 4.1.2 Outlet triangle

The outlet velocity triangle is calculated using the same methods as with the inlet. The outlet velocity triangle can be seen on Figures 4.6a and 4.6b. The flow through the outlet is, due to conservation of mass and incompressibility, the same as the flow through the inlet. The meridional velocity,  $c_{2m}$ , is calculated similarly to the inlet, based on Equation 4.6. Blade blockage is again taken into account via Equations 4.7 and 4.8.

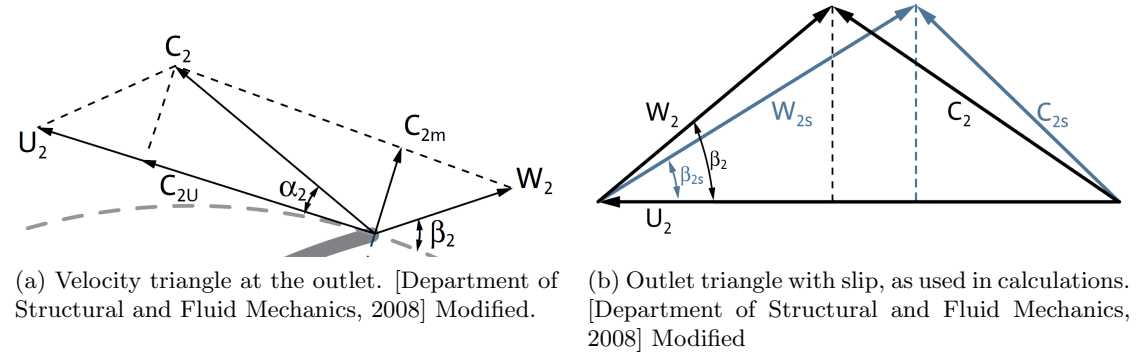


Figure 4.6: Outlet velocity triangle.

However, in the outlet triangle a value of the absolute flow angle,  $\alpha_2$ , cannot be accurately assumed as in the inlet. This means that the circumferential component of the absolute velocity,  $c_{2u}$ , cannot be calculated from Equation 4.9. Instead, Equation 4.12 is employed [Gülich, 2008].

$$c_{2u} = u_2 \cdot \left( \gamma - \frac{c_{2m}}{u_2 \cdot \tan(\beta_{2B})} \right) \left[ \frac{m}{s} \right] \quad (4.12)$$

$\gamma$  is the slip factor, described later in Section 4.1.4 and found in Equation 4.21. The angle between the blade angle,  $\beta_{2B}$ , and the flow angle including blockage,  $\beta'_2$ , is here called the deviation angle, and is denoted  $\delta'$ . Since  $c_{2u}$  is no longer zero, it must be considered when calculating  $w_2$ .  $c_2$  is again found from Pythagoras, and finally the outlet absolute flow angle  $\alpha_2$  can be found from Equation 4.14.

$$\delta' = \beta_{2B} - \beta'_2 \quad [^\circ] \quad (4.13)$$

$$\alpha_2 = \arctan \left( \frac{c_{2m}}{c_{2u}} \right) \quad [^\circ] \quad (4.14)$$

The deviation angle is shown in Figure 4.7.

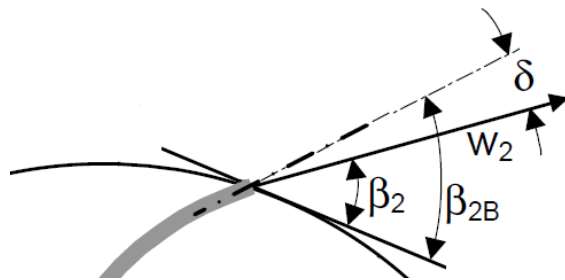


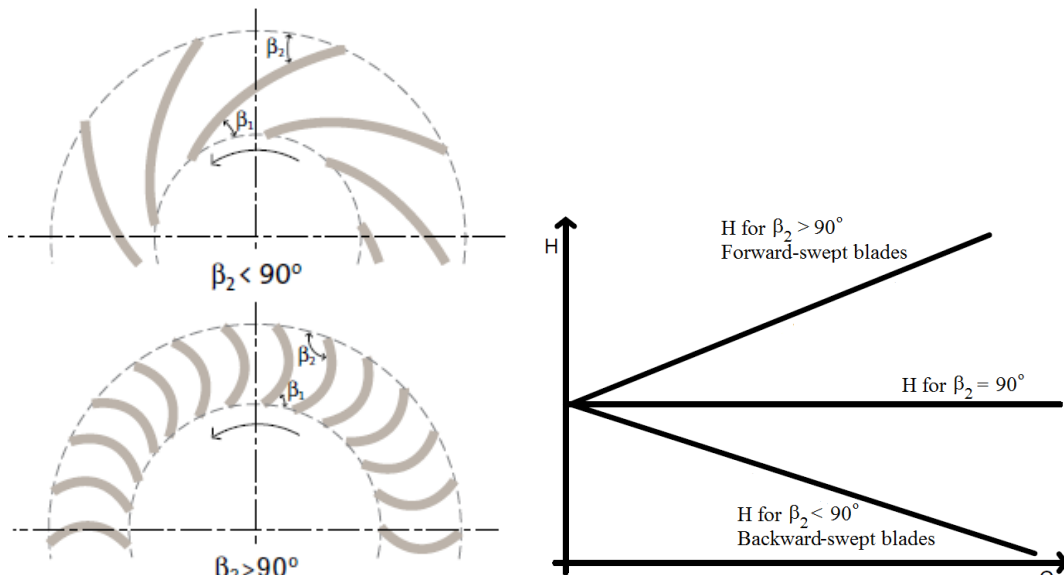
Figure 4.7: The deviation-, blade- and relative flow angles and the relative velocity at the impeller outlet.[Department of Structural and Fluid Mechanics, 2008,p. 61] Modified

#### 4.1.3 Outlet angle impact on the head

From the Equations 4.2, 4.5, 4.6 and 4.16 with the following assumptions; no inlet rotation ( $c_{1u} = 0$ ) and the system is ideal ( $\gamma = 1$ ), Equation 4.15 can be derived. Equation 4.15 shows that the head varies linearly with the flow and the slope depends on the relative outlet flow angle,  $\beta_2$  [Department of Structural and Fluid Mechanics, 2008,p. 66].

$$H = \frac{u_2^2}{g} - \frac{u_2}{\pi \cdot 2 \cdot r_2 \cdot b_2 \cdot g \cdot \tan(\beta_2)} \cdot Q \quad [m] \quad (4.15)$$

This can be seen in Figure 4.8b where the head varies as a function of the flow and the relative outlet flow angle.



(a) Impeller blades with backwards swept ( $\beta_2 < 90^\circ$ ) and forward swept ( $\beta_2 > 90^\circ$ ) blades. [Department of Structural and Fluid Mechanics, 2008]

(b) The head varies as a function of the flow and the relative outlet angle. Based on [Department of Structural and Fluid Mechanics, 2008]

Figure 4.8: The effect of varying relative outlet angle on the head gain.

Figure 4.8b is based on an ideal system, a real pump curve will look a bit different since losses, slip and inlet rotation will have an influence on the head and will vary with the flow.

#### 4.1.4 Slip

Velocity triangles and calculations based solely on geometry largely ignore the complicated flow conditions in the interior of the impeller. However, the interior is crucial in making sure the velocities in the fluid come out as described in the outlet triangle.

If a blade is to generate force, there must be a pressure difference between the pressure and suction surfaces of the blade. Since the pressure distributions on a blade is entirely dependent on the velocity distributions around the blade, the flow must be different on the pressure and suction side of the blade. This means that the flow does not follow the blade shape exactly. Consequently, a difference between the flow and blade angle is necessary for transfer of work in the impeller. As mentioned, this angle is called the deviation angle. Slip is the degree to which the flow follows the blade.

The slip factor can be calculated from Equation 4.16, defining the blade-congruent flow with  $\infty$  the following applies:

$$c_{2u\infty} - c_{2u} = (1 - \gamma)u_2 \left[ \frac{m}{s} \right] \quad (4.16)$$

where  $\gamma$  is the slip factor, and  $(1 - \gamma)$  is referred to as the slip. If  $\gamma=1$  then the flow is blade-congruent. A small  $\gamma$  means a large deviation angle between actual blades and flow. With Equation 4.16 and 4.17 an expression for the slip factor can be found, see Equation 4.18.

$$\tan(\beta_{2B}) = \frac{c'_{2m}}{u_2 - c_{2u\infty}} \quad [-] \quad (4.17)$$

$$\gamma = \frac{c_{2u}}{u_2} + \frac{c_{2m} \cdot \tau_2}{u_2 \cdot \tan(\beta_{2B})} \quad [-] \quad (4.18)$$

Without an actual pump test,  $c_{2u}$  will be unknown. This means that the slip factor,  $\gamma$ , cannot be calculated from Equation 4.18.

An alternative method for predicting the slip factor can be seen in the following equations. The slip factor is predicted from number of blades, the blade angle at the outlet, and two constants,  $k_w$ , and  $f_1$ . For a radial centrifugal pump  $f_1$  has a fixed value of 0,98.  $k_w$  is calculated from  $\epsilon_{Lim}$ , which is based on the number of blades and the blade angle at the outlet. If  $\epsilon_{Lim}$  exceeds  $d_{1m}^*$ ,  $k_w$  is set to a value of 1.

$$\epsilon_{Lim} = \exp\left(-\frac{8,16 \cdot \sin\beta_{2B}}{z_{La}}\right) [-] \quad (4.19)$$

$$k_w = 1 - \left(\frac{d_{1m}^* - \epsilon_{Lim}}{1 - \epsilon_{Lim}}\right)^3 [-] \quad (4.20)$$

$$\gamma = f_1 \cdot \left(1 - \frac{\sqrt{\sin\beta_{2B}}}{z_{La}^{0.7}}\right) \cdot k_w [-] \quad (4.21)$$

The dimensionless  $d_{1m}^*$  is  $\frac{d_{1m}}{d_2}$ . In the model,  $d_{1m} = d_1$ . The slip factor influences the outlet velocity triangles as described in Equation 4.12. It should be noted that the influence happens gradually from the inlet to the outlet.

The slip is generally not considered a loss, since it is necessary for the transfer of energy to the fluid. The losses in the pump are covered in Section 4.2.

## 4.2 Overview of losses

Euler's equation and the velocity triangles give a simple and loss free description of the impeller performance. In reality there are hydraulic and mechanical losses in the pump. These causes the pump performance to be lower than predicted by the equations. Table 4.1 shows different losses in the pump. First the mechanical losses will be described and then the hydraulic losses.

	<b>Loss</b>	<b>Larger flow (<math>Q_{La}</math>)</b>	<b>Lower head (<math>H</math>)</b>	<b>Higher power consumption (<math>P</math>)</b>
Mechanical losses	Bearing			X
	Shaft seal			X
Hydraulic losses	Flow friction		X	
	Mixing		X	
	Shock		X	
	Disc friction			X
	Leakage	X		

Table 4.1: The table shows how different types of impeller related losses affects the flow, head and power consumption. Table based on [Department of Structural and Fluid Mechanics, 2008,p. 78]

Due to the model being restricted to the impeller, only losses related to the impeller have been included. In addition to hydraulic losses in Table 4.1, recirculation losses occur at low flows. These have also not been included, due to being insignificant at relevant levels of flow.

The hydraulic losses cause the actual head to be lower than the theoretical head, as can be seen at Figure 4.9. The disc friction- and the leakage losses are not shown on the Figure 4.9 as they do not directly change the head.

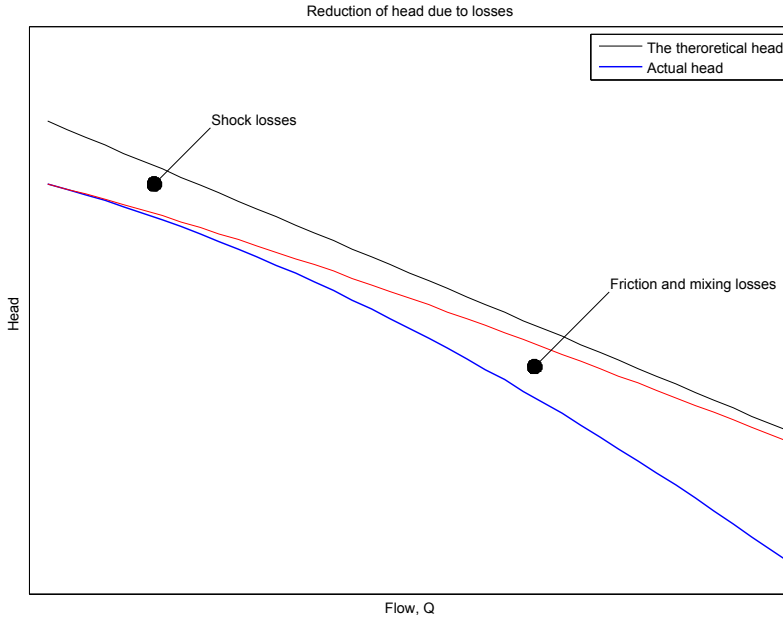


Figure 4.9: Hydraulic losses cause the theoretical head to be reduced. The losses which cause a lower flow and a higher power consumption are not represented.

The shock loss decreases as the flow increases, this is due to the fact that the velocity of the impeller and the flow velocity in the impeller throat becomes similar in value as the flow increases. The friction and mixing losses get higher as the flow increases due to the higher velocities. Leakage causes the shock, friction and mixing losses to be higher due to the fact that it creates a higher flow in the impeller, which will be explained further in Section 4.2.2 under Leakage.

#### 4.2.1 Mechanical losses

Mechanical losses due to mechanical friction losses in the pump coupling, which, depending on the pump type, consist of bearings, shaft seals and gears. Here the combined bearing loss and shaft seal loss will be described.

The friction losses caused by the bearing and the shaft seal can vary in size dependent on the pressure and the rotational speed. However, the variations due to these are so small that it is often modeled to be constant at a given rotational speed, see Equation 4.22.

$$P_{loss,mechanical} = P_{loss,bearing} + P_{loss,shaft seal} = \text{constant} [W] \quad (4.22)$$

The mechanical losses are estimated from the flow and the rotational speed, relative to references values,  $Q_{Ref}$  and  $n_{Ref}$  respectively. The mechanical loss depends on the power consumption in the best efficiency point,  $P_{Opt}$ . These relations and additional constants and exponents can be seen in Equation 4.23.

$$\frac{P}{P_{Opt}} = 0,0045 \cdot \left( \frac{Q_{Ref}}{Q} \right)^{0,4} \cdot \left( \frac{n_{Ref}}{n} \right)^{0,3} [W] \quad (4.23)$$

$n_{Ref}$  and  $Q_{Ref}$  are 1500 rpm and  $1 \frac{m^3}{h}$  respectively.  $P_{Opt}$  is the power consumption in the operation point of maximum efficiency. [Gülich, 2008,p. 135]

The mechanical losses is only a loss in the power consumption, not in head.

The MATLAB program *mech\_loss.m* models the different mechanical losses throughout the system.

#### 4.2.2 Hydraulic losses

There are several hydraulic losses in a centrifugal pump as seen at Table 4.1. Hydraulic losses occurs because of friction or due to the change in direction and velocity of the fluid through the pump.

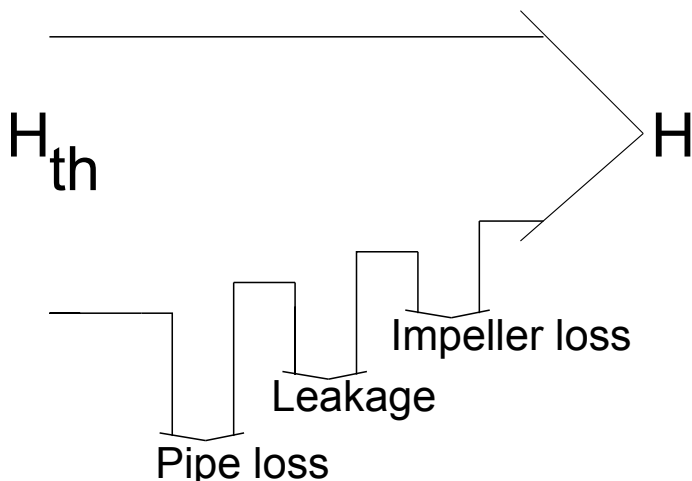


Figure 4.10: The hydraulic head losses. The arrow starts at the theoretical head and then comes to the actual head when the losses have been taking into account. The impeller losses includes the friction, mixing and shock losses.

The pipe loss gives a head loss outside the pump. Leakage, friction, mixing, shock and disc friction losses occurs in the impeller. The losses on Figure 4.10 are the losses used in the model with the exception of the pipe loss due to the fact that it occurs outside the pump.

#### Friction loss in pipes

Friction loss in pipes is the loss of energy in the fluid as it flows through the pipes. At the wall in a pipe the fluid velocity is zero and the maximum velocity of the fluid is found in the center of the pipe. The molecules in the fluid rub against each other due to the velocity differences across the pipe. This friction causes some of the kinetic energy to

transform to heat energy, which is considered a loss. The loss in the pipe depends on the Darcy friction factor, the length of the pipe, the fluid velocity and the hydraulic diameter of the pipe. The Darcy friction factor,  $f$  is the inner surface roughness. Equation 4.24 shows the equation for the loss in pipes.

$$H_{loss,pipe} = f \cdot \frac{L \cdot V^2}{D_h \cdot 2g} [m] \quad (4.24)$$

The hydraulic diameter is the ratio of the cross-sectional area to the wetted circumference, see Equation 4.25.

$$D_h = \frac{4 \cdot A}{O} [m] \quad (4.25)$$

When the pipe is a circular pipe, the hydraulic diameter is equal to the pipe diameter. The circular pipe has the smallest interior surface compared to other cross-section area, which gives it the smallest flow resistance.

The Darcy friction coefficient depends on the Reynolds number. The Reynolds number is a dimensionless number which expresses how turbulent the flow is.

$$Re = \frac{V \cdot D_h}{\nu} [-] \quad (4.26)$$

Table 4.2 shows which fluid flow corresponds to which Reynolds number. Laminar flow occurs at relatively low velocities. The motion of the particles of the fluid in a laminar flow is well-ordered with the particles moving in straight lines parallel to the pipe walls. The turbulent flow occurs at higher velocities where eddies leads to lateral mixing. The transition flow is a mix of the laminar and turbulent flow.

$Re < 2300$	Laminar flow
$2300 < Re < 5000$	Transitional flow
$Re > 5000$	Turbulent flow

Table 4.2: The fluid flow in a pipe described by the Reynolds number.

The Darcy friction coefficient for laminar flow for pipes with a circular cross-section can be seen in Equation 4.27. The coefficient is only dependent on the Reynolds number for laminar flows.

$$f_{laminar} = \frac{64}{Re} [-] \quad (4.27)$$

The Darcy friction coefficient for turbulent flow depends on the Reynolds number and the pipe roughness (known as the relative roughness),  $\epsilon = \frac{k}{D_h}$ . The friction increases in old pipes due to corrosion and sediments. A Moody chart is a non-dimensional graph that shows the Darcy friction factor as a function of the Reynolds number and the surface roughness,  $\epsilon$ , for laminar and turbulent flows. A Moody chart can be seen at Figure 4.11.

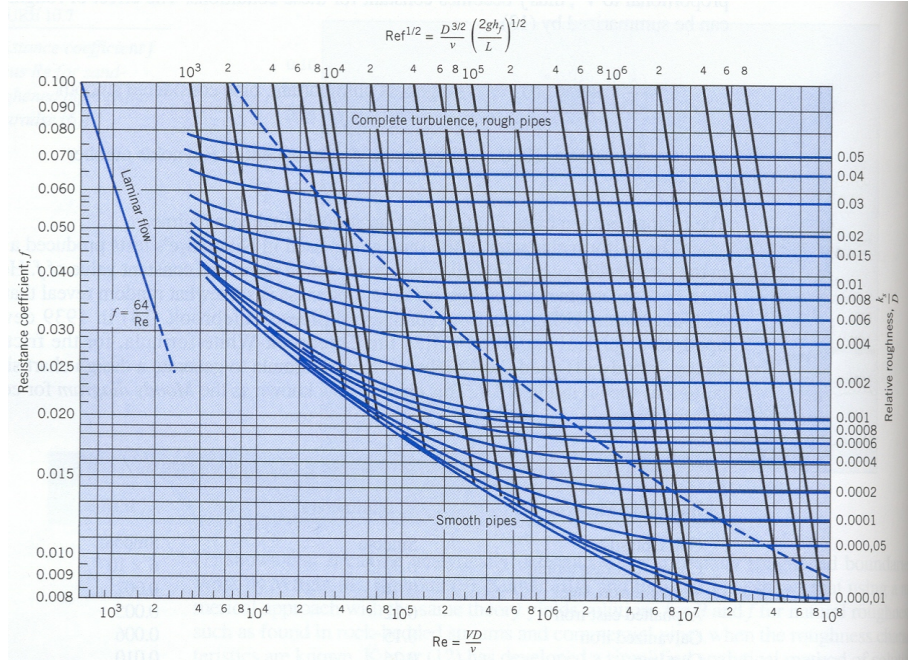


Figure 4.11: Moody chart which shows the Darcy friction factor as a function of the Reynolds number and the relative roughness,  $\epsilon$ . [University of Texas in Austin, 2012]

## Leakage

Leakage loss occurs because of circulation through gaps between the fixed and the rotating parts of the pump. Leakage increases the flow in the impeller compared to the flow through the pump which results in a loss of efficiency. The leakage flow and the useful flow running through the pump is part of the entire pump flow, see Equation 4.4 in Section 4.1.1. It is assumed that the leakage flow runs radially inwards due to the pressure difference in the pump and that the only leakage occurs between the impeller and the pump casing. The leakage loss is dependent on the axial velocity of the fluid in the gap,  $c_{ax}$ , the distance from the impeller eye to the seal,  $d_{sp}$ , and the diameter of the seal,  $s$ . The leakage flow is shown in Equation 4.28.

$$Q_{sp} = \pi \cdot d_{sp} \cdot s \cdot c_{ax} \left[ \frac{m^3}{s} \right] \quad (4.28)$$

where

$$c_{ax} \propto H_p \quad (4.29)$$

$$H_p = \frac{u_2^2 - u_1^2}{2 \cdot g} + \frac{w_1^2 - w_2^2}{2 \cdot g} - Z_{La} [m] \quad (4.30)$$

The axial velocity in the gap depends on the Reynolds number and the pressure difference across the seal which is based on the static pressure rise created by the impeller in Equation 4.30. Appendix C.2 elaborates on Equations 4.28 and 4.29.

Leakage loss in the impeller have been modeled in the MATLAB program *leakage\_losses.m*.

### Friction, mixing and shock losses

Flow friction is due to the contact between the fluid and the surface of the rotating impeller and the pump casing. The magnitude of the friction loss depends on the fluid velocity relative to the surface and the roughness of the surface. The flow friction reduces the head because of a pressure loss. The deceleration of flow causes the flow to run less uniformly. This causes an increase in the momentum exchange between streamlines, causing small-scale turbulence. Head losses due to deceleration and turbulence are termed mixing losses. All the equations for finding the friction and mixing losses can be found in Appendix C.1. The loss in head due to friction and mixing losses in the impeller can be seen in Equation 4.31, where  $\zeta_{La,R}$  is the loss coefficient.

$$Z_{La,R} = \frac{\zeta_{La,R} \cdot u_2^2}{2g} [m] \quad (4.31)$$

The shock losses occurs when a sudden deceleration of the flow happens at the impeller inlet. This gives a non-uniform flow distribution in the channel. The equations for the shock loss can be found in Appendix C.1. The shock loss is seen in Equation 4.32.

$$Z_{La,C} = \frac{\zeta_{La,C} \cdot u_2^2}{2g} [m] \quad (4.32)$$

The total hydraulic loss in the impeller is found in Equation 4.33.

$$Z_{La} = Z_{La,R} + Z_{La,C} [m] \quad (4.33)$$

The MATLAB program *impeller-loss.m* models the friction, mixing and shock losses in the impeller.

### Disc friction

Disc friction is increased power consumption due to the impeller rotation in a fluid filled pump casing. The fluid in the cavities begins to rotate and creates primary and secondary vortices (see Section 3.1.1 under cavities). The disc friction is caused by the energy transfer from the impeller surface to the surface of the pump casing. As can be seen in Equation 4.34, the disc friction power,  $P_{loss,disk}$ , is dependent on the density,  $\rho$ , the circumferential velocity,  $u_2$ , the outlet diameter,  $d_2$ , the axial distance to the wall at the periphery,  $E$ , and  $k$ , an empirical value found from Equation 4.35. Here  $\nu$  is the kinematic viscosity of the fluid and  $m$  is an exponent varying from  $\frac{1}{6}$  to  $\frac{1}{9}$  depending on the roughness of the surface [Department of Structural and Fluid Mechanics, 2008,p. 92].

$$P_{loss,disk} = k \cdot \rho \cdot u_2^3 \cdot d_2 (d_2 + 5E) [W] \quad (4.34)$$

$$k = 7,3 \cdot 10^{-4} \cdot \left( \frac{2 \cdot \nu \cdot 10^6}{u_2 \cdot d_2} \right)^m [-] \quad (4.35)$$

The program *Disc\_Friction\_losses.m* models the disc friction caused by the impeller.

### 4.3 Overview of impeller model

To utilize the theory presented in sections 4.1.1 through 4.2.2, an overall model have been set up, including both ideal calculations of head gain and loss calculations. A flowchart of this is seen in Figure 4.12.

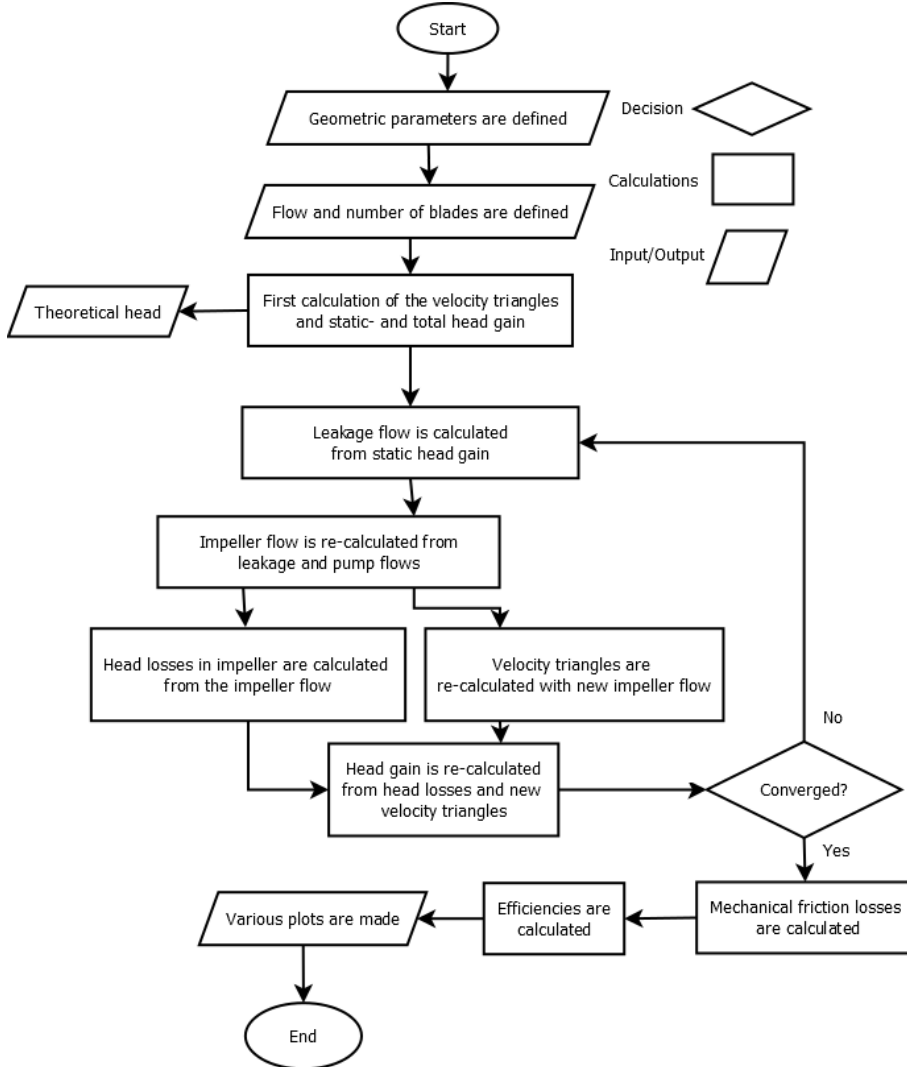


Figure 4.12: Flowchart of the model for each point of flow rate and blade number.

The model functions as follows:

- The inputs to the model are the pump flow,  $Q$ , and the geometry of the pump and impeller. Based on these inputs, the model calculates an initial head gain with no leakage and no head losses,  $H_{th}$  and a static head gain,  $H_p$ . Initial values of velocities and angles are calculated as well.
- Using the static head increase, a leakage flow,  $Q_{sp}$ , is calculated and added to the pump flow, yielding the impeller flow,  $Q_{La}$ .
- Using the impeller flow, the velocity triangles are re-calculated. Simultaneously the head loss in the impeller,  $Z_{La}$ , is calculated. Subtracting this from the theoretical head, the net head gain is found.

- This procedure is repeated until the result converges, after which the disc friction and mechanical losses are calculated.
- The model calculates the efficiencies and several plots are made.

In Appendix B the model is documented and explained. All subprograms mentioned throughout the chapter, describing losses and the main MATLAB programs are contained in Appendix A.2.

The model has the following limitations:

- The blades, however sloped, may not be curved along the height of the blade.
- In the model, only impeller losses are accounted for. Other losses in the hydraulic system is not represented.

*Through the first part of the report, equations used in the model have been presented along with a presentation of the pump used, the Grundfos NK 32-125 with a 142 mm impeller. In Part II of the report, the verification of the model will be presented. The model is in Part II compared to the data sheet of the Grundfos pump and experimental pump data.*



# **Part III**

## **Model verification**



# Verification of the model by product data sheet

5

This chapter contains model results, performance curves from the data sheet of the pump, a comparison between the two and a comparison with impeller theory in Chapter 4. The purpose of this chapter is to evaluate the usability of the model. The pump investigated is the Grundfos NK 32-125, with the 142 mm diameter impeller used as reference. The model can be found in Appendix A.2 and the data sheet for the pump in Appendix A.3.

## 5.1 Reference pump data

The Grundfos pump used in the experiments is a NK 32-125, which is a dry runner, endsuction pump. This is a series with varying size impellers (same number of blades), from a outer diameter of 115 to 142 mm (the 142 mm being NK 32-125/142). Figure 5.1 and Figure 5.2 show the difference in head and efficiency for the different size impellers.

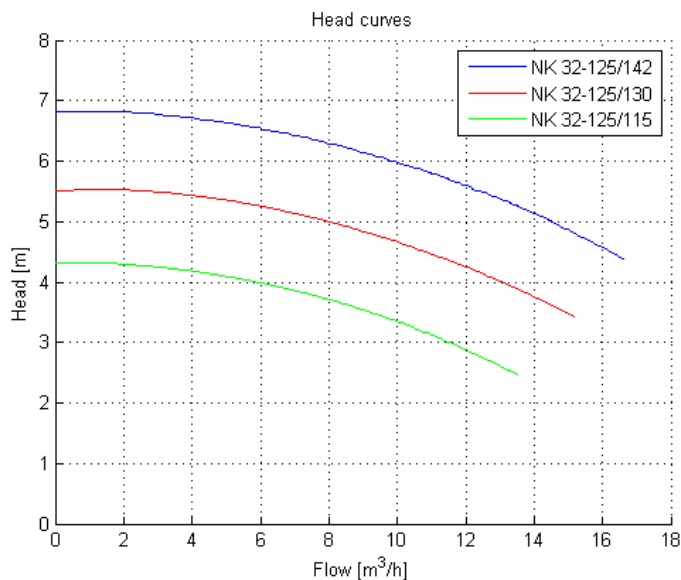


Figure 5.1: Head curve for the three impellers with the outer diameters of 115, 130 and 142 mm. Based on Appendix A.3

Figure 5.1 shows that the smaller impellers yield lower head. The efficiency peak point is generally at a lower flow for the smaller impellers (Figure 5.2). Performance curves can be found in Appendix A.3.

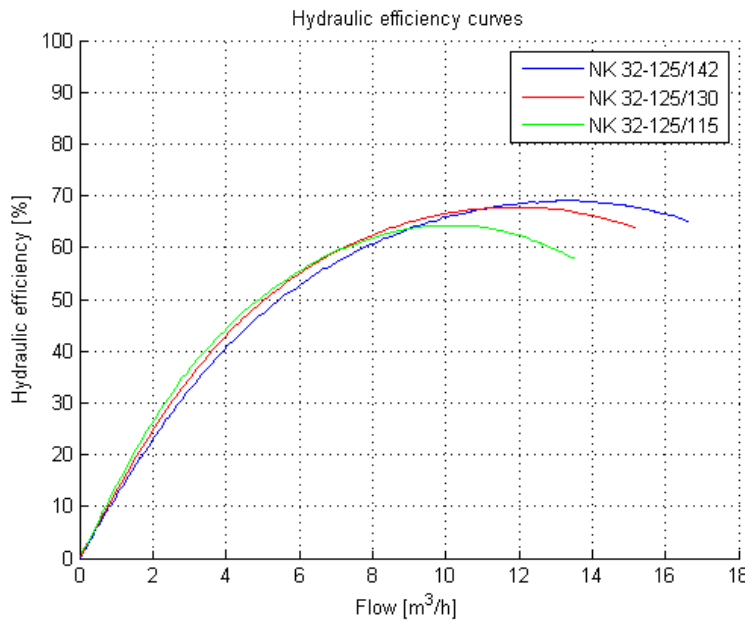


Figure 5.2: Hydraulic efficiency curve for the three impellers with the outer diameters of 115, 130 and 142 mm. Based on Appendix A.3

The smaller impeller diameters are based on the 142 mm impeller, ground to smaller size. Further in the report the 142 mm impeller is used, as the pump was designed for this.

The NK 32-125/142 has 5 blades, a rated speed at 1340 rpm, a rated flow of 12,6  $\frac{m^3}{h}$  and a rated head of 5 m. Using Equation 3.2 the NK 32-125/142 specific speed ( $n_q$ ) is  $\approx 28$ , making it a radial pump (See Table 3.1). This is the impeller which was used for developing the model, and the basis for the impeller development in Chapter 6.

The NK 32-125/142 data sheet (see Appendix A.3) is used to evaluate the model. Figure 5.3 shows the performance curves of the NK 32-125/142. A performance chart shows the performance characteristic of a pump e.g. the head or efficiency against flow rate at a constant speed [Thin et al., 2008].

It should be noted, that the NK 32-125 has curved channels with twisted blades ( $\lambda$  varying along blade height), and that the model has blades which stand perpendicular to the side discs ( $\lambda = 90^\circ$ ). See Figure 4.4 for clarification of  $\lambda$ . Thusly, the results of the model can be expected to vary somewhat from those found in the data sheet. The model does not, as mentioned in Section 4.2, take recirculation losses in the impeller into account. Since losses outside the impeller in general have been omitted, the model can be expected to have an artificially higher efficiency and head curve.

*It has been noticed that the pump curve from the data sheet has a varying rotational speed and is not fixed at 1340 rpm. Due to simplification the data sheet is assumed to be at a fixed speed at 1340 rpm.*

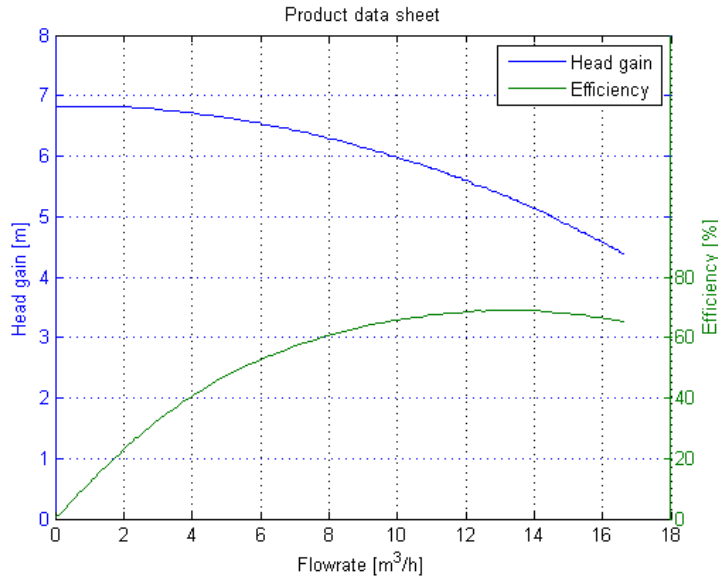


Figure 5.3: Head and efficiency curves from the data sheet of the NK 32-125/142. Based on Appendix A.3

## 5.2 Comparison between model and reference impeller.

The model is based on the theory from Chapter 4. A flowchart describing the model can be found in Section 4.3. Section 4.3 explains how the model is structured, and Appendix B describes the equations used and which assumptions are made.

To evaluate if the model fits, the geometric parameters from the CAD drawing provided by Grundfos (see Appendix A.1 for CAD drawing and Appendix B.B.1 for the list of the parameters) are used as inputs for the model. The provided CAD drawings show the impeller and the pump housing without an annular seal. The performance charts from the model and the ones provided by Grundfos are compared in Figure 5.4 and 5.5.

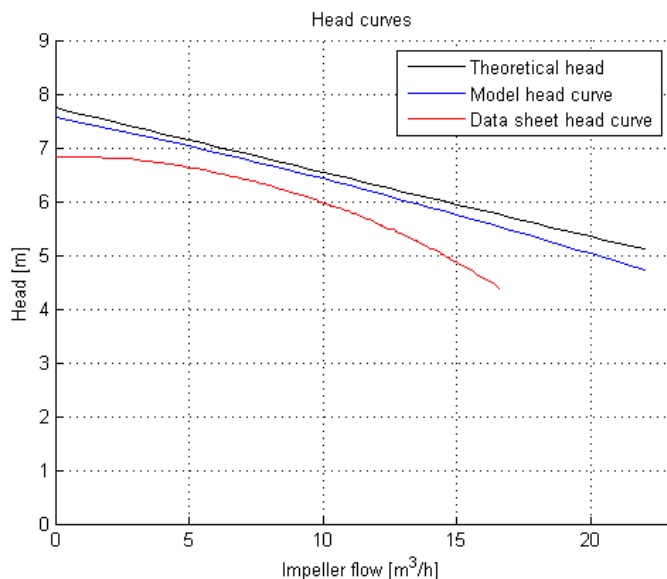


Figure 5.4: Head gain as a function of flow from both model and data sheet. Theoretical head as a function of flow from the model. Based on Appendix A.3

Figure 5.4 shows the theoretical head and the actual head gain from the model and compares them to the head gain from the data sheet. The theoretical head is the highest and the actual head from the model gain is a bit lower. The losses in the impeller increases when the flow increases. The head gain from the model is more linear than the data sheet curves. The difference between the head curve from the data sheet and the one from the model indicates that the model is missing one or more losses. Figure 5.5 is the efficiency curve for the model and the data sheet respectively.

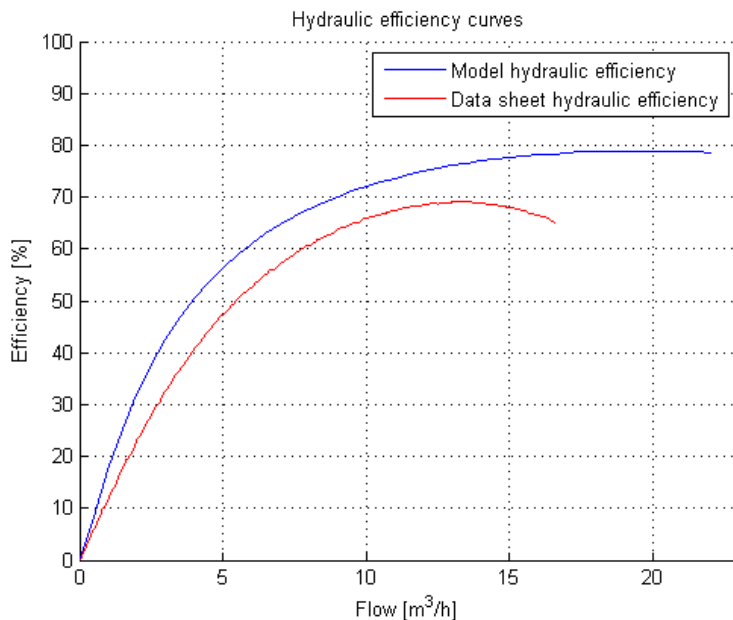


Figure 5.5: Efficiency as a function of flow from both model and data sheet. Based on Appendix A.3

Two significant differences between the efficiency curves on Figure 5.5 are:

- The model has higher efficiency than the data sheet.
- The model efficiency rises faster and levels out significantly more, compared to the data sheet.
- The top efficiency point occurs at a higher flow in the model than in the data sheet.

The missing head loss causes the model efficiency to be higher than the data sheet curve. A loss which increases with the flow would cause the efficiency to decrease similarly and thus approach the efficiency of the data sheet.

*From comparison between the made model and the data sheet, it is concluded that the model is not sufficiently accurate to be used as basis for a test, since significant losses have been omitted. Due to this, additional losses will be added to the model prior to the pump test, see Section 5.4*

## 5.3 Evaluation of model

### 5.3.1 Number of blades influence on the head

The model is set up to test some basic claims in the known impeller theory, namely in [Department of Structural and Fluid Mechanics, 2008]. The tendencies of these should be unaffected by the omission of losses in other parts of the pump. By matching the model results to the overall theory, the correspondence of the two theoretical sources, which the model is based on, [Department of Structural and Fluid Mechanics, 2008] and [Gülich, 2008] is checked. In order to compare the model to the theory, the pump hydraulic efficiency with varying number of blades in the impeller is plotted. A contour plot can be seen in Figure 5.6. Theory states that an impeller in a centrifugal pump should generally have from 5 to 10 blades to get the highest efficiency [Department of Structural and Fluid Mechanics, 2008,p. 16].

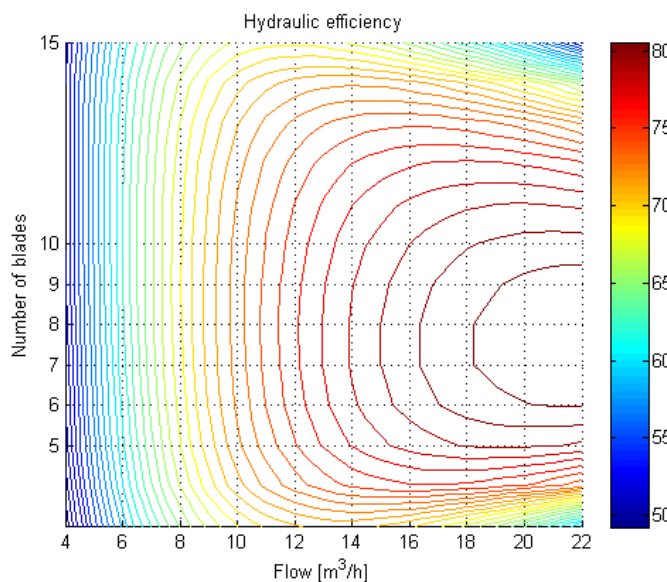


Figure 5.6: The efficiency of the pump, according the model, plotted as a function of flow and number of impeller blades. Note that the scale starts from 49% and not from 0%.

As can be seen in Figure 5.6 the efficiency, regardless of flow, is at its highest when the number of blades are in the region of 6-9. E.g. the maximum hydraulic efficiency for a pump with an impeller with 8 blades running at a flow at  $21 \frac{m^3}{h}$  lies at 81%. This supports the theory according to [Department of Structural and Fluid Mechanics, 2008,p. 16].

The influence of the number of blades on the efficiency is examined in further detail. This examination is based on the plot seen in Figure 5.6. For further examination the interval of 5 to 10 blade is examined, further.

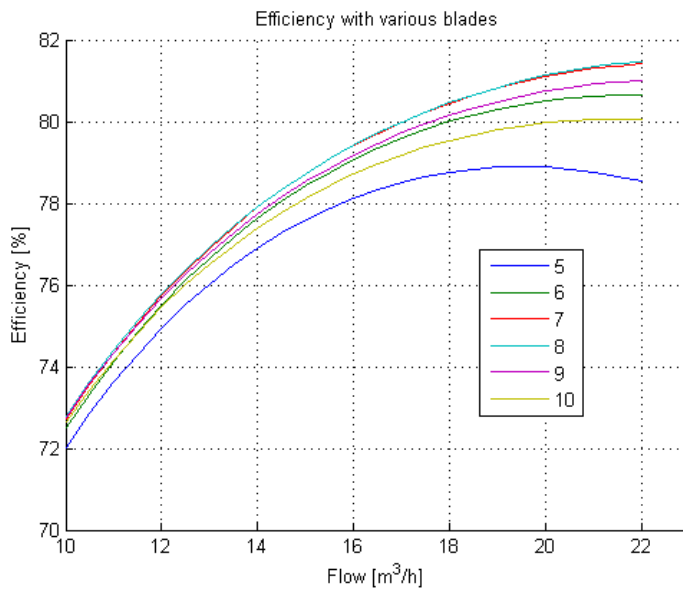


Figure 5.7: The efficiency of the pump, as a function of flow, with various number of blades. Note that the flow starts at  $10 \frac{m^3}{h}$

The simulation in Figure 5.7 shows that at low flows, the number of blades in the impeller have an insignificant effect on the hydraulic efficiency. As the flow gets progressively higher, the significance of the number of blades increases. The optimal number of blades according to the model is 7-8 at any flow. However, the differences are quite small, and the calculations are based on numerous geometric approximations. E.g. blade width or the vane width would have to change with every added blade to make room for them all. Figure 5.8 shows the influence of the number of blades on the head. It can be seen that when the flow increases, the number of blades necessary to get the highest head decreases. This follows naturally from the lower efficiency with many ( $>10$ ) blades.

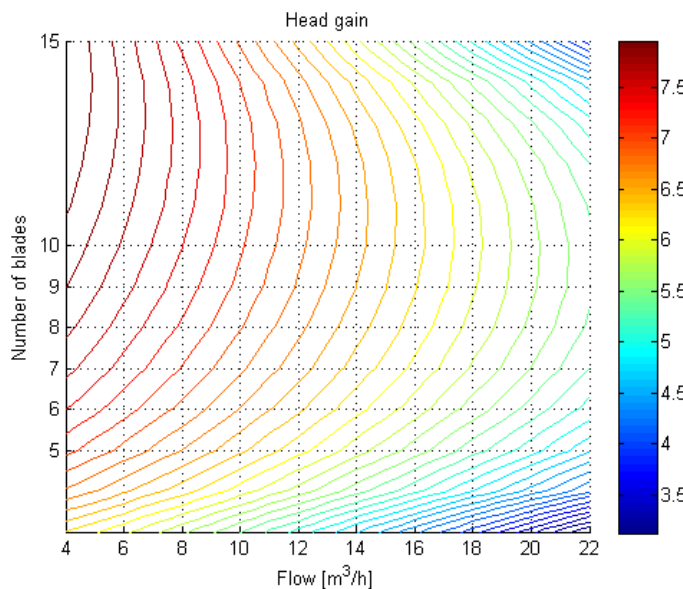


Figure 5.8: The head as a function of flow, with various numbers of blades.

It can be concluded that the model is an adequate indicator of the general theory, regarding blade quantity.

### 5.3.2 The outlet angle influence on the head

Number of blades changes the head and the efficiency. Accordingly to Equation 4.15 in Section 4.1.3, the outlet angle changes the slope of the head, from decreasing with flow with an angle lower than  $90^\circ$  to increase with the flow with an angle higher than  $90^\circ$ . Figure 5.9 shows the head as a function of the flow and five different outlet angles.

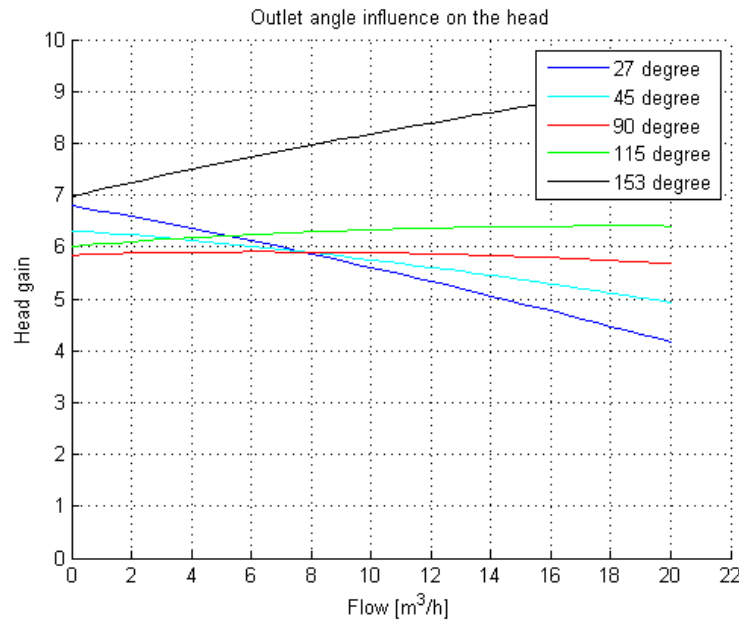


Figure 5.9: The outlet angle influence on the head.

Figure 5.9 shows that even with  $\beta_2 = 90^\circ$  the head gain is not constant as the theory in Section 4.1.3 states. This is due to the losses in the system. Additionally it is notable that the head at  $90^\circ$  is lower initially than is the case with both higher and lower outlet angles. This is likely caused by the shorter vanes and that several calculations in the velocity triangles are inversely proportional with  $\sin(\beta_{2B})$ , which has its highest value at  $\beta_{2B} = 90^\circ$  (The difference between  $\beta_2$  and  $\beta_{2B}$  is the deviation angle,  $\delta$ , caused by the slip).

Even though the head at a high outlet angle is high, the efficiency curve does not change much, due to the fact that the shaft power rises as well. This can be seen in Figure 5.10.

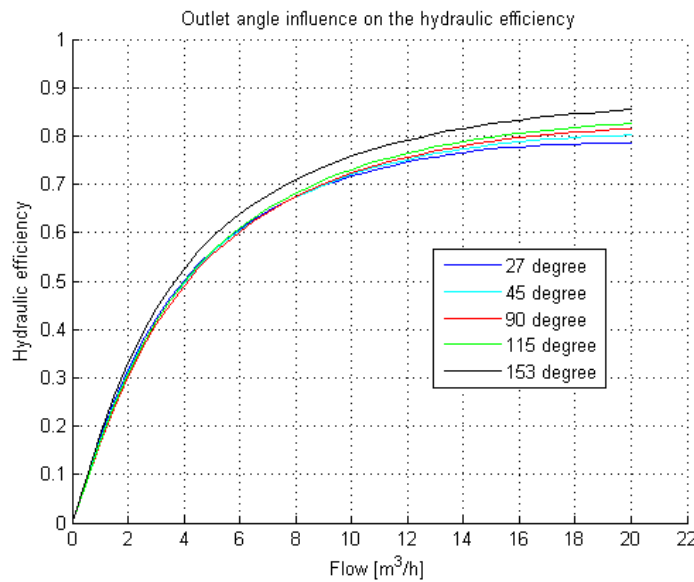
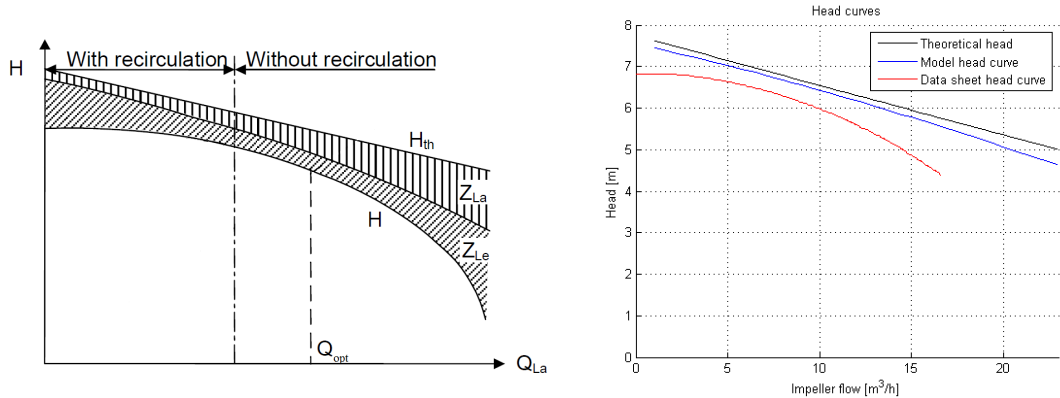


Figure 5.10: Efficiency curves when the outlet angle changes

*Since the results of the model correctly reflects known tendencies in the theory, both regarding the number of blades and the outlet angle, the model is assumed to be an adequate estimator of the pump impeller performance. However, an evaluation of the missing loss is needed in order to make an accurate comparison to the overall pump performance and thereby a final assessment of the pump.*

## 5.4 Additional model loss

Figure 5.11a indicates that the theoretical head and the actual head gain, calculated only with impeller losses, in Figure 5.11b correspond to the theory about losses influence on the head. By comparing Figure 5.11a and 5.11b it can be seen that the missing loss is the diffuser loss and recirculation loss. If a diffuser loss corresponding to the one in Figure 5.11a is added it can be assumed that the efficiency in Figure 5.5 would be more similar to the data sheet efficiency in Figure 5.3.



(a) Recirculation and diffusers losses influence on the head.  $Z_{La}$  is the impeller losses and  $Z_{Le}$  is the diffuser losses. [Gülich, 2008] Modified  
(b) The head curves from Figure 5.4 as a function of the impeller flow,  $Q_{La}$  instead of pump flow,  $Q$ . Based on Appendix A.3

Figure 5.11: Comparison between model and theory in regards to the different types of losses.

### Diffuser losses

This section will aim to describe the diffuser losses seen in Figure 5.11a. The following assumptions and equations are based on [Gülich, 2008]. The following height and radii in the volute have been measured. The different radii can be seen at Figure 5.12.

- $b_3 = 1,5 \cdot 10^{-2}$  [m] (The height at  $r_3$ .)
- $r_3 = 7,3 \cdot 10^{-2}$  [m]
- $r_4 = 8,9 \cdot 10^{-2}$  [m]

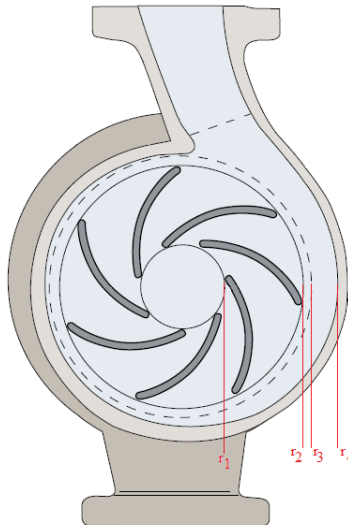


Figure 5.12: The different radii of the impeller, diffuser and volute. [Department of Structural and Fluid Mechanics, 2008,p. 22] Modified

Following assumptions have been made:

- The diffuser has a constant height, which is assumed to be as  $b_2$ .
- The diffuser has a constant width.
- $\alpha_3$  depends on  $\alpha_2$  and has been estimated based on the data sheet.

### Shock loss in the vaneless diffuser.

The loss coefficient and the head loss can be found in Equation 5.1 and 5.2 respectively [Gülich, 2008].

$$\zeta_{ls} = (\varphi_{2,La})^2 \cdot \left( \frac{\tau_2 - b_2}{b_3} \right)^2 = \left( \frac{c_{2m}}{u_2} \right)^2 \cdot \left( \frac{\tau_2 - b_2}{b_3} \right)^2 [-] \quad (5.1)$$

$$Z_{ls} = \frac{\zeta_{ls}}{2 \cdot g} \cdot u_2^2 [m] \quad (5.2)$$

### Friction loss in vaneless diffuser with constant width.

Equation 5.3 and 5.4 find the loss coefficient and the head loss respectively. [Gülich, 2008]

$$\zeta_{lr} = \frac{2 \cdot c_f \cdot r_2}{b_3 \cdot \sin(\alpha_3) \cdot \cos^2(\alpha_3)} \cdot \left( \frac{c_{2u}}{u_2} \right)^2 \cdot \left( 1 - \frac{r_2}{r_4} \right) [-] \quad (5.3)$$

$$Z_{lr} = \frac{\zeta_{lr}}{2 \cdot g} \cdot u_2^2 [m] \quad (5.4)$$

The total diffuser loss is described in Equation 5.5.

$$Z_{Le} = Z_{ls} + Z_{lr} [m] \quad (5.5)$$

The QH curve on Figure 5.11a shows that the diffuser loss,  $Z_{Le}$ , is high at the low and high flow region. The diffuser loss is found in Equation 5.5 does not fit the one represented in the QH curve.

The loss coefficient in Equation 5.1, except the velocity part of the equation, is built on the geometric parameters. Neglecting leakage flow, the meridional velocity  $c_{2m}$  is directly proportional with the flow, which means that when the flow increases, so does the shock loss.

Equation 5.3 describes the friction in the vaneless diffuser is based on geometric parameters, except the velocity part of the equation with  $c_{2u}$ ,  $c_f$  and  $\alpha_3$ .  $c_{2u}$  decreases with the flow.  $c_f$  is dependent on the Reynolds number. Since the flow is described as turbulent by the Reynolds number, the change in the value for  $c_f$  is very small.  $\alpha_3$  is estimated to be a function of  $\alpha_2$ , which does not change significantly with the flow. The small changes in size of  $c_f$  and  $\alpha_3$  makes the circumferential velocity the variable which changes the friction loss the most. Since this decreases with the flow, the friction loss decreases with the flow.

Since recirculation loss only occurs at low flows it will not be added to the model, since it will add to the model's complexity without adding to the certainty of the model due to the extra assumptions needed in the recirculation loss equations.

It is expected that the model with the impeller and diffuser loss (without recirculation) will fit in the middle and high flow region, but will deviate significantly in the low flow area.

## 5.5 Influence of diffuser loss

Figure 5.13 shows four different head curves. It can be seen that with adding first the impeller losses and later the diffuser loss to the theoretical head curve, the model head curve gets closer to the data sheet curve. The model with the added diffuser loss diverges from the data sheet curve in the low and high flow region. The difference in the low flow region is assumed to be due to the recirculation loss.

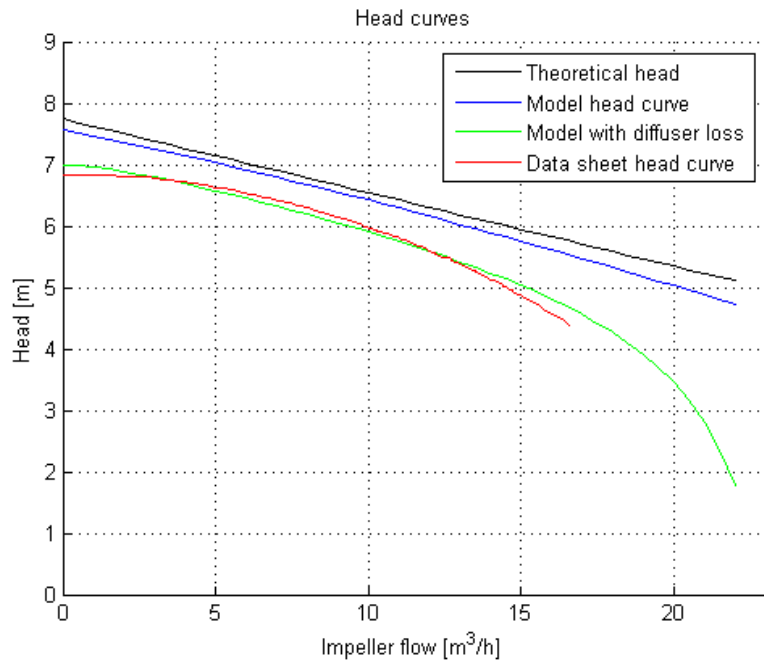


Figure 5.13: Different head as function of the flow. The model head curve with added diffuser loss lies closer to the data sheet head curve. Data sheet based on Appendix A.3.

Figure 5.14 shows the efficiency of the model with the impeller loss, the model with both the impeller and the diffuser loss and the data sheet. The model with the impeller and diffuser losses has a higher efficiency curve than the data sheet and peaks at the same flow.

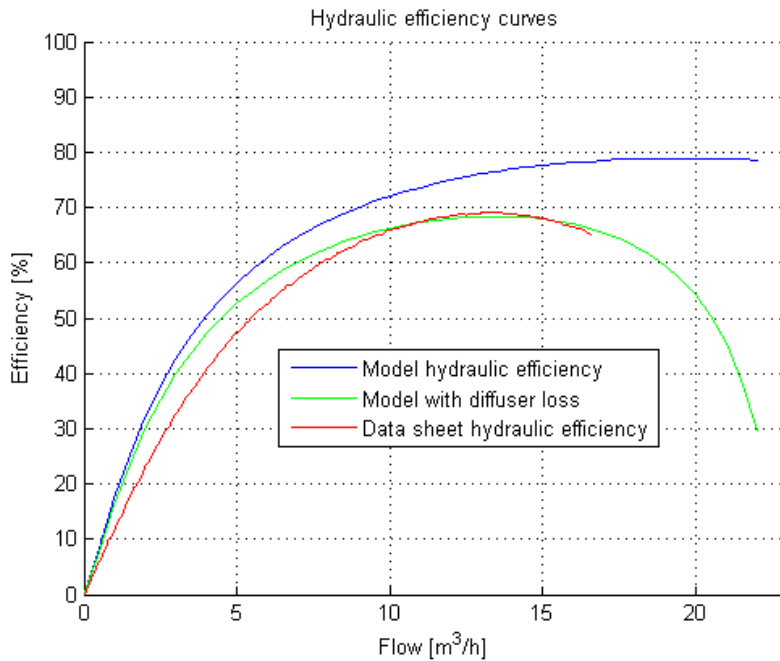


Figure 5.14: The different efficiency curves. The efficiency curve of the model is closer to the data sheet curve after the diffuser loss is added, and now peaks at the same flow rate. Data sheet based on Appendix A.3.

### Deviation in head and efficiency

The deviation in head between the model with only the impeller loss and the model with both impeller and diffuser losses can be seen at Figure 5.15. The deviation is relative to the data sheet head. It can be seen that by adding the diffuser loss to the model, the head deviation is decreased. The head curve from the model has an absolute deviation of maximum 4,9% and a absolute deviation at the rated flow of 2% with the added diffuser loss.

Figure 5.16 shows the deviation of the efficiency between the model with the impeller loss and the model with both impeller and diffuser losses. It should be noted that the deviation in the low flow region appear exaggerated due to the fact that the efficiencies have small values.

The absolute deviation in efficiency at the NK 32-125/142 operating point is under 2,5%. The small deviation in the operating point makes the model a valid model, when in Chapter 6 a impeller to the NK 32-125 pump will be designed, as long as the pump runs in the same operating area.

*In Section 5.1 the assumption that the pump data sheet was with a fixed rotational speed at 1340 rpm was made. If the model had a rotational speed which would vary like the data sheet, the head would in the low flow area increase and in the high head area decrease in head. Futher explanation can be found in Appendix E.*

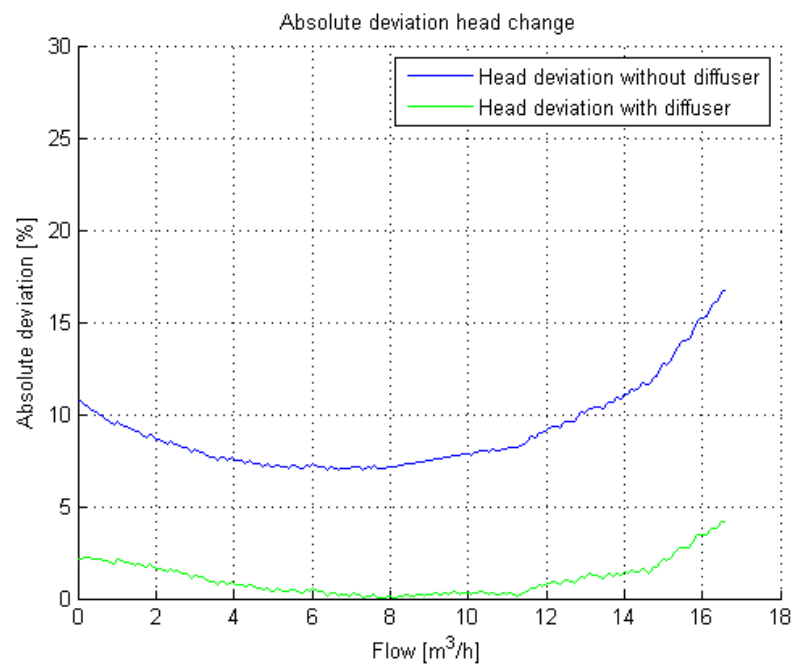


Figure 5.15: Deviation in the model with impeller loss and diffuser loss. The deviation is relative to the data sheet head.

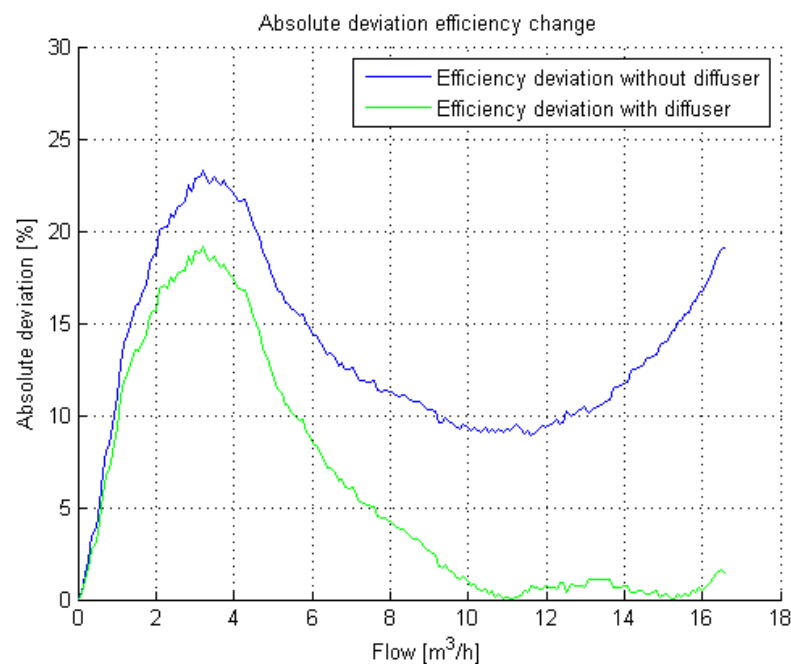


Figure 5.16: Model efficiency deviation relative to data sheet with and without diffuser loss.



# Design of model test impeller 6

---

A new impeller to the NK 32-125 pump will be designed in order to perform tests with parameters more alike those the model is limited to. The impeller will be designed in this chapter and tested. The test results are presented in Chapter 7.

The impeller model is limited to blades with a constant angle between blade and side disc ( $\lambda$ ), both along the blade length and blade height. Meaning the model does not allow the blade to neither twist nor curve along its height. Making an impeller with the same parameters the model is limited to should give the same or close to the same results as the model predicts. In Chapter 5 it can be seen that there is a difference in head gain and in efficiency point between the model and the data sheet. The new impeller for the NK 32-125 pump will be used to make a final verification of the model based on a comparison between experimental data and model results, if time permitted.

## Design Goal

- Similar design to the NK 32-125/142 impeller, but better adapted to the limitations of the model.
- Achieve test results similar to the model results of the 142 mm impeller. The model results can be seen in Figure 5.4 and Figure 5.5 in Section 5.2.

## Design parameters

In order to achieve results similar to those simulated in Chapter 5, the design will be the same as the NK 32-125/142 impeller, with the exceptions that the blades are now perpendicular to the side discs (i.e.  $\lambda = 90^\circ$ ) and the blades no longer curve along the height. Radii, other angles, distances etc. will remain the same. The geometric parameters of the NK 32-125/142 impeller can be found in Appendix B.1 [Grundfos, 2012a].

### 6.1 Design of the non-twisted blade impeller

The design of the non-twisted blade impeller is similar to the NK 32-125/142 impeller, except that the blades are perpendicular to the side discs. A CAD drawing of the original NK 32-125/142 impeller can be seen on Figure 6.1.

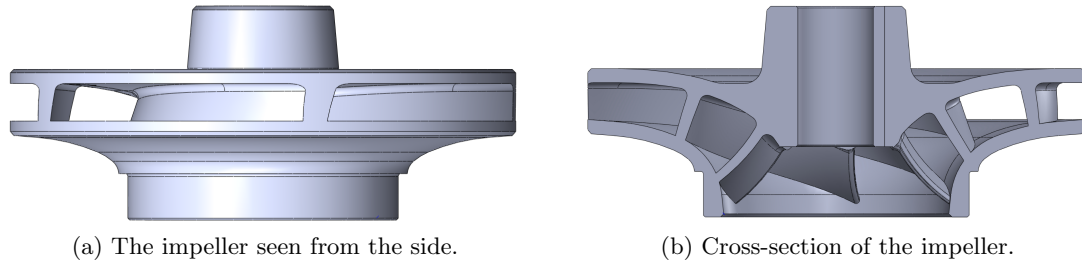
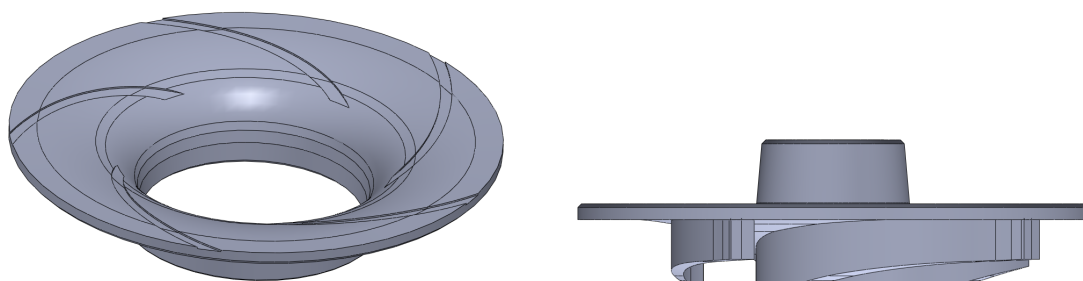


Figure 6.1: Impeller profiles of the NK 32-125/142. The inlet is at the bottom of the impeller.[Grundfos, 2012a]

Figure 6.2a shows the inlet and the bottom of the new impeller. The entire design can be seen in a CAD drawing in Appendix A.4. Note the preserved curvature in the bottom side disc, which causes the inlet blade height to be larger than the outlet blade height. The curved lines on the bottom of the disc are the assembly grooves for fitting the blades into when the impeller is assembled. The assembly grooves are 0,5 mm deep, but this will not change the blade height from the design, since the blades have been made 0,5 mm taller to fit.



(a) The “bottom” of impeller. The lines on the drawing are 0,5 mm assembly grooves. (b) Profile cut where the difference in height at inlet and outlet can be seen.

Figure 6.2: Profiles of the designed impeller to fit with the NK 32-125/142. The inlet is at the bottom of the figure.[Grundfos, 2012a]

The curvature of the blades, which is the reason for the change of design can be seen in Figure 6.3. The curvature is larger at the inlet of the blades and gradually fades along the blade length towards the outlet.

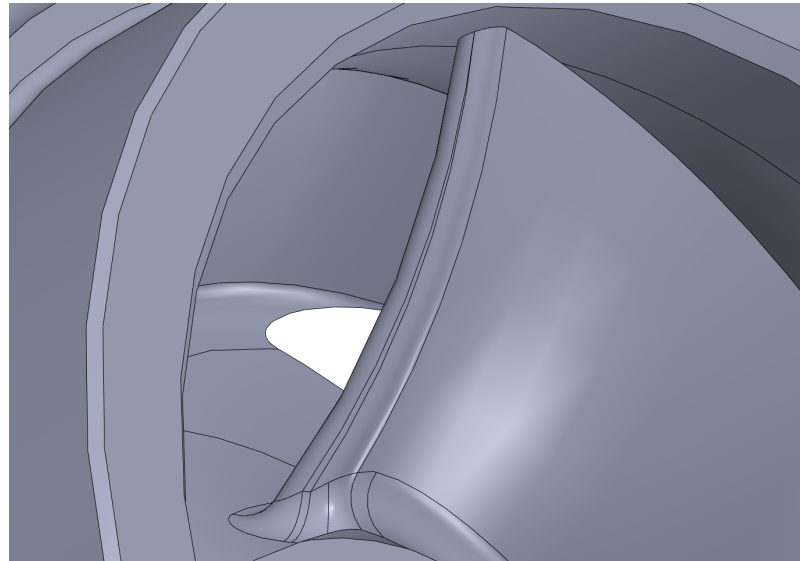
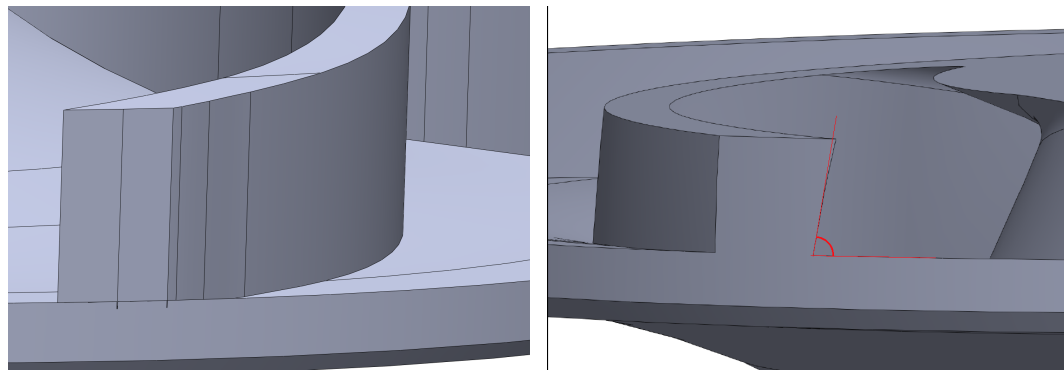


Figure 6.3: The inlet of the NK-32/125-142 impeller, demonstrating the curved blade the model does not account for.[Grundfos, 2012a]

Figure 6.4 demonstrates the angle change at the impeller outlet. It can be seen that the impeller stands perpendicular to the side disc in Figure 6.4a, where Figure 6.4b has turned blades (i.e.  $\lambda \neq 90^\circ$ ).



(a) The blade at the outlet of the designed impeller.

(b) The blade at the outlet of the NK-32/125-142 impeller [Grundfos, 2012a]. The red angle line shows  $\lambda \neq 90^\circ$ .

Figure 6.4: Impeller blades at the outlets, demonstrating the angle change. The blade of the designed impeller is turned upside-down relative to the NK-32/125-142 impeller. Based on [Grundfos, 2012a].

Figure 6.5 shows all of the blades of the designed impeller. The blades are 0,5 mm higher in order to fit in the assembly grooves and still get the right proportions. The opening in the middle is where the shaft is connected to the impeller.

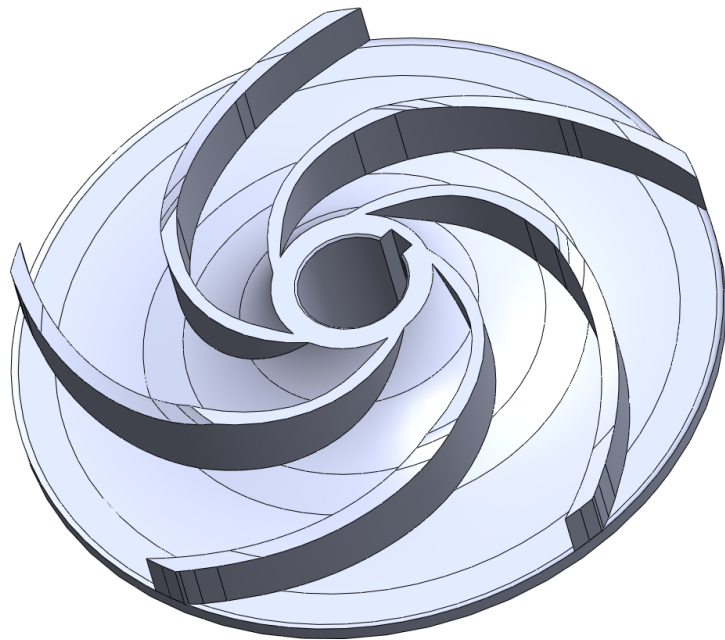


Figure 6.5: The “upper” part of the impeller. The blades fits in the assembly grooves in the bottom part of the impeller (See Figure 6.2a). Based on [Grundfos, 2012a].

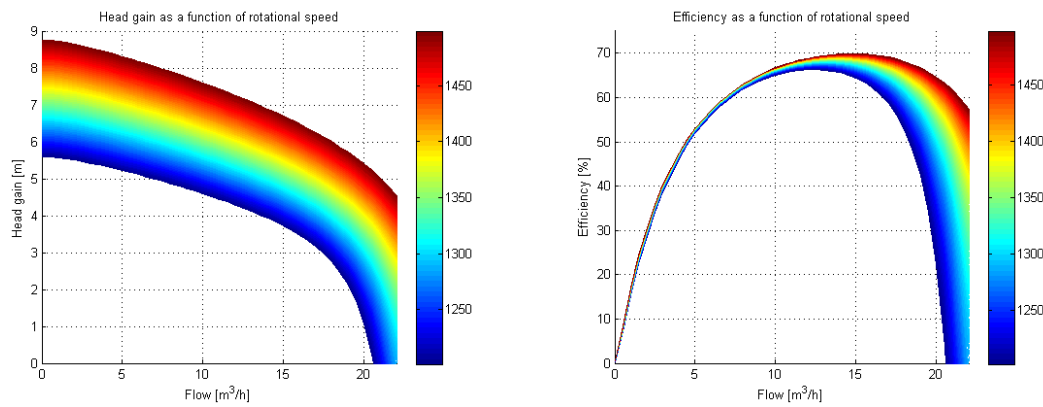
*In Appendix D a pump test corresponding to the ISO 9906 standard is set up. The test journal for the pump test is located in Appendix E.*

# Test data verification of model

7

The model is designed after a fixed rotational speed at 1340 rpm, but the fabricated pump has a rated rotational speed at 1400 rpm, a rated flow at 13,1  $\frac{m^3}{h}$  and a rated head at 5,5 m (see Appendix A.3). Therefore, the verification of the model will be based on a fixed rotational speed at 1400 rpm and not the 1340 rpm the model was designed for.

The change in rotational speed changes the head and efficiency curves. Figure 7.1 shows how the model head (including both impeller and diffuser losses) and efficiency changes with the flow and the the rotational speed but with the same geometric parameters.



(a) Head as a function of flow and rotational speed. (b) Hydraulic efficiency as a function of rotational speed

Figure 7.1: The rotation speed influence on the head and the hydraulic efficiency.

As it can be seen on Figure 7.1 both the efficiency and the head changes with the rotational speed. The head curve for the pump lies higher at a higher rotational speed and the best efficiency point is higher and at a higher flow when the rotational speed is higher than the model's fixed rotational speed at 1340 rpm.

The deviation between the model's hydraulic efficiency with the data sheet of the pump with at a rotational speed at 1340 rpm and 1400 rpm respectively can be seen at Figure 7.2. Note that the rotational speed in the model is fixed at 1340 rpm and 1400 rpm, while the rotational speed in the data sheet varies. In the low flow area the 1400 rpm model efficiency has a larger deviation, but from around 5  $\frac{m^3}{h}$  the two deviation curves follows each other. A certain error margin is expected in the low flow area due to the fact that the data sheets only estimates a head and efficiency in this region. It can be seen that the

model with the 1400 rpm has a larger absolute deviation in the high and low flow area but a smaller deviation at the rated flow than the 1340 rpm model.

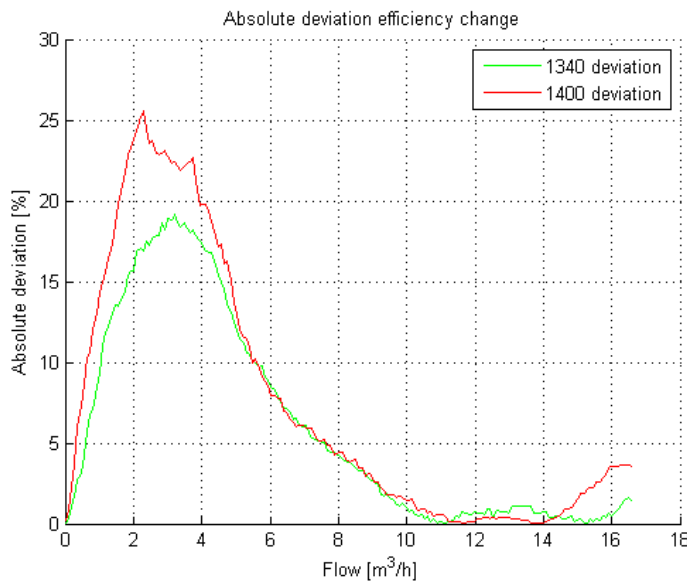


Figure 7.2: Deviation in efficiency for the model with the fixed rotational speed at 1340 rpm and 1400 rpm. Note that the scale in deviation ends at 30% and not 100%.

In Figure 7.3 the deviation between the model and the data sheet for 1340 rpm and 1400 rpm respectively can be seen. The deviation between the two curves shows a deviation increase of maximum 5% when the rotational speed rises from 1340 rpm to 1400 rpm. The small increase in deviation between the model results compared to the data sheets indicates that the model is valid even if the rotational speed changes. Note that the maximum deviation between model and data sheet is 8%.

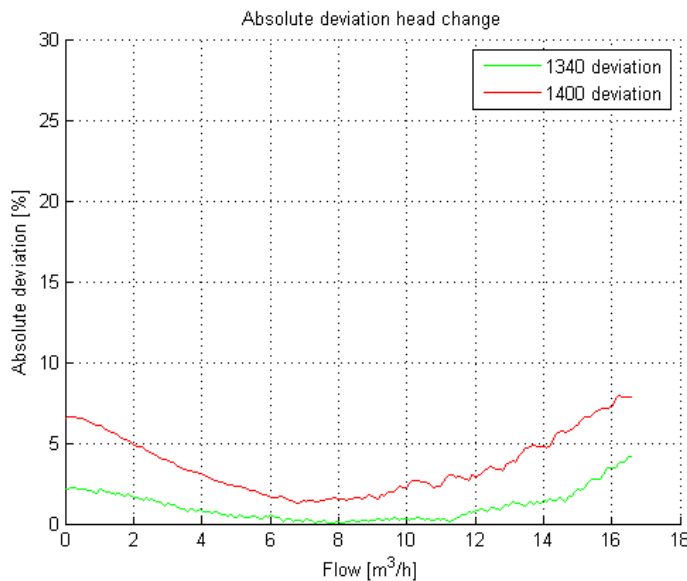


Figure 7.3: Deviation in head between the datasheet and the model for fixed rotational speeds at 1340 rpm and 1400 rpm. Note that the scale in deviation ends at 30% and not 100%.

The change from 1340 rpm to 1400 rpm has not had a significant effect of the accuracy of the model. The model is therefore considered valid for 1400 rpm as well as 1340, and the test will be carried out at 1400 rpm and compared to the model.

*The deviations in the model would, if the rotational speed in the model would change as in the data sheet, be different. The deviation would in the low flow area increase and in the high flow area increase as well, since the rotational speed in the data sheet exceeds the fixed rotational speed in the model.*

### Predicted results from model and data sheet

Figure 7.4 and Figure 7.5 show the model predicted results of the pump test and the data sheet curves. Figure 7.4 shows the model with fixed rotational speed at 1400 rpm predicted head and efficiency curve.

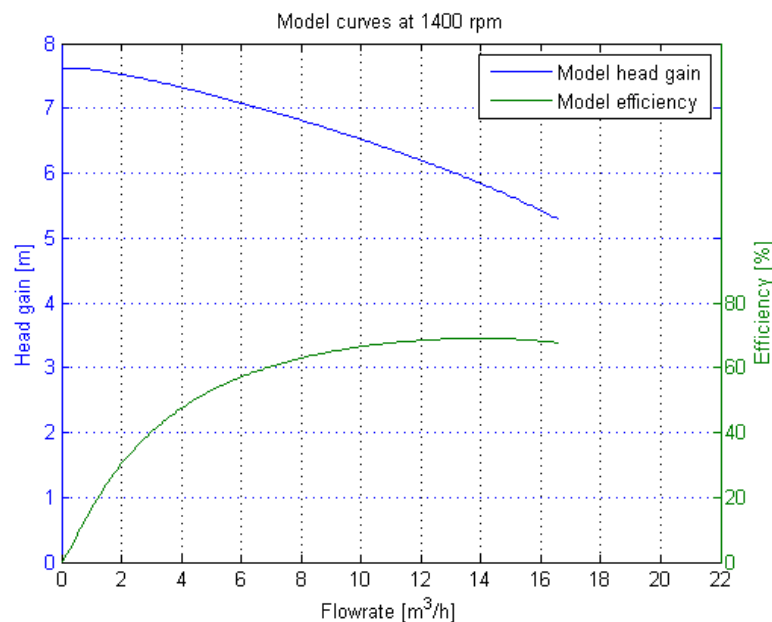


Figure 7.4: Head and efficiency curves from the model with a fixed rotational speed at 1400 rpm.

Figure 7.5 shows the data sheet prediction of the model with a rated rotational speed at 1400 rpm. The data sheet can be found in Appendix A.3.

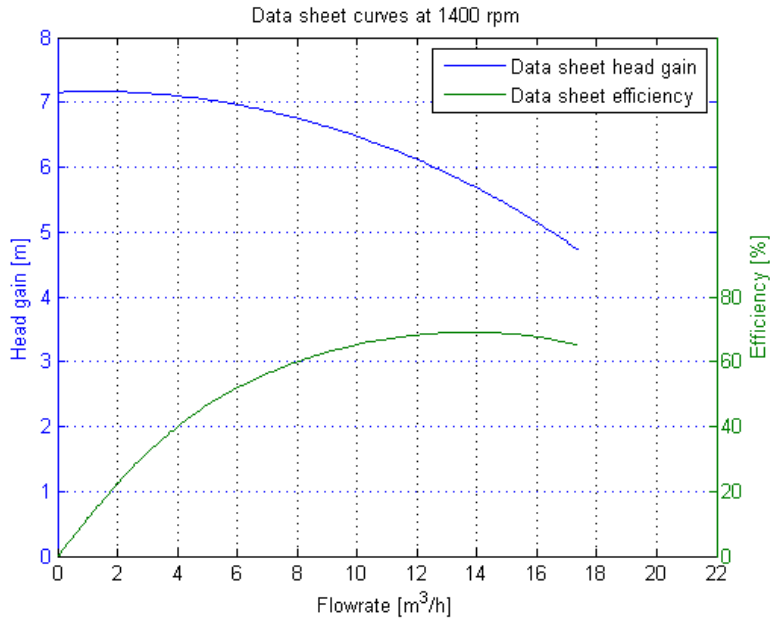


Figure 7.5: Efficiency curves from the model and the data sheet, which are scaled to varying rotational speed from 1469 to 1419 rpm. Based on Appendix A.1.

The model and the data sheet predictions of the test data are very similar. So in the following Section 7.1 when comparing the test data with the model at a fixed rotational speed at 1400 rpm and with the data sheet with a varying rotational speed, it is expected that the test data lies close to both the model and the data sheet. When comparing test data to the data sheet, these will have to be scaled to the same variation in speed.

## 7.1 Pump characteristics from test data

The pump characteristics are based on the experiments and calculations in Appendix E. Figure 7.6 shows the head and efficiency curves from the pump test. Figure 7.6a shows the head measurements. The blue crosses on the figure are error bars describing the deviation in data points and in measurement devices. The line between the points is a curve fit based on the data points positions. Figure 7.6b shows the efficiency as a function of the flow with error bars. The test hydraulic efficiency peak point is due to limited available flow not possible to determine, it seems likely that the test peak efficiency point will be around the same as the data sheet (i.e. at 13,1  $\frac{m^3}{h}$ ).

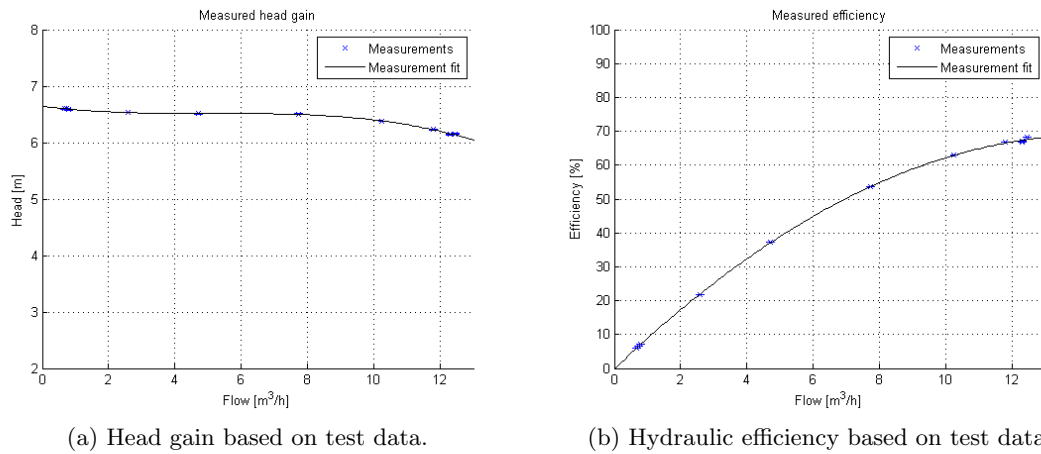


Figure 7.6: Pump performance based on the pump test. The rotational speed is fixed at 1400 rpm. Data have not been scaled. Error bars are based on device uncertainties and a 95% confidence interval of measured data.

Since the deviations in data points and in measurement devices are insignificant, the error bars will not be used on the rest of the figures in this chapter.

Figure 7.7 shows how the pipe, expansion and contraction losses effects the head and efficiency. The pipe, expansion and contraction losses are explained further in Appendix E. The added losses causes the curves from the pump test to lie higher on both the head and efficiency scale.

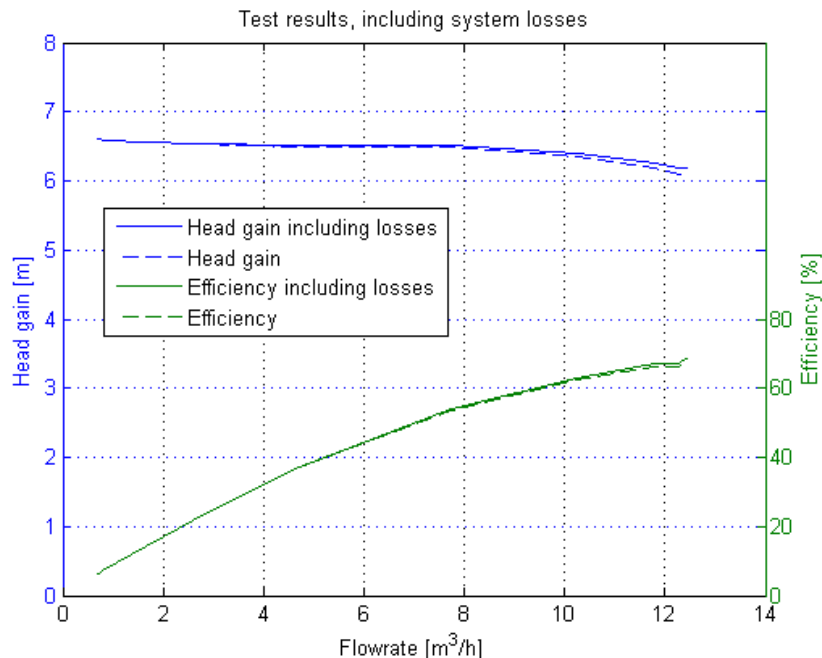
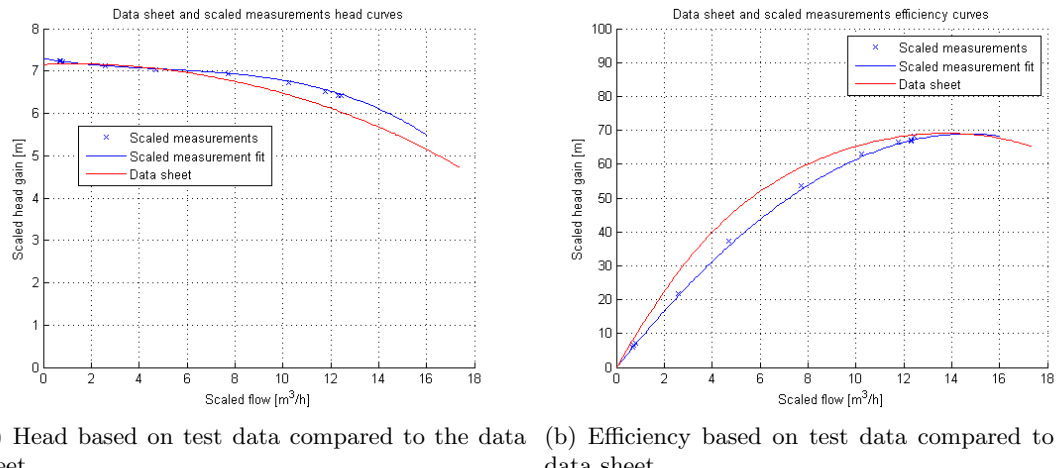


Figure 7.7: Head and efficiency curves from the pump test with and without pipe, expansion and contraction losses.

The pump characteristic based on the test data with the added losses, which is seen in Figure 7.7, has been scaled to make a comparing between the data sheet and the pump characteristic. The scaling of the rotational speed is elaborated in Appendix E.3.3. Figure 7.8 shows the head and efficiency curve for the data sheet and the pump test. Comparing the data sheet and the pump characteristic it is possible to affirm that the pump test data is valid and can be used to verify the model.

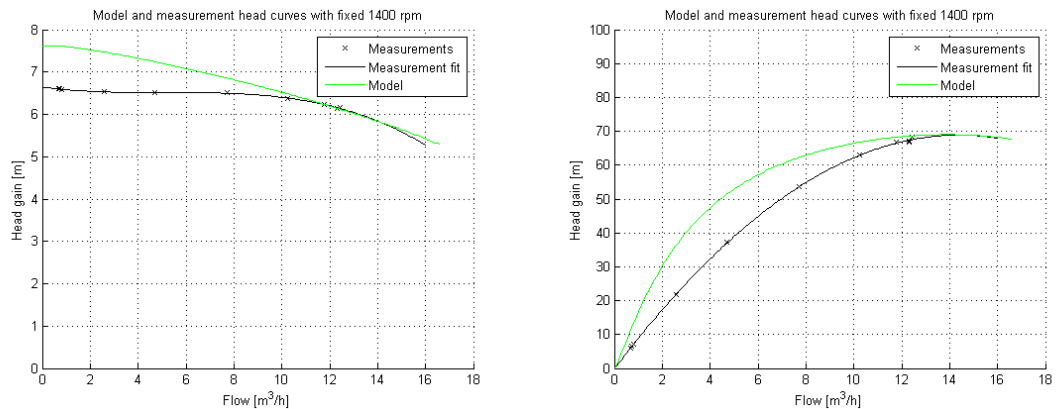


(a) Head based on test data compared to the data sheet.  
(b) Efficiency based on test data compared to the data sheet.

Figure 7.8: Pump performance based on the pump test with added losses. The rotational speed is varying for both the data sheet and the test data. Data sheet is based on Appendix A.3.

It can be seen in Figure 7.8 that there is a small difference between the data sheet and the scaled test data. In the low flow area the head curve fits but the efficiency curve for the scaled test data lies under the data sheet. In the high flow area the efficiencies fit but the head curve for the scaled test data is higher than on the data sheet, this indicates that there is an inconsistency in the shaft power (used to calculate the test data efficiency), which is higher in the test data.

The pump characteristic from the test data with added losses is compared to the model in order to verify the model. The comparison to the model can be seen on Figure 7.9.



(a) Head based on test data compared to the model. (b) Efficiency based on test data compared to the model.

Figure 7.9: Pump performance based on the pump test with added losses. The rotational speed is fixed at 1400 rpm for both the model and the test data. Note that the test data here has not been scaled. Datasheet is

The model and the test data with added losses with a fixed rotational speed fits both on the efficiency and the head with a flow around  $12 \frac{m^3}{h}$ . The model lies higher than the test data when concerning both the head and efficiency.

*It can be concluded by comparing Figure 7.8 and Figure 7.9 that the model fits in the high flow area (including the pump's rated flow at  $13,1 \frac{m^3}{h}$ ) when predicting the performance of a NK 32-125/142 Grundfos pump. The accuracy of the model increase when the flow increases, which is clear on Figure 7.9 but also on Figure 7.2 and Figure 7.3.*



# Conclusion 8

---

The main goal of this project has been to produce a model for prediction of the performance of the Grundfos NK 32-125 pump, verify the model by setting up and carrying out an ISO approved pump test and achieve an understanding of the theories applied for centrifugal pump modeling.

Based on the description of the centrifugal pump and its theory, a model describing the pump performance is set up. The theory behind the model is based on the different velocities in the impeller, the flow through it and the losses caused by it. The velocities of the impeller are found by using velocity triangles and correcting with blockage, incidence and slip. The losses includes mechanical and hydraulic losses. The model has several limitations. It has a fixed rotational speed and the only losses subtracted is the impeller losses including leakage flow.

The model is verified in the second part of the report by the means of a data sheet for the NK 32-142/142 with a rated rotational speed at 1340 rpm and a comparison to general impeller theory. The model reflects known tendencies in the theory, both regarding the number of blades and the outlet angle influence on the head and efficiency. Comparing the model with [Gülich, 2008] graph over the influence of losses and recirculation on pump characteristics, it is concluded that a diffuser loss is needed in order to improve the accuracy of the model.

The model is predicted to have an increase in head gain in the low flow area and a decrease in head in the high flow area, if the rotational speed of the pump is changed from fixed to varying like in the data sheet for the NK 32/125-142.

A new impeller is designed with blades perpendicular to the side discs in order to test the accuracy of the model when using a impeller with parameters more alike those the model is limited to.

Due to lack of time and a pump with a rated rotational speed at 1400 rpm, the verification of the model is based on the change in the rotational speed as the model variable instead of the designed impeller. Changing the rotational speed from 1340 rpm to 1400 rpm results in a slight increase in the head and efficiency of the model.

A final verification of the model is made experimentally. A pump test corresponding to the ISO 9906 standard is designed from specifications given by International Standard 9906. However, due to difficulties in the setup construction, the used test setup does not fulfill the ISO 9906 standard. The test data is corrected to only present the head and hydraulic efficiency of the pump. The data sheets used in the comparison have varying rotational speed while the model have fixed rotational speed. The validity of the test data and thereby the test is verified by scaling the rotational speed so a comparison between

the test data and the data sheet is possible.

The final verification of the model uses the validated test data. The model deviates significantly in the low flow area, but fits accurately at higher flows. The model is therefore considered valid in the high flow area thereby including the rated flow at  $13,1 \frac{m^3}{h}$ , for the NK 32-125/142 with a rated rotational speed at 1400 rpm.

# Model improvement proposals

# 9

---

*This chapter consists of a series of proposals, there could be implemented in order to improve the accuracy of the model.*

## Both fixed and rotational speed in the model

The data sheet has been scaled to fit varying rotational speeds at different flows. The model is constructed to run at a constant rotational speed, but includes parameters that have been scaled to make the model fit the data sheet better (See diffuser loss in Section 5.4).

Rebuilding the model to vary the rotational speed depending on the flow would require a known compliance between rotational speed and flow, making the rotational speed a function of the flow. The compliance between rotational speed and flow could be found from a polynomial fit of corresponding flows and rotational speeds from the data sheet. The scaling laws and an example of scaling of rotational speed can be found in Appendix E. The model could be changed so it would always find the optimum speed, depending on the flow, thereby improving the model as a tool to predict the optimal operating point.

## Improve diffuser loss calculations

As described in Section 5.4 there are significant losses in the pump outside of the impeller, namely in the pump diffuser and volute. However, the diffuser loss found in Section 5.4 is dependent on a fit to a data sheet, which as mentioned has a different premise than the model. This means the diffuser loss is not as accurate as wanted.

To improve the accuracy and reliability of the diffuser loss, the two major assumptions of the calculation could be eliminated; The volute radius,  $r_4$ , and the diffuser flow angle,  $\alpha_3$ . In the model the volute radius is an estimated mean of an increasing value, ranging from being almost equal to the diffuser radius,  $r_3$ , to almost being twice of that. To better calculate the diffuser loss, rather than estimate a mean value of  $r_4$ , an integral could be set up to account for the increase in volume in the volute and thereby accurately estimate  $\alpha_3$ .

**Verification with designed impeller**

In Chapter 6 an impeller with blades perpendicular to the side discs and no curvature along the blade height was designed to better fit within the limitations of the model. Due to lack of time this impeller was never tested, and the original 142 mm impeller was instead used to conduct the pump test described in Appendix E.

Since the shape of the impeller blades (i.e. curved along the blade height) most likely have a positive effect on the pumps performance, a test with the designed impeller would account for shortcomings in the model regarding the geometric parameters. In addition to not accounting for the shape of the impeller blades, the model omits recirculation losses and losses outside of the impeller and the diffuser. Performing the test with the impeller designed in Chapter 6 would therefore allow a better assessment of the significance of these losses, and thereby a better assessment of the model.

# Bibliography

---

- Danfoss (2012a). *MBS33*. <http://ic.danfoss.com/TechnicalInfo/literature/manuals/04/ICPDP20X202.pdf>.
- Danfoss (2012b). *VLT Low Harmonic Drive for AAF006 Operating Instructions*.  
[http://mcliterature.danfoss.com/WebPublish/doc\\_MG37A102.pdf](http://mcliterature.danfoss.com/WebPublish/doc_MG37A102.pdf).
- Department of Structural and Fluid Mechanics (2008). *The Centrifugal Pump*. Grundfos Management A/S, 1. edition.
- Grundfos (2012a). *CAD drawing of NK 32-125/142*. Provided by Troels Jepsen, Grundfos.
- Grundfos (2012b). *Grundfos Webcaps*.  
<http://net.grundfos.com/App1/WebCAPS/custom?&userid=GDK&lang=DAN.html>.
- Gülich, D.-I. J. F. (2008). *Centrifugal Pumps*. Springer. ISBN: 978-3-540-73694-3.
- Hydraulic Institute, Europump and U.S. Department of Energy (2001). Pump life cycle costs: A guide to lcc analysis for pumping systems, executive summary. Report, Hydraulic Institute and Europump and U.S. Department of Energy.
- Munson, Young and Okiishi (2006). *Fundamentals of fluid mechanics*. John Wiley & Sons, Inc., 5. edition. ISBN: 0-471-67582-2.
- MyTub (2012). *Belimo Nr24a-sr Rotary Act 24v 10nm Mudul*.  
[http://www.mytub.co.uk/product\\_information.php?product=477994](http://www.mytub.co.uk/product_information.php?product=477994).
- National Instruments (2012). *NI USB-6341*.  
<http://sine.ni.com/nips/cds/view/p/lang/en/nid/209069>.
- One Technology Way (1999). *AD594-AD595*.  
[http://www.analog.com/static/imported-files/data\\_sheets/AD594\\_595.pdf](http://www.analog.com/static/imported-files/data_sheets/AD594_595.pdf).
- Robort W. Fox, Philip J. Pritchard and Alan T. McDonald (2010). *Introduction to fluid mechanics*. John Wiley & sons, inc., 7. edition. ISBN: 978-0-470-23450-1.
- Siemens (2005). *Sitrans F M Magflo*. [http://cache.automation.siemens.com/dnl/DY/DY5NTQ3AAAA\\_17532493\\_HB/SFIDKPS027W401.pdf](http://cache.automation.siemens.com/dnl/DY/DY5NTQ3AAAA_17532493_HB/SFIDKPS027W401.pdf).
- Stepanoff, A. J. (1957). *Centrifugal and Axial Flow Pumps*. Krieger Publishing Company, 2. edition. ISBN: 0-89464-723-7.
- Tech Instrumentering (2012). *Tofting TF-100P data sheet*. [www.tech.dk](http://www.tech.dk). Provided by Kim Andersen.

- The Danish Energy Saving Trust (2012). *What is an A-rated pump?*  
=http://www.savingtrust.dk/consumer/products/indoor-climate/a-rated-pumps/what-is-an-a-rated-pump.
- The International Organization for Standardization (1999). Iso 9906:1999 -  
rotordynamic pumps - hydraulic performance acceptance tests - grades 1 and 2.
- Thin, K. C., Khaing, M. M. and Aye, K. M. (2008). Design and performance analysis of  
centrifugal pump. *World Academy of Science, Engineering and Technology*,  
(46):422-429.
- University of Texas in Austin (2012). Moody diagram. Report,  
[http://www.ce.utexas.edu/prof/kinnas/319LAB/lab\\_s09.html](http://www.ce.utexas.edu/prof/kinnas/319LAB/lab_s09.html). Found  
20.05.2012.

## **Part IV**

## **Appendices**



# **Contents on the CD**

---

A

- A 1: CAD drawing of NK 32-125/142 impeller and housing. [Grundfos, 2012a]
- A 2: Model in MATLAB.
- A 3: Data sheets of Grundfos NK 32-125. [Grundfos, 2012b]
- A 4: CAD drawing of designed impeller, based on A 1.
- A 5: 2D CAD drawing of Grundfos NK32-125 pump. [Grundfos, 2012a]
- A 6: Designed test setup based on A 5.
- A 7: Constructed test setup based on A 5.
- A 8: Raw test results in csv.
- A 9: Data sheet of the National Instrument USB-6341 control unit. [National Instruments, 2012]
- A 10: Data sheet of the Danfoss MBS33 pressure transmitter. [Danfoss, 2012a]
- A 11: Data sheet of the Belimo NR24A-SR motorvalve. [MyTub, 2012]
- A 12: Data sheet of the Tofting TF-100P flow transducer. [Tech Instrumentering, 2012]
- A 13: Data sheet of the Danfoss FC302 VLT inverter drive. [Danfoss, 2012b]
- A 14: Data sheet of the Analog Devices AD595 temperature transducer. [One Technology Way, 1999]
- A 15: Labview program.
- A 16: PDF prints of web pages and web sources.
- A 17: The report as PDF file



# Documentation of model B

This appendix describes the structure of the model and which assumptions and equations are used. All mentioned equations except Equation 4.1 which describes the total head are from the source [Gülich, 2008,p. 131-140]. Equation 4.1 is from [Department of Structural and Fluid Mechanics, 2008,p. 65]. All model MATLAB files are found in Appendix A.2. This appendix contains:

- Step by step explanation of the model
- The model's geometric parameters

Every step of the flowchart (Figure B.1) has a number, which fits with a corresponding number in the list below. In the list the steps, the assumptions and equations used will be explained.

1. The geometry of the impeller and the house has been measured from the pump drawing of the Grundfos NK32-125/142 pump. Some measurements, like the ones of the leakage loss parameters, has been made with some reservation due to the fact that the annular seal is missing from the pump drawing (see Appendix A.4).
2. The flow is set from 0 to  $22 \frac{m^3}{h}$  and the number of blades,  $z_{La}$ , is set from 3 to 15. The reasoning for 3 blades as the minimum number of blades is due to restrictions in the equation for the slip factor (Equation 4.21 in Section 4.1.4). This equation is valid only for  $z_{La} \geq 3$ .
3. The initial inlet and outlet velocity triangles calculates the velocities in the impeller including blockage. The outlet velocities are calculated with slip. The velocity triangles are calculated based on the equations in Section 4.1. The static head rise in the impeller is calculated from Equation 4.1 in Section 4.1. The static head rise is initial since the losses has not yet been taken into account. From the velocity triangles the theoretical head is calculated using Equation B.1.

$$H_{th} = \frac{u_2 \cdot c_{2u} - u_1 \cdot c_{1u}}{g} [m] \quad (\text{B.1})$$

4. Leakage flow  $Q_{sp}$  is calculated from the static head gain and the two assumptions:
  - The loss coefficient  $\zeta_{EA}$  for the inlet and outlet loss is set to 1,2.
  - The loss per chamber coefficient  $\zeta_K$  is set to 1,3.

In [Gülich, 2008,p. 137] Gülich says that the coefficients is found experimentally and lies around  $\zeta_{EA} = 1$  to 1,2 and  $\zeta_K = 1$  to 1,3. The leakage flow can be seen in Figure B.2 as a function of the pump flow. The leakage flow decreases as the pump flow increases.

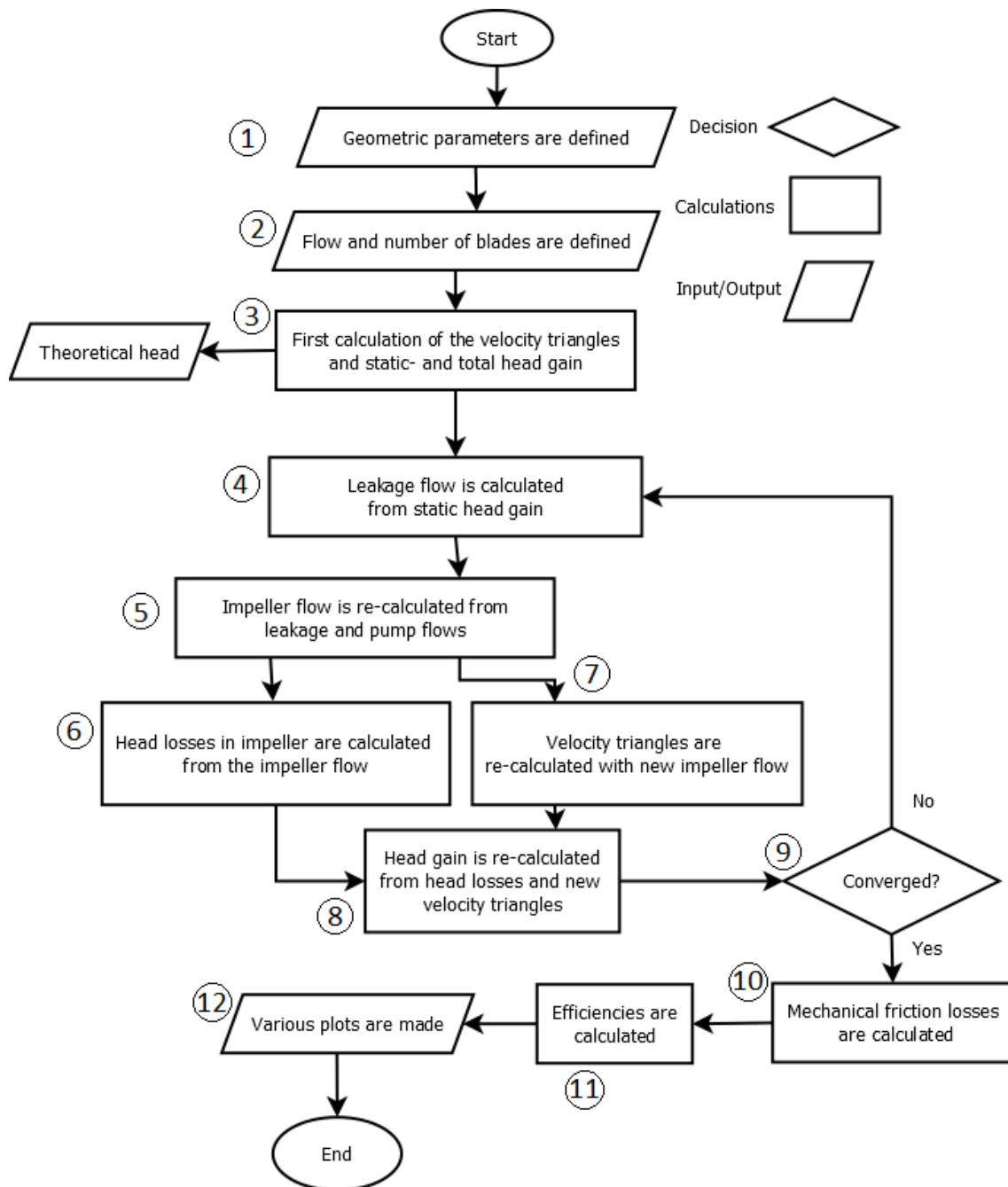


Figure B.1: Flowchart over the model. The process is repeated for each flowvalue. The numbers are used to describe the course of the program.

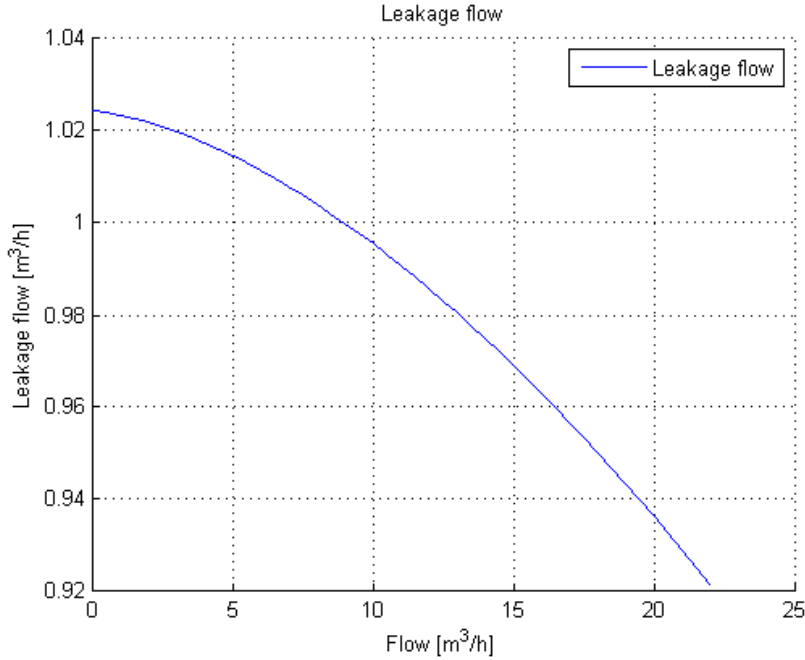


Figure B.2: Leakage flow,  $Q_{sp}$ , as a function of the pump flow,  $Q$ .

5. The leakage flow is added to the flow running into the impeller,  $Q_{La}$ .
6. The head losses in the impeller are calculated based on the equations in Appendix C.1. Figure B.3 shows the head losses as a function of the pump flow. The head losses contains the shock losses, friction and mixing losses. The friction and mixing losses increases and the the shock losses decreases when the flow increases.

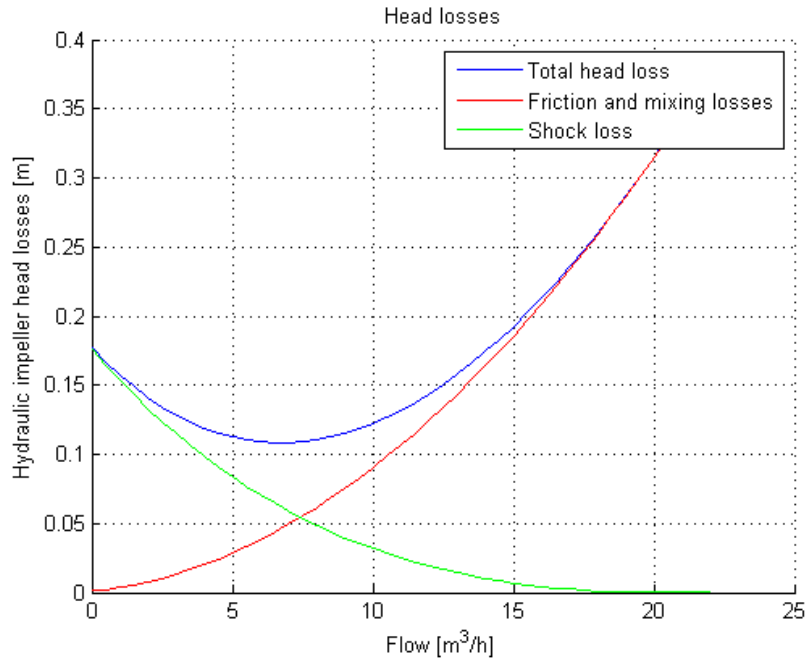


Figure B.3: Head losses as a function of the pump flow.

7. The velocity triangles are calculated with the new impeller flow which includes the

- leakage flow.
8. Head gain is calculated with the head losses in the impeller and the new velocities due to the leakage flow.
  9. Since leakage flow loss, head losses and velocity triangles are all dependent on each other, the program runs step 4-8 until it converges.
  10. The mechanical friction loss is the disc friction loss and the mechanical loss. The disc friction loss is based on Equation 4.23 and the mechanical loss is based on Equation 4.34 which are found in Section 4.2.1 and 4.2.2 respectively.
  11. The hydraulic efficiency is found. Equation B.2 shows the hydraulic efficiency of the pump. The total efficiency  $\eta_{total}$  (Equation B.3) is the ratio between the hydraulic power and the supplied power.

$$\eta_{hyd} = \frac{P_{hyd}}{P_{shaft}} \cdot 100 \text{ [%]} \quad (\text{B.2})$$

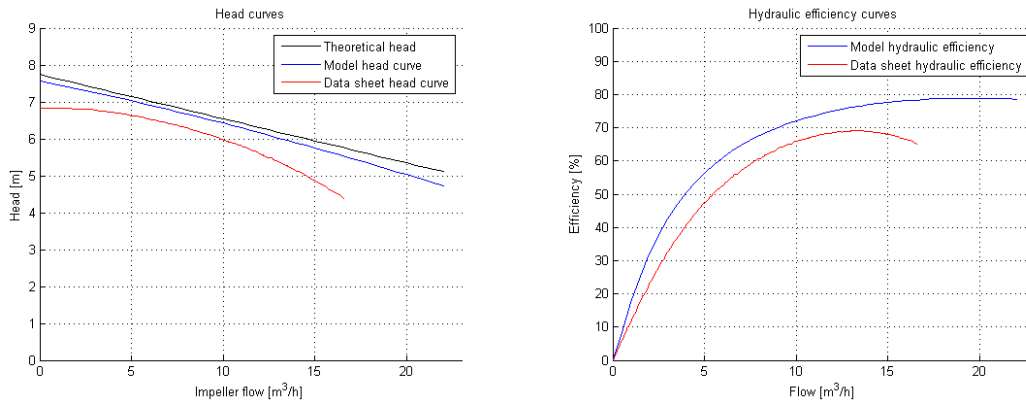
$$\eta_{total} = \frac{P_{hyd}}{P_{motor}} \cdot 100 \text{ [%]} \quad (\text{B.3})$$

$P_{hyd}$  is the hydraulic power transferred from the impeller to the fluid.  $P_{shaft}$  is the shaft power transferred from the motor to the shaft.  $P_{motor}$  is the supplied power from external electricity source to the motor and the controller. Equation B.4 shows how the different powers are connected.

$$P_{hyd} < P_{shaft} < P_{total} \text{ [W]} \quad (\text{B.4})$$

The total efficiency is lower than the hydraulic efficiency due to the fact that in the total efficiency both the hydraulic and the mechanical efficiency are included.

12. The final procedure before the model is terminated, is the plotting of various parameters. Figure B.4 shows two examples of this; a head curve and an efficiency curve.



(a) The head curve from the model.

(b) The efficiency curve from the model.

Figure B.4: Model results. Data sheet data based on Appendix A.3.

The data sheet for the pump with the performance curves, which is used to verify the model, is based on an impeller with twisted blades. The theory used in the model has only curved blades. This effects the model outputs which are slightly different than the curves given in the data sheet for the pump.

## B.1 Geometric parameters of the model

Table B.1 is a parametric table, where the parameters are extracted from the CAD drawing (Appendix A.1). Figure B.5 explains where the seal length, width and diameter are measured.

Symbol	Explanation	Value	Unit
$n$	Motorspeed	1340	rpm
$a_1$	Distance between vanes at inlet	$1,626 \cdot 10^{-2}$	m
$a_2$	Distance between vanes at outlet	$2,71 \cdot 10^{-2}$	m
$r_1$	Radius of impeller inlet	$2,591 \cdot 10^{-2}$	m
$r_2$	Radius of impeller outlet	$7,1 \cdot 10^{-2}$	m
$b_1$	Inlet blade height	$1,448 \cdot 10^{-2}$	m
$b_2$	Outlet blade height	$1,09 \cdot 10^{-2}$	m
$\beta_{1B}$	Inlet blade angle	14	°
$\beta_{2B}$	Outlet blade angle	27	°
$\lambda_1$	Angle between vane and side discs at inlet	90	°
$\lambda_2$	Angle between vane and side discs at outlet	90	°
$\epsilon$	Roughness	$4,5 \cdot 10^{-5}$	
$L_{sch}$	Length of blade	$102,225 \cdot 10^{-3}$	m
$d_{sp}$	Diameter from eye to seal	0,07595	m
$L_{sp}$	Length seal	$2,88 \cdot 10^{-3}$	m
$s$	Width of seal	$2,5 \cdot 10^{-4}$	m
$d_{si}$	Diameter from eye to seal after the chamber	0,07595	m
$L_i$	Length of second seal after chamber	$1 \cdot 10^{-3}$	m
$s_i$	Width of second seal after chamber	$2,5 \cdot 10^{-4}$	m
$e_1$	Blade thickness at inlet	$2,07 \cdot 10^{-3}$	m
$e_2$	Blade thickness at outlet	$2,07 \cdot 10^{-3}$	m
$e$	Axial distance to wall at the periphery of the impeller	$1 \cdot 10^{-4}$	m

Table B.1: Geometric parameters extracted from CAD drawings [Grundfos, 2012a].

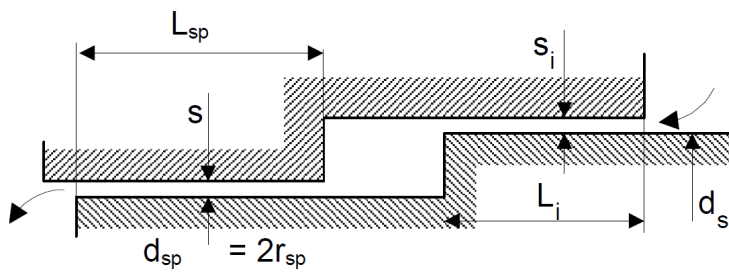


Figure B.5: Drawing explaining where the seal length, width and diameter are measured.



# Loss equations C

---

## C.1 Impeller loss equations

The equations used for calculating the impeller losses; the friction, and mixing and shock losses. The equations are based on [Gülich, 2008,p. 140].

Average relative velocity in impeller channels.

$$w_{av} = \frac{2 \cdot Q_{La}}{z_{La} \cdot (a_2 \cdot b_2 + a_1 \cdot b_1)} \left[ \frac{m}{s} \right] \quad (\text{C.1})$$

Reynolds number and friction coefficient. The roughness coefficient,  $\epsilon$  can be found on the moody chart in Figure 4.11 in Section 4.2.2.

$$Re = \frac{w_{av} \cdot L_{sch}}{\nu} [-] \quad (\text{C.2})$$

$$c_f = \frac{0,136}{\left( -\log \left( 0,2 \cdot \frac{\epsilon}{L_{sch} + \frac{12,5}{Re}} \right) \right)^{2,15}} [-] \quad (\text{C.3})$$

Hydraulic diameter

$$D_h = \frac{2(a_2 \cdot b_2 + a_1 \cdot b_1)}{a_2 + b_2 + a_1 + b_1} [m] \quad (\text{C.4})$$

Dissipation coefficient

$$c_d = (c_f + 0,0015) \cdot \left( 1, 1 + 4 \cdot \frac{b_2}{d_2} \right) [-] \quad (\text{C.5})$$

### Friction and mixing losses

$$\zeta_{La,R} = 4 \cdot c_d \frac{L_{sch}}{D_h} \left( \frac{w_{av}}{u_2} \right)^2 [-] \quad (\text{C.6})$$

Relative velocity vector

$$w_1 = \sqrt{c_{1m}^2 + (u_1 - c_{1u})^2} \left[ \frac{m}{s} \right] \quad (\text{C.7})$$

Average velocity in impeller throat

$$w_{1q} = \frac{Q_{la}}{z_{La} \cdot a_1 b_1} \left[ \frac{m}{s} \right] \quad (\text{C.8})$$

### Shock loss at impeller inlet

$$\zeta_{La,C} = 0,3 \cdot \left( \frac{w_1 - w_{1q}}{u_2} \right)^2 [-] \text{ Only for } \frac{w_{1q}}{w_{1m}} > 0,65 \quad (\text{C.9})$$

### Impeller loss

$$\zeta_{La} = \zeta_{La,R} + \zeta_{La,C} [-] \quad (\text{C.10})$$

Impeller friction, mixing and shock loss in head.

$$Z_{La} = Z_{La,R} + Z_{La,C} [m] \quad (\text{C.11})$$

$$Z_{La,R} = \frac{\zeta_{La,R} \cdot u_2^2}{2g} [m] \quad (\text{C.12})$$

$$Z_{La,C} = \frac{\zeta_{La,C} \cdot u_2^2}{2g} [m] \quad (\text{C.13})$$

The MATLAB function `impeller-loss.m` calculates the impeller loss and the function is used in the model.

## C.2 Leakage loss equations

The equations used for calculating the leakage loss. The equations are based on [Gülich, 2008, p. 137]. Using the geometric parameters, static pressure rise created by the impeller,  $H_p$ , and the circumferential speed,  $u_2$ , the loss coefficient for the inlet and outlet,  $\zeta_{EA}$ , and the loss coefficient for loss per chamber,  $\zeta_K$ , the leakage loss is found.

The loss coefficients are assumed to be  $\zeta_{EA} = 1, 2$  and  $\zeta_K = 1, 3$ . The second assumption is that the leakage flows radially inwards.

Reynolds number

$$Re_{u_2} = \frac{u_2 \cdot r_2}{\nu} [-] \quad (\text{C.14})$$

The rotation factor  $k$  as a function of the Reynolds number and the seal geometry

$$y_{sp} = Re_{u_2}^{0,3} \cdot \frac{s \cdot d_{sp}}{d_2^2} \sqrt{\frac{s}{L_{sp}}} [-] \quad (\text{C.15})$$

$$k = 0,9 \cdot y_{sp}^{0,087} [-] \quad (\text{C.16})$$

Pressure difference across seal

$$\Delta H_{sp} = H_p - k^2 \frac{u_2^2}{2g} \left( 1 - \frac{d_{sp}^2}{d_2^2} \right) [m] \quad (\text{C.17})$$

The leakage flow rate,  $Q_{sp}$ , can be calculated from the axial velocity in the gap,  $c_{ax}$ , the Reynolds number and the friction coefficient. All the variables are dependent and the Gauss-Seidel method is used as the converging method.

Axial velocity in gap

$$c_{ax} = \sqrt{\frac{2g\Delta H_{sp}}{\zeta_{EA} + \lambda \frac{L_{sp}}{2s} + \sum_i \left(\frac{d_{sp}}{d_{si}}\right)^2 \left(\frac{s}{s_i}\right)^2 \left(\zeta_K + \lambda_i \frac{L_i}{2s_i}\right)}} \left[\frac{m}{s}\right] \quad (\text{C.18})$$

Reynolds numbers

$$Re = \frac{2s \cdot c_{ax}}{\nu} [-] \quad (\text{C.19})$$

$$Re_u = \frac{2s \cdot u_{sp}}{\nu} [-] \quad (\text{C.20})$$

$$u_{sp} = \frac{\pi \cdot d_{sp} \cdot n}{60} \left[\frac{m}{s}\right] \quad (\text{C.21})$$

Leakage flow rate

$$Q_{sp} = \pi \cdot d_{sp} \cdot s \cdot c_{ax} \left[\frac{m^3}{s}\right] \quad (\text{C.22})$$

Equation C.19 will be used to find if the flow is laminar or turbulent.

The following equations are used to found the friction coefficient, which is used in Equation C.18. Friction coefficient for laminar flow,  $e_x$ =eccentricity=0.

$$\lambda_0 = \frac{96}{Re} \left(1 - 0,6 \frac{e_x}{s}\right) [-] \quad (\text{C.23})$$

$$\lambda = \lambda_0 \cdot \left(1 + 0,2 \cdot \left(\frac{Re_u}{2000}\right)\right)^{1,03} [-] \quad (\text{C.24})$$

Friction coefficient for turbulent flow,  $e_x$ =eccentricity=0.

$$A = 0,135 \cdot \frac{\epsilon}{s} [-] \quad (\text{C.25})$$

$$\lambda_0 = \frac{0,31}{\left(\log \left(A + \frac{6,5}{Re}\right)\right)^2} [-] \quad (\text{C.26})$$

$$\lambda = \lambda_0 \cdot \left(1 + 0,19 \cdot \left(\frac{Re_u}{Re}\right)^2\right)^{0,375} [-] \quad (\text{C.27})$$



# **Standard measurement criteria D**

---

*In this chapter, the outlines of the International Standard ISO 9906 [The International Organization for Standardization, 1999] are described. The information in this chapter is used throughout the report for determining correct setup of the experiment system.*

## **D.1 Data criteria**

For testing a pump system there are standards which are recommendable to fulfill. The guidelines of these are described in the International Standard ISO no. 9906 [The International Organization for Standardization, 1999], this will be referred to as the ISO.

In the ISO, there are two grades of precision, where grade 1 is the most precise. The difference in grades is determined by the setup and the data precision. The report aims for a fulfillment of a grade 2 test as a minimum.

Regarding variations in measured data the ISO describes the requirements as follows; note that the quotes below are for unsteady conditions. Steady conditions are defined as a test with so small variance that only 1 set of readings is required per data point (See Table D.1).

*"At each test point, repeated readings of the measured quantities shall be made at random intervals of time, but not less than 10 s (...)"* [The International Organization for Standardization, 1999,p. 15]

*"The difference between these repeated readings of the same quantities will be a measure of the unsteadiness of the test conditions, which are at least partly influenced by the pump under test as well as by the installation."* [The International Organization for Standardization, 1999,p. 15]

"(...) and the value of each separate reading and of the efficiency derived from each set of readings shall be recorded. The percentage difference between the largest and smallest values of each quantity shall not be greater than that given in Table 4. It should be noted that a wider difference is permitted if the number of readings is increased (see Table 4)." [The International Organization for Standardization, 1999,p. 15]

*"Table 4 - Limits of variations between repeated measurements of the same quantity  
(based on 95% confidence limits)" [The International Organization for Standardization, 1999,p. 15]*

Each data point must be based on a number of sets of continuous measurements. Each set must consist of data measured over at least 10 seconds, though no specification on how many measurements should be in a set is found. The number of sets for each data point depend on the variations in the test data as seen in Table D.1 (Referred to as Table 4 in the above quote).

The variation in the test data is interpreted to be the difference between the largest and smallest value of a 95% confidence interval of the measurements in each data point, relative to the average value of the data point. E.g. 5 sets of 100 measurements are made in a data point, the variation would then be the difference between the largest and smallest value of the 95% confidence interval of all 500 values.

Conditions	Number of sets of readings	Permissible difference between largest and smallest readings of each quantity, related to the mean value			
		Flow rate, pump total head, torque, power input		Speed of rotation	
		grade 1 %	grade 2 %	grade 1 %	grade 2 %
Steady	1	0,6	1,2	0,2	0,4
Unsteady	3	0,8	1,8	0,3	0,6
	5	1,6	3,5	0,5	1,0
	7	2,2	4,5	0,7	1,4
	9	2,8	5,8	0,8	1,6
	13	2,9	5,9	0,9	1,8
	> 20	3,0	6,0	1,0	2,0

Table D.1: Permissible difference between largest and smallest readings of quantities under steady state conditions, copy of the ISO Table 4 [The International Organization for Standardization, 1999,p. 15].

The speed of rotation during tests is permitted to be in the range of 50-120% of the specified optimal speed [The International Organization for Standardization, 1999,p. 15].

The uncertainties for the instruments are called systematic uncertainties. Even after calibration the measurement unit may have a certain uncertainty of measurements. The maximum permitted uncertainties are listed in Table D.2.

Quantity	Permissible value	
	Grade 1 [%]	Grade 2 [%]
Flow rate	±1,5	±2,5
Speed of rotation	±0,35	±1,4
Torque	±0,9	±2,0
Pump total head	±1,0	±2,5

Table D.2: Permissible transducer uncertainties for grade 1 and grade 2 tests. Based on [The International Organization for Standardization, 1999,p. 19]

For testing the pump, if not otherwise defined, for real applications the fluid in the test is "clean cold water". The conditions of "clean cold water" is showed in Table D.3.

Characteristics	Unit	Permitted max.
Temperature	°C	40
Kinematic viscosity	m <sup>2</sup> /s	1,75 · 10 <sup>-6</sup>
Density	kg/m <sup>3</sup>	1050
Non-absorbent free solid content	kg/m <sup>3</sup>	2,5
Dissolved solid content	kg/m <sup>3</sup>	50

Table D.3: International Standard for "cold clean water". [The International Organization for Standardization, 1999,p. 16]

## D.2 Dimensions criteria

The dimensions of the test setup for the pump experiments have been standardized to comply with standards for grade 1 tests, including NPSH tests (for future use), presented by the ISO [The International Organization for Standardization, 1999]. Even should other parameters prevent a fulfillment of a grade 1 test, the dimensions of the setup will still be valid for grade 2.

For finding some parameters of the standardized setup, the type number,  $K$ , of the pump is needed. The type number is dimensionless and is determined from the point of highest efficiency in the pump, as seen in Equation D.1 [The International Organization for Standardization, 1999,p. 6].

$$K = \frac{2\pi n Q'^{\frac{1}{2}}}{(g H')^{\frac{3}{4}}} [-] \quad (\text{D.1})$$

$$= \frac{2 \cdot \pi \cdot \frac{1340}{60} \cdot 0,0035^{\frac{1}{2}}}{(9,82 \cdot 5)^{\frac{3}{4}}} [-] \\ = 0,447565 [-] \quad (\text{D.2})$$

The type number for the pump is used to determine various minimum lengths in the test setup.  $Q'$ ,  $H'$  and  $n$  are the flow, head and rotational speed in the design point.

To avoid flowswirl and asymmetrical velocity distributions, the experiment setup is made with respect to the standards. A drawing of the test setup is shown in Figure D.1. It is a

general goal to avoid bends and other disturbances that can cause swirl. Flowswirl is best avoided by arranging the installation so the measurement sections will have minimal impact on the flow distribution [The International Organization for Standardization, 1999,p. 12]. In the installation the flow should have an axially symmetrical velocity distribution and an uniform static pressure distribution.

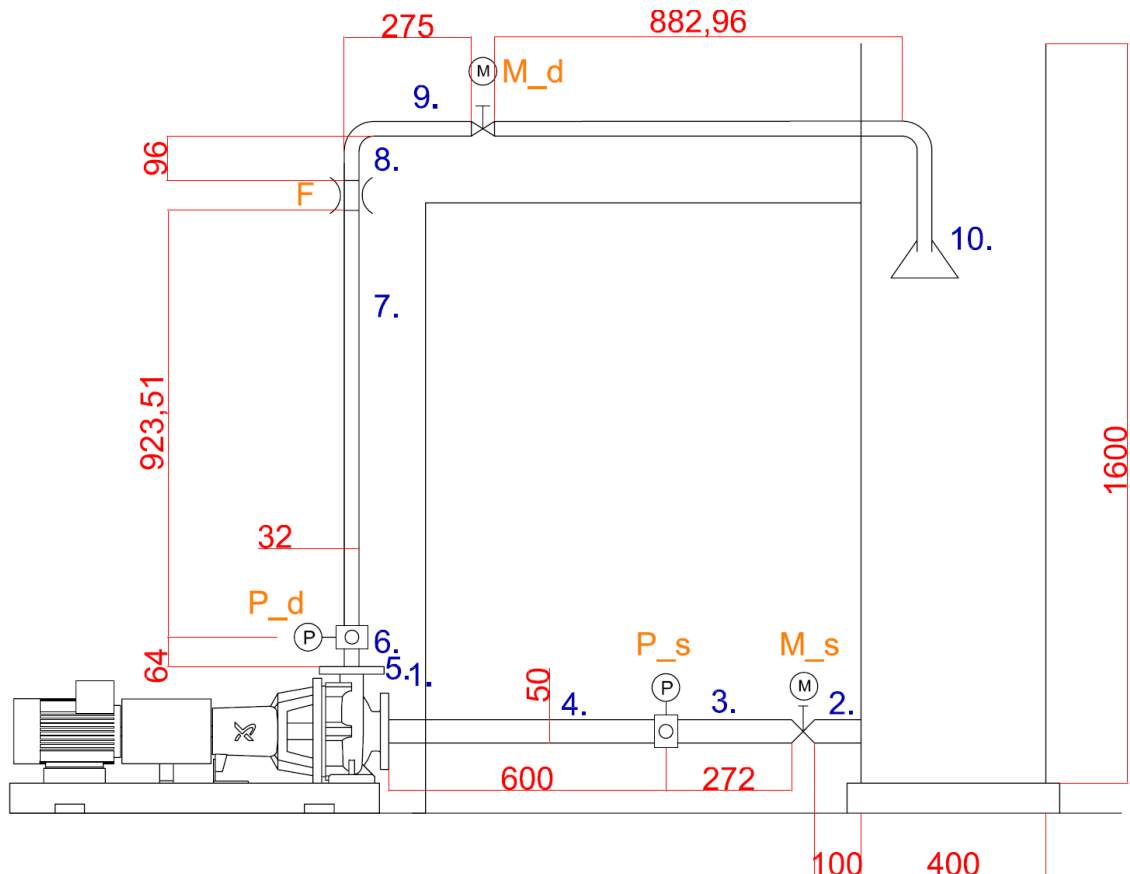


Figure D.1: Drawing of the test setup in accordance with [The International Organization for Standardization, 1999]. All measurements are presented as required minimums and in mm. The pipe diameters are inner diameters, Based on Appendix A.5.

The dimensions of Figure D.1 have been numbered. The relevant ISO regulation and the minimum size determination for each number is found in the following.

1. The width of the pipe is dictated by the inlet width of the pump [The International Organization for Standardization, 1999,p. 25], hence 50 mm is used, see Appendix A.3.
2. Starting from the water tank, the length of the pipe before the first valve is set by the standard to twice the pipe diameter, since there are no measurement units until after the valve. Distance will be  $2 \cdot d_{inlet} = 2 \cdot 50 \text{ mm} = 100 \text{ mm}$  [The International Organization for Standardization, 1999,p. 25].
3. According to the standard, a system with a free surface reservoir must have a straight length of pipe before any measurement unit [The International Organization for Standardization, 1999,p. 12]. Equation D.3 describes the length of this pipe, using the type number from Equation D.1.

$$L_{straight} = (K + 5) \cdot d_{inlet} \text{ [mm]} \quad (\text{D.3})$$

$$\begin{aligned} L_{straight} &= (0,447565 + 5) \cdot 50 \text{ [mm]} \\ &= 272 \text{ mm} \end{aligned} \quad (\text{D.4})$$

The length found in Equation D.4 is the straight length between the nearest disturbance and the measurement tapping on the inlet side of the pump.

4. For NPSH tests, the distance between the inlet pressure measurement and the pump inlet is  $12 \cdot d_{inlet} = 12 \cdot 50 \text{ mm} = 600 \text{ mm}$  [The International Organization for Standardization, 1999,p. 39].
5. Outlet piping diameter is dictated by the pump outlet diameter [The International Organization for Standardization, 1999,p. 28], which is 32 mm, seen in Appendix A.3.
6. The distance between the pump outlet and the outlet pressure measurement is 64 mm. This is dictated for  $L_{pressure} = 2 \cdot d_{outlet}$  [The International Organization for Standardization, 1999,p. 28].
7. Between the outlet pressure measurement and the flow measurement there is a straight pipe of length 923 mm. This complies with the rule of  $L = 5 \cdot d_{outlet}$  that is required by the MagFlo [Siemens, 2005,p. 22].
8. The length between the flow measuring device and the  $90^\circ$  bend is 96 mm. This is due to the MagFlo data sheet requirement of  $L = 3 \cdot d_{outlet}$  [Siemens, 2005,p. 22].
9. The return piping is not determined from the ISO standard. The return valve has been placed 275 mm in, to distance it from the flow transducer and the  $90^\circ$  bend. The final pipe length is determined by the remaining distance to the tank.

An AutoCAD file of the ISO test setup dimensions can be seen in Appendix A.6.



# Testing of pump system E

In this chapter the experimental setup and the experimental description will be explained along with the uncertainties and the accuracy of the experiments.

The NK 32-125 will be tested with the standard impeller described in Chapter 5 with a fixed rotational speed at 1400 rpm.

## E.1 Test setup

The build test setup varies from the designed in Figure D.1 due to construction. The dimensions have been altered slightly. The dimensions of the test setup are seen in Figure E.1 and a description of the measurement devices is seen in Appendix F.

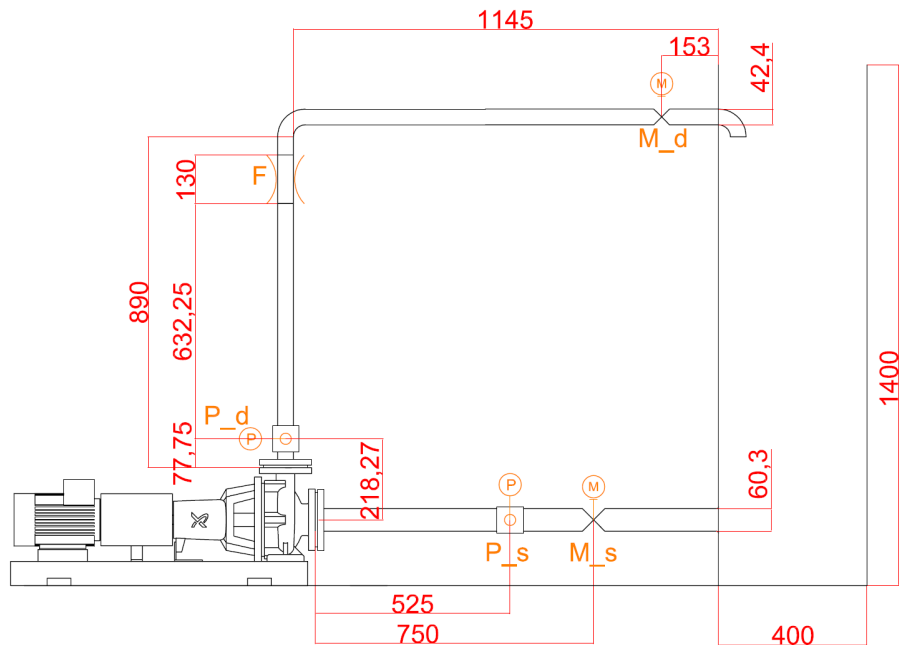


Figure E.1: The experimental test setup with measurements. All measurements are in mm. Based on Appendix A.5.

The constructed test setup is not in accordance to the demands set in the ISO, due to pipe diameters being different from pump flange diameters, changes in pipe lengths, etc. [The International Organization for Standardization, 1999]. The different size pump used

also changes the system type number (Equation D.1). This can cause larger error than permitted for the tests, which is further discussed in Section E.3.

## E.2 Experimental method

The test setup is a closed system and a drawing of the test setup is shown in Figure E.1.

The setup in Figure E.2 consists of a pump with a valve and a pressure transducer on both suction and discharge side. A flow meter is placed in the system. A still water tank is connecting suction and pressure sides.

The designed and constructed test setup both have a flow meter which is placed as the ISO instructs, but when performing the test, it is clear that the inserted flow meter is defect. A new flow meter of the type Tofting TF-100P (See Appendix A.12 for data sheet) is placed as seen in Figure E.2 (the box named Q). The new flow meter is placed after the 90° bend in a distance that comply with the ISO (see Appendix D Section D.2 for further details).

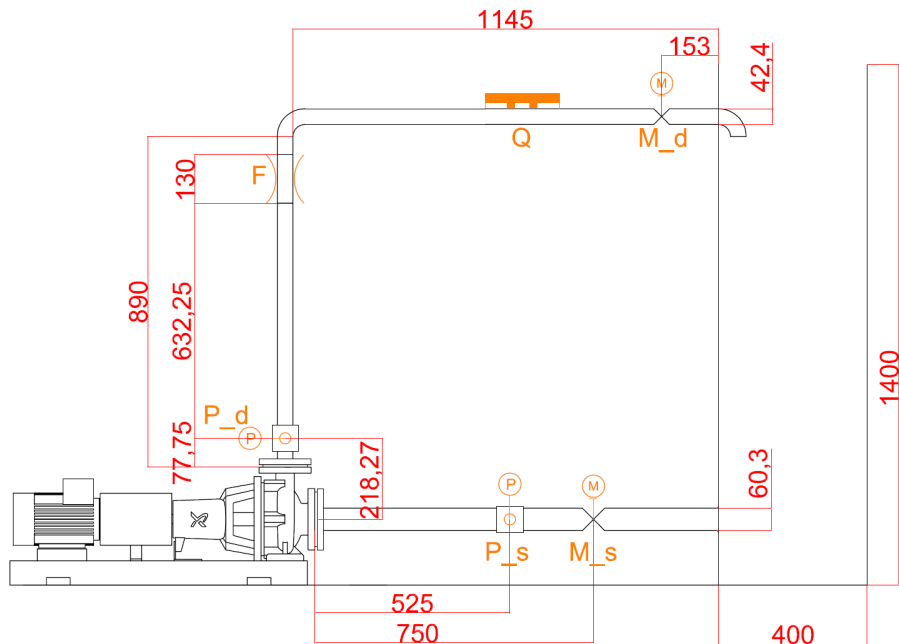


Figure E.2: The experimental test setup with measurements, and including the new flow meter. All measurements are in mm. Based on Appendix A.5.

Under the test the discharge and suction pressures are measured with the LabVIEW program. The motorized valves are controlled with the LabVIEW program. The flow measurements are determined by visual observation of the flow meter display.

### E.2.1 Calculation of pump characteristics from test data

The test setup provides the discharge and suction pressures, the rotational speed, the torque and the flow. These data will, with some calculations, provide the pump head, the

shaft power and the hydraulic efficiency as a function of the flow. The equations used in finding the pump characteristics are from [Department of Structural and Fluid Mechanics, 2008] and [Robert W. Fox et al., 2010].

The head gain is calculated from the pressure difference as seen in Equation E.1.

$$H = \frac{\Delta p}{\rho \cdot g} [m] \quad (\text{E.1})$$

Bernoulli's equation can be rewritten to represent the pressure, as seen in Equation E.2. The pressure equation can be rewritten like Equation E.3 and Equation E.4. The pressure difference can be used in Equation E.1. The value of  $\rho$  is determined by the temperature of the water.

$$\Delta p = \left( p + \frac{v^2 \rho}{2} + z g \rho \right)_d - \left( p + \frac{v^2 \rho}{2} + z g \rho \right)_s [Pa] \quad (\text{E.2})$$

$$\Delta p = \Delta p_{stat} + \Delta p_{dyn} + \Delta p_{geo} [Pa] \quad (\text{E.3})$$

$$= (p_d - p_s) + \frac{1}{2} \rho \left( \frac{Q}{\frac{\pi}{4}} \right)^2 \cdot \left( \frac{1}{d_{out}^4} - \frac{1}{d_{in}^4} \right) + \Delta z g \rho [Pa] \quad (\text{E.4})$$

The inner pipe diameter at the inlet and the outlet of the pump is, due to the difference between the designed and constructed test setup, 38,4 mm and 58,3 mm respectively. The height,  $\Delta z$ , between the two pressure transmitters, is 205,15 mm.

The unknown parameters,  $p_d$ ,  $p_s$  and  $Q$  and, are all measured in the experiment.

The shaft power is calculated with a fixed rotational speed of 1400 rpm as in Equation E.5. The torque,  $T$ , is found as Equation F.6 in Appendix F describes.

$$P_{shaft} = T \cdot \omega [W] \quad (\text{E.5})$$

Equation E.6 uses the pressure difference found in Equation E.4 to find the hydraulic power.

$$P_{hyd} = Q \cdot \Delta p [W] \quad (\text{E.6})$$

The hydraulic efficiency based on the hydraulic power and the shaft power is seen in Equation E.7.

$$\eta_{hyd} = \frac{P_{hyd}}{P_{shaft}} \cdot 100 \% \quad (\text{E.7})$$

Figure E.3 shows the head and efficiency from the test.

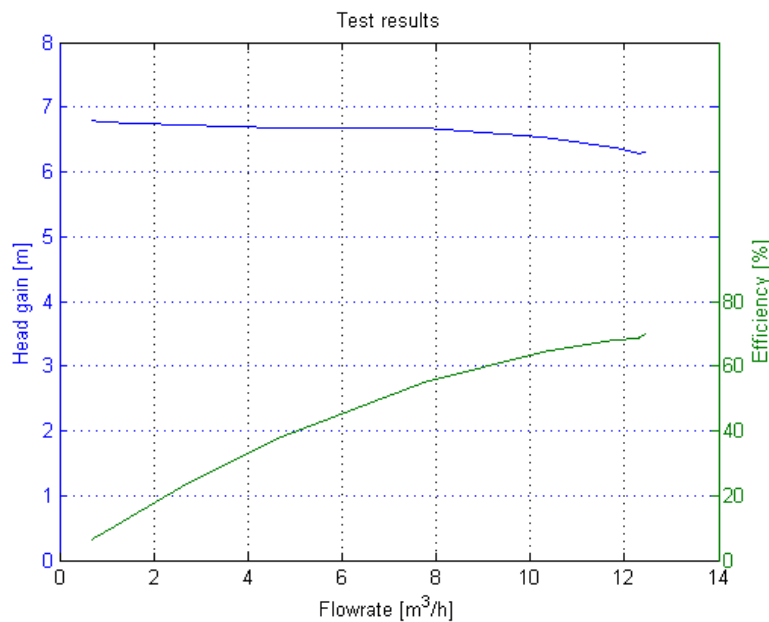


Figure E.3: Test results.

### E.3 Validity of test and measurement uncertainties

For validation of the measured data from the pump, analyzing the uncertainties of the data is needed. The uncertainties are presented throughout this section as a percentage deviation from the mean values. For upholding the grade 2 standard, the uncertainties will have to be in accordance to the maximum permitted uncertainties of the ISO [The International Organization for Standardization, 1999], seen in Table D.1. Each data point value has been found from 3 sets of 100 measurements each over 10 seconds.

The validity of the test results can be defined from the different requirements set in the ISO. There are, as described in Appendix D, requirements for the setup, the transducers used and the data collected.

#### E.3.1 Validity of test setup

In Section D.2 the required test setup dimensions for grade 1 and 2 tests is presented. The required lengths and widths of the piping in the setup are shown in Figure D.1. The constructed setup is presented in Figure E.1 and Figure E.2.

It can be seen that the physical test setup does not correspond to the the minimum requirements.

*"The outlet measuring section should be arranged in a straight section of pipe coaxial with the pump outlet flange and of the same diameter."* [The International Organization for Standardization, 1999,p. 28]

The quotation from the ISO applies for the inlet measuring section as well. The constructed setup have a difference in diameter between the piping and the pump flange.

The minimal distance between the pressure transducer and the pump has not been fulfilled, which can cause increased swirl to the pump. Though the dimensional difference is small, the test setup is not valid for grade 2 tests.

### E.3.2 Validity of transducers

By comparing Table D.2 containing the maximum permissible uncertainties allowed by the ISO [The International Organization for Standardization, 1999] and Table F.1 of the uncertainty values of the different transducers, it can be seen that all the transducers have uncertainties less than the permitted values. The comparison can be seen in Table E.1

Quantity	Grade 2 requirement [%]	Used [%]
Flow rate	±2,5	±0,2
Speed of rotation	±1,4	±0,5
Torque	±2,0	±0,5
Pump total head	±2,5	±0,8*

Table E.1: Permissible and used transducer uncertainties. \*per pressure unit. [The International Organization for Standardization, 1999,p. 19]

### E.3.3 Validity of data

Table D.1 shows the maximum permitted uncertainty values by repeated measurements. Figure E.4 shows the deviation of the limits of the 95% confident interval from the mean value. Comparing with Table D.1 it can be seen that all deviations are significantly below the permitted maximum. The maximum deviation for the test when using 3 sets is 1,8 %.

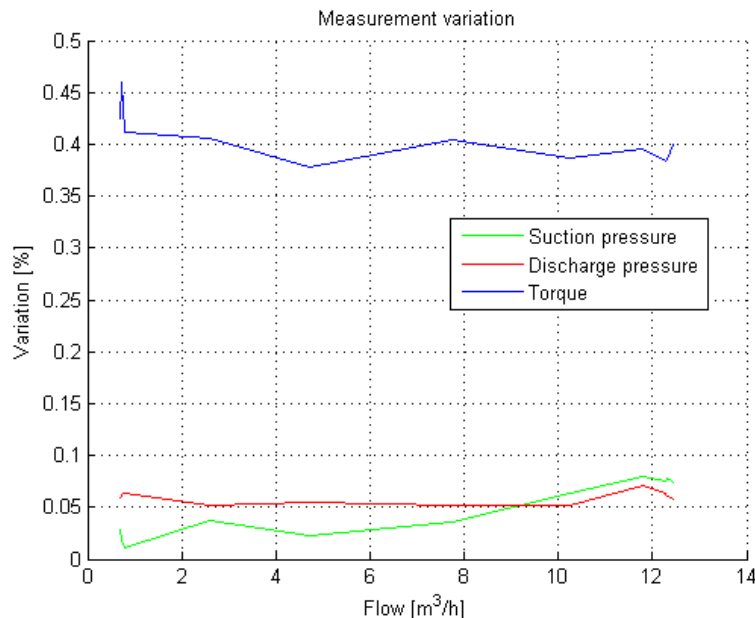


Figure E.4: Percentage deviation from the mean value with a 95% confidence interval

### System losses

The data measurements can be used to find the head and efficiency for the pump including the piping between the measurement devices. To get the precise head gain and the efficiency for the pump, additional losses are added.

The pipe loss between the pressure transducers and the pump is added. The loss is based on Equation 4.24 in Section 4.2.2.

Due to the constructed setup having a difference in diameter between the piping and the pump flange, contraction and expansion losses occur. These losses are found using Equations E.8 and E.9 [Department of Structural and Fluid Mechanics, 2008,p. 86-88].

$$H_{loss,expansion} = \zeta \cdot \frac{v_1^2}{2 \cdot g} \quad [m] \quad (\text{E.8})$$

$$H_{loss,contraction} = \zeta \cdot \frac{v_2^2}{2 \cdot g} \quad [m] \quad (\text{E.9})$$

The  $\zeta$  values are different for the expansion and contraction, and are found as described in Figure E.5. The area ratios are 0,74 at the inlet of the pump and 0,69 at the outlet of the pump.

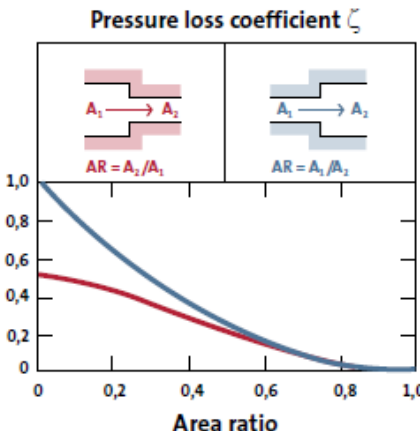


Figure E.5: Pressure loss coefficients of contraction and expansion. [Department of Structural and Fluid Mechanics, 2008,p. 88]

Figure E.6 shows the head and efficiency curves with and without system losses. The head and efficiency with added system losses lies higher. The efficiency lie higher due to the fact that the added system losses only changes the hydraulic power and not the shaft power.

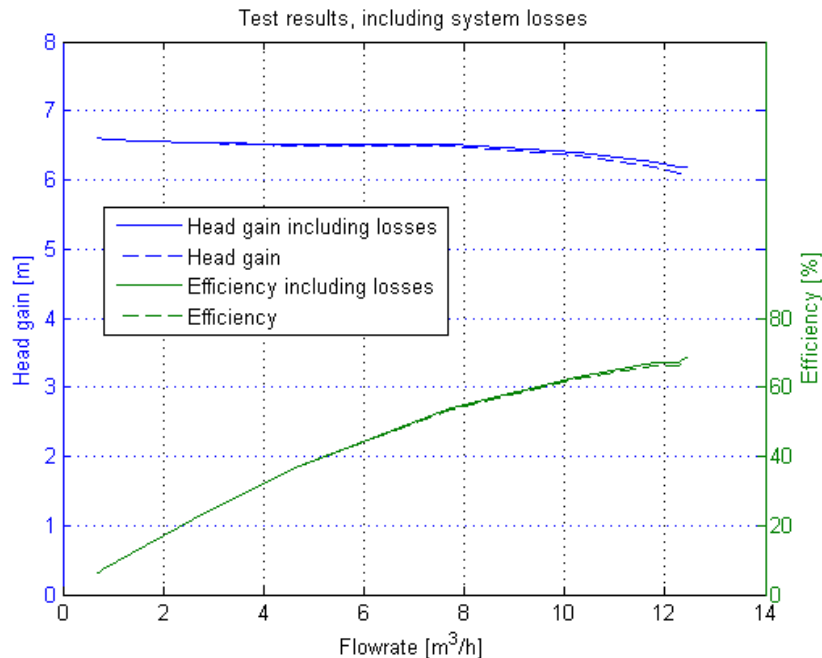


Figure E.6: Head and efficiency curves with and without system losses.

## Scaling

The reference data sheet has been scaled to a varying rotational speed from 1424 to 1469 rpm, while the testing was done with a constant speed of 1400 rpm. In order to compare the data to the scaled data sheet, the measured data will have to be scaled with rotational speed as well. The scaling laws used for this can be seen in Equations E.10, E.11 and E.12 [Department of Structural and Fluid Mechanics, 2008,p. 68]. For head, flow and power, respectively.

$$H_{new} = H_{old} \cdot \frac{n_{new}}{n_{old}} \quad [m] \quad (E.10)$$

$$Q_{new} = Q_{old} \cdot \left( \frac{n_{new}}{n_{old}} \right)^2 \quad \left[ \frac{m^3}{s} \right] \quad (E.11)$$

$$P_{new} = P_{old} \cdot \left( \frac{n_{new}}{n_{old}} \right)^3 \quad [W] \quad (E.12)$$

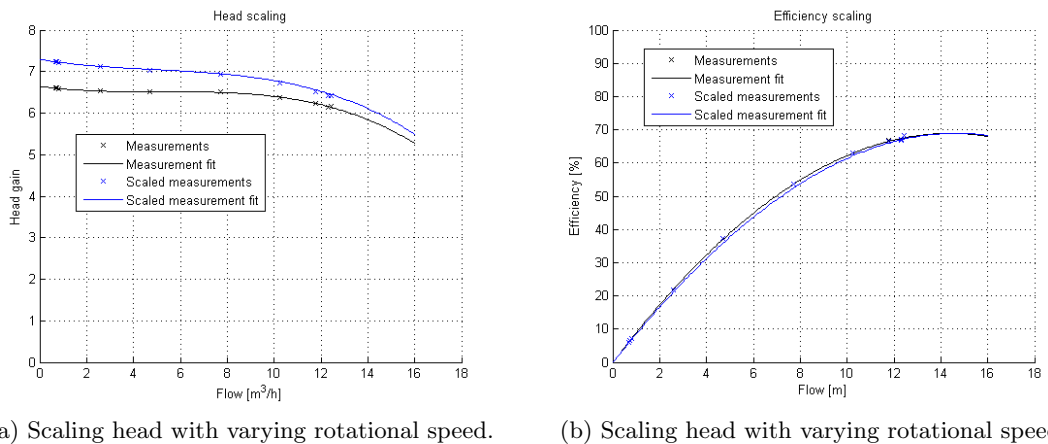
To best approach the data found in the data sheet, values for rotational speed was found for each measuring point in the data sheet (note that the varying rpm values are not found on the data sheet pdf in Appendix A.3, but can be found in Grundfos webcaps). The iterative process of scaling progressed as follows:

1. A rotational speed was found in the data sheet based on measured flow.
2. A scaled flow was calculated using Equation E.11.
3. A new rotational speed was found in the data sheet based on the scaled flow.
4. Steps 1-3 were repeated until convergence was reached.

5. Scaled head and shaft power were calculated using Equations E.10 and E.12.
6. Scaled efficiency was calculated using scaled values of head, flow and shaft power.

The results of scaling the measured data can be seen in Figure E.7. Generally the head gain rises with a higher rotational speed (See Figure 7.1a), and since the actual pump interval used in the data sheet is higher than the 1400 rpm used in the test, the head curve rises.

Scaling efficiency with speed of rotation will not, as with the head, simply increase or decrease the value. The efficiency curve will, when scaled with speed of rotation, move right when the speed is increased, changing to have its peaks at a higher flow (but at the same value). Reducing the speed will push the efficiency peak toward lower flows. Figure E.7b shows the scaled and unscaled efficiency plots of the pump test.



(a) Scaling head with varying rotational speed. (b) Scaling head with varying rotational speed.

Figure E.7: The effects of scaling measurement data.

*The test setup does not fulfill the requirements for a grade 2 test due to dimensions. Under the test it was noted that the system flow would not get higher than  $12,6 \frac{m^3}{h}$ , which is under the rated flow at  $13,1 \frac{m^3}{h}$  for the pump, and significantly below the  $17 \frac{m^3}{h}$  that is the highest flow shown in the data sheet. The devices used have uncertainties less than the permitted values. The test data has been calculated to include pipe, expansion and contraction loss. To be able to compare the test data with added losses to the data sheet, scaling of rotational speed is used.*

# Measurement devices F

---

In this appendix, the different measurement devices are presented. Their function in the test setup, their input and output characteristics and what is needed to produce measurable data are presented for each of the devices.

## F.1 National Instruments USB-6341 digital acquisition device

The National Instruments control unit used to power LabVIEW is the NI USB-6341. The unit can tolerate 10V as input as well as producing 10V for output channels. As it the maximum voltages needed for the motorized valve, this unit has been used. See Appendix A.9 for further information on the unit.

### F.1.1 Transferring from current to voltage

Several of the measurement devices produce a current output. The National Instruments USB-6341 is unable to measure current, so conversion to voltage is needed. Using the applications of Ohm's Law, the running current can be measured as voltage by using a known resistor. For the devices, a  $464\ \Omega$  resistor is used. The output current for the devices are in the range of 4-20 mA. The USB-6341 can measure up towards 10 V. Equation F.1 shows that the maximum output voltage will be just under 10 V and the minimum value will be in the accepted voltage range as well.

$$V = I \cdot R [V] \quad (\text{F.1})$$
$$1,86 = 0,004A \cdot 464\Omega [V]$$
$$9,28 = 0,020A \cdot 464\Omega [V]$$

Using the resistor in Equation F.1 the full voltage range of the NI USB-6341 is used. In Figure F.1 the applied circuit is shown.

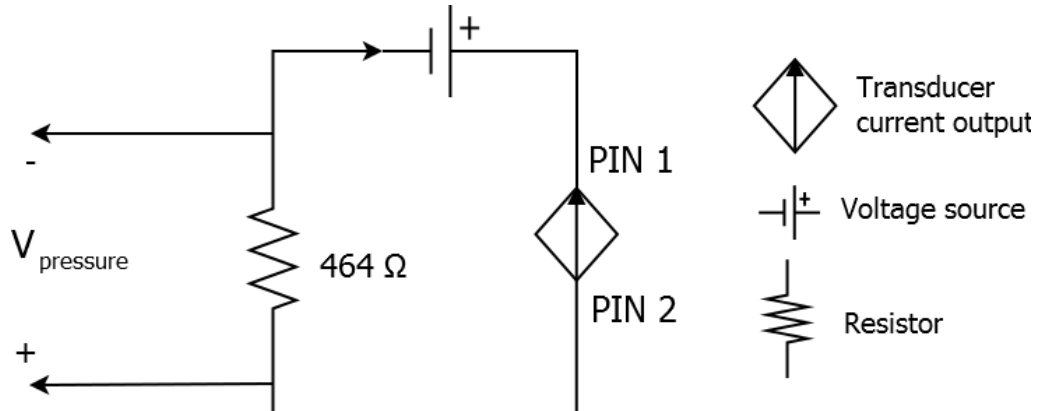


Figure F.1: Circuit for transforming measurement device output to voltage.

The circuit shown in Figure F.1 is used for transforming the current output for torque meter and pressure transmitter.

## F.2 Pressure measurement

The pressure in the system will be measured with a Danfoss MBS33 pressure transmitter, which is showed in Figure F.2. This will measure an absolute pressure of 0 to 2,5 bar, and output a corresponding current from 4 to 20 mA. The data sheet can be found in Appendix A.10.



Figure F.2: The Danfoss MBS33 pressure transmitter. [Danfoss, 2012a]

The function for converting voltage to bars is found from linear correlation between pressure and current in the pressure gauge, as can be seen in Equation F.3.

$$p = a \cdot V + b \quad [\text{Bar}] \quad (F.2)$$

$$a = \frac{\Delta p}{\Delta V} = 0,3367 \quad \left[ \frac{\text{Bar}}{\text{V}} \right]$$

$$b = p - a \cdot V \quad [\text{Bar}]$$

$$= 2,5 - 0,3367 \cdot 9,28 = -0,625 \quad [\text{Bar}] \quad (F.2)$$

$$p = 0,3367 \cdot V - 0,625 \quad [\text{Bar}] \quad (F.3)$$

The LabVIEW program (see Appendix G) will therefore measure the voltage drop over the resistance and transform it into bars using Equation F.3.

The pressure is measured before and after the pump, see Appendix D, Section D.2 for further details.

### F.2.1 Motorized valve

The motorized valve used in the setup is a Belimo NR24-SR (Appendix A.11), which is shown in Figure F.3. The valve is controllable for  $90^\circ$  with a voltage input. The motorized valve is controlled by the LabVIEW program. More on the control on the valve can be seen in Appendix G.



Figure F.3: Belimo NR24A-SR motorized valve used in the experiment setup. [MyTub, 2012]

The motorized valve in Figure F.3 is controlled by a voltage range of  $0 - 10V$  which rotates the valve from  $0 - 90^\circ$ .

### F.2.2 Flow measurement

The flow throughout the test setup is measured using a Tofting TF-100P, by attaching the flow measurement set on the pipe on the discharge side of the pump. The flow is shown on the display of a hand-held device. The data sheet for the TF-100P can be seen in Appendix A.12. For future uses, a Siemens MagFlo 1100 flow transducer and a MagFlo 3000 transmitter have been mounted on the setup, but have not been used in the experiments.

The readings of the Tofting TF-100P have been done manually by visual observation of the display.

### F.2.3 Motor measurements

For measuring the parameters related to the motor of the Grunfoss NK32-125 pump, a Danfoss VLT FC302 frequency converter is used. The motor parameters controlled and measured by the frequency converter are rotational speed, torque and power. The frequency directly controls the rotational speed. The torque is then given as an output.

The output of the frequency converter for measuring torque is a current, which then is converted to a voltage and then to torque. The method converting from current to voltage

is shown in F.1. The rated torque is found in Equation F.4 by using the rated power and the rated rotational speed.

$$\begin{aligned}
 T_{rated} &= \frac{P}{\omega} [Nm] \\
 &= \frac{P}{\frac{rpm}{60} \cdot 2 \cdot \pi} [Nm] \\
 &= \frac{370W}{\frac{1400}{60} \cdot 2 \cdot \pi} [Nm] \\
 &= 2,524Nm
 \end{aligned} \tag{F.4}$$

From Equation F.4, the torque can be set between 0-2,524 Nm. For finding the conversion factors, the torque range is compared to the output voltage range shown in Equation F.1. The function for the conversion is shown in Equation F.6.

$$\begin{aligned}
 T &= a \cdot V + b [Nm] \\
 a &= \frac{\Delta T}{\Delta V} \left[ \frac{Nm}{V} \right] \\
 &= \frac{0 - 2,524}{9,28 - 1,856} \left[ \frac{Nm}{V} \right] \\
 &= -0,34 \frac{Nm}{V}
 \end{aligned}$$

$$\begin{aligned}
 b &= T - a \cdot V [Nm] \\
 &= -2,524 - (-0,34) \cdot 9,28 [Nm] \\
 &= 0,631Nm
 \end{aligned} \tag{F.5}$$

$$T = -0,34 \cdot V + 0,631 [Nm] \tag{F.6}$$

#### F.2.4 Uncertainties

The uncertainties of the system have to be in compliance with [The International Organization for Standardization, 1999]. The measurement uncertainties for the different transducers can be seen in Table F.1.

Quantity	Measurement uncertainty [%]
Danfoss MBS33 pressure transducer	±0,8
Tofting TF-100P flowmeter	±0,2
Danfoss VLT FC 302 speed measurement	±0,5
Danfoss VLT FC 302 torque measurement	±0,5

Table F.1: Transducer uncertainties. The data sheets of the devices is shown in Appendices A.10,A.12, A.14, A.13

Comparing the uncertainties for the different transducers in Table F.1 to the maximum permitted systematic uncertainties for grade 1 and grade 2 shown in Table D.2, it is seen

that the used transducers complies fully with both grade 1 and grade 2 test procedures. A comparison to grade 1 and grade 2 requirements can be seen in Table E.1.

### F.2.5 Device numbers

The device numbers on the devices used in the test setup can be found in Table F.2.

<b>Device</b>	<b>AAU nr.</b>	<b>AUC nr.</b>
Voltage source	-	LBNR 29335
Danfoss MBS33 pressure transducer	-	-
Siemens MagFlo 1100 flow rate transducer	-	35893
Tofting TF-100P flowmeter	88461	-
Danfoss VLT FC 302	83280	-
Motor and pump	95822	-
LabVIEW box	91586	-
Valves	-	-

Table F.2: Device numbers.



# LabVIEW program G

---

*For efficient measuring of the Grundfos NK32-125 pump, a program have been set up using the G visual coding language in LabVIEW. This program, meant for automated measuring will be explained throughout this appendix. The program can be found in Appendix A.15.*

The program is repeatedly measuring and logging data from the different transducers in respect to different valve closing scenarios while controlling the motorized valve itself. LabVIEW runs the program while The National Instrument USB-6341 control unit, see Appendix A.9, controls the circuitry. The different aspects of the program will be explained in the following. A series of simplified examples is used throughout the chapter, as the full program contains data which would unnecessarily complicate the explanation. The full program can be seen at the end of the chapter in Figure G.7.

As the program runs with repeated measurements, loops are needed. A flowchart of the program is shown in Figure G.1.

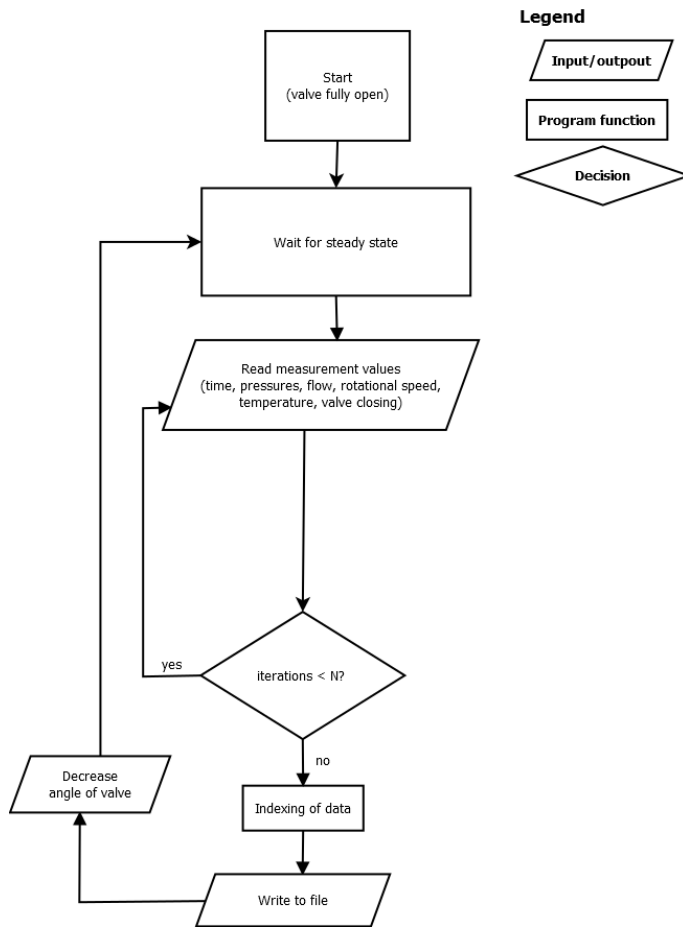


Figure G.1: Flowchart of the measuring program.

The single entities of the program flowchart seen in Figure G.1 will be explained during the appendix.

During the experiment, the flow rate measurement and the temperature check was made by manual reading due to faulty equipment. The LabVIEW program has the option of measuring the entities for future use. The calculations and programming related to these entities are still presented throughout the chapter along with the entities measured by LabVIEW in the experiment.

For measuring physical data, *Create channel* blocks for each channel are used, shown in Figure G.2.

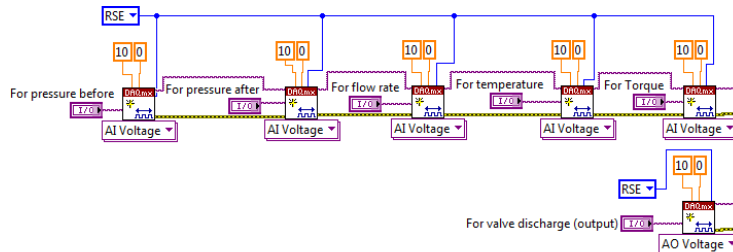


Figure G.2: Channels created for the measuring program.

The four channels in series are the physical inputs to the system, all analog (pressures, flow, torque and temperature). In Figure G.3 the analog output for controlling the motorized valve is shown. The channels are set to *Reference Single Ended (RSE)*, which means the measured voltages are referenced to ground.

In the flowchart in Figure G.1, it is seen that the measurements are to be repeated while changing the opening of the motorized valve. For the repetition, a *While Loop* is used. As the output voltage for the motorized valve needs to be changed every time the loop is run, a function called *Shift register* is used. By connecting functions to the Shift register, the changes caused by a run in the loop will be applied as an initial condition through the next run. In Figure G.3 a simplified example of the While loop with a Shift register, which resembles the usage in the measuring program, is shown. The number of times the loop has to run (iterations) can be set by the user of the program.

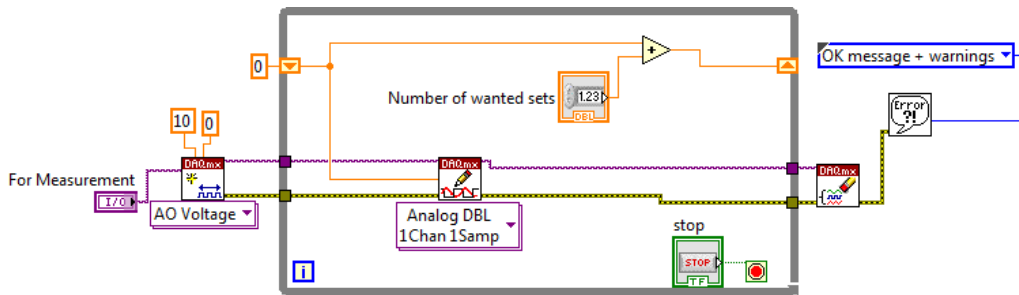


Figure G.3: Example of While loop with Shift register for initial condition changes through iterations.

In the loop shown in Figure G.3, the value sent to the analog voltage output is zero. Then, by each iteration, the voltage will increase by  $\frac{10V}{\text{number of wanted sets}}$  (e.g: for 40 measuring points, voltage will increase by  $\frac{10}{40} = 0,25V$  after each iteration), which is controllable from the user interface. The initial condition for the first run of the loop has been given to be 0 in the diagram. The change will in the example occur as quickly as possible, as there is no time delay. A time delay have been added to the program, seen in Figure G.4 and explained further down in the section.

To give the system time to settle into steady state, a time delay is set to occur after the change of output voltage, and thereby giving the valve and system time to adjust. The time delay is made by using a block called *Wait (ms)*. This block allows the user to delay the program by a specified number of milliseconds. The block is shown in Figure G.4, connected to a control which makes the user able to adjust the waiting period.

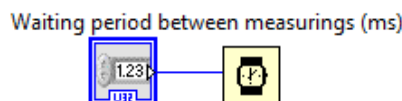


Figure G.4: *Wait (ms)* block connected to a numeric control block.

As all measurement channels are connected, the data of the different transducers needs to be separated before collection of data can occur. By using a series of the block *Index array*, the data stream can be separated into the correct measurement data sets. The separation of measured data is shown in a simplified example in Figure G.5.

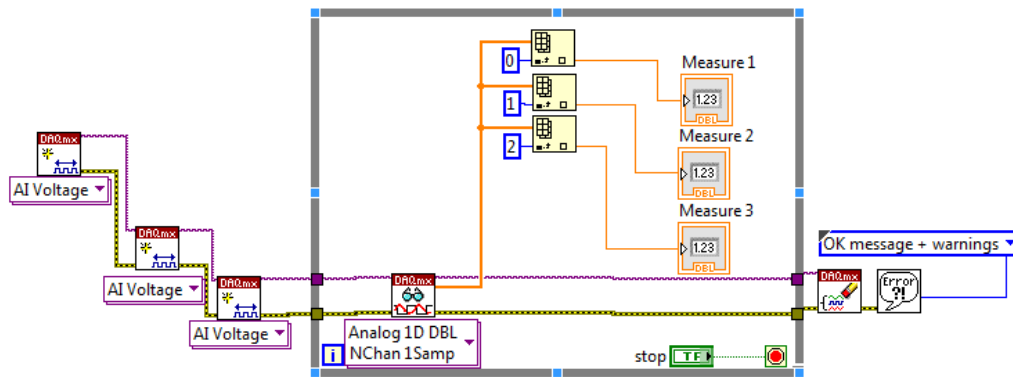


Figure G.5: A simplified example of the function *Index array*.

In the example on Figure G.5, three input voltages are collected and by using *Index array*, separated into different data outputs. This is similarly done in the measurement program for all input values.

All the physical measurements are in voltage, as seen in Figure G.2. As the desired data has various units (*bar*,  $^{\circ}\text{C}$ , *rpm*, *T*), voltage measurements are converted based on the setup and the data sheets of the different transducers (found in Appendix A.12 for flow measurement, A.10 for pressure measurements and A.13 for rotational speed measurement).

In Figure G.6 the different calculations in the measurement program for the transducers are shown. The calculations as well as the circuitry for the different transducers can be seen in Appendix F.

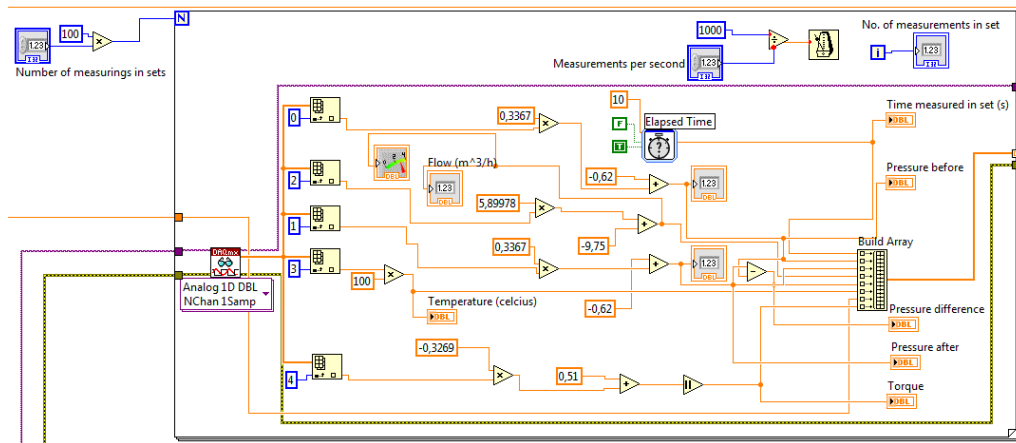


Figure G.6: The transducer calculations in LabVIEW.

In Figure G.6, the measurements and calculations are positioned in a *For Loop*. The For loop repeats the included functions until the initial conditions of the loop have been fulfilled. For the loop in the program, the For Loop will repeat itself a specified number of times. The included *Wait until* block specifies the rate of the loop by starting the iteration when the time is a multiplication of a user specified number of milliseconds. The control block named *Number of measurements in sets* in Figure G.6 specifies how many times the For Loop should run. For fulfilling the ISO criteria of measuring for at least 10 seconds, seen

in Appendix D.1, the number of iterations and the rate of iterations multiplied should be at least 10000.

As the procedures of changing the output parameter (the valve voltage), waiting for steady state, measuring the inputs from the system and then repeating needs to be in a certain order, a block called *Flat sequence* is used. This series of loops can make the program run in a specified sequence.

When the *For loop* collecting and recalculating the input data, the data is indexed and send to a specified file via the *Write to spreadsheet* block. The data for each measuring set is send to the specified tabular file.

In Figure G.7 the overall program for measurement is shown.

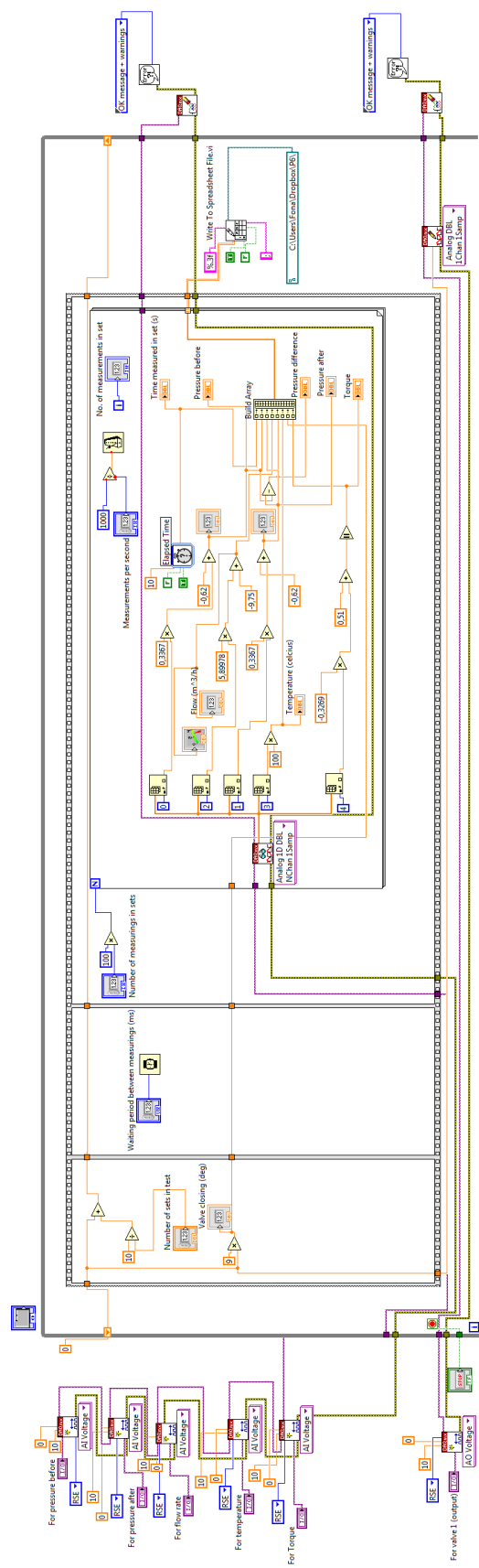


Figure G.7: Measurement program for the tests of the impellers.